

July 2021

Advanced Organic Polymers for the Nanoscale Fabrication of Fiber-based Electronics Using the Electrospinning Technique

William Serrano Garcia
University of South Florida

Follow this and additional works at: <https://digitalcommons.usf.edu/etd>



Part of the [Electrical and Computer Engineering Commons](#), and the [Other Education Commons](#)

Scholar Commons Citation

Serrano Garcia, William, "Advanced Organic Polymers for the Nanoscale Fabrication of Fiber-based Electronics Using the Electrospinning Technique" (2021). *USF Tampa Graduate Theses and Dissertations*. <https://digitalcommons.usf.edu/etd/9228>

This Dissertation is brought to you for free and open access by the USF Graduate Theses and Dissertations at Digital Commons @ University of South Florida. It has been accepted for inclusion in USF Tampa Graduate Theses and Dissertations by an authorized administrator of Digital Commons @ University of South Florida. For more information, please contact digitalcommons@usf.edu.

Advanced Organic Polymers for the Nanoscale Fabrication of Fiber-based Electronics Using the
Electrospinning Technique

by

William Serrano Garcia

A dissertation submitted in partial fulfillment
of the requirements for the degree of
Doctor of Philosophy in Electrical Engineering
Department of Electrical Engineering
College of Engineering
University of South Florida

Major Professor: Sylvia W. Thomas, Ph.D.

Arash Takshi, Ph.D.

Jing Wang, Ph.D.

Norma Alcantar, Ph.D.

Vincenzo Guarino, Ph.D.

Chang-Yong Nam, Ph.D.

Date of Approval:

June 15, 2021

Keywords: P3HT, BBL, semiconductors, sensors, coaxial junctions, nanofibers

Copyright © 2021, William Serrano Garcia

Dedication

To those who pointed at the correct path.

To those who noticed that not only one path was correct.

To those who noted that creating a path was also appropriate.

To all of those who affected my decisions:

My mother *Susana García Agosto* and my father *William Serrano Ríos*, mentors, and meaningful friends.

And in memory of my beloved father whose support, love, and dedication are a bastion of poetry and there is no method by which it can be weighted, in this world or in another.

A los que señalaron el camino correcto.

Para aquellos que notaron que no solo un camino era correcto.

Para aquellos que notaron que crear un camino también era apropiado.

A todos los que afectaron mis decisiones:

Mi madre *Susana García Agosto* y mi padre *William Serrano Ríos*, mentores y amigos significativos.

Y en memoria de mi amado padre cuyo apoyo, amor y dedicación son un baluarte de la poesía y no hay método por el cual se pueda ponderar, ni en este mundo ni en otro.

Acknowledgments

This work is made possible by many years of research, reading, collaboration, and reflection, and there is no way to express my deep gratitude to the countless mentors, advisors, colleagues, and friends who have given uninterrupted advice and mentorship during all these years. But I must give, at least, the most genuine and sincere thanks to those who helped me in shaping the scientist I am today and expressing the ideas in this work:

To Idalia Ramos and Nicholas Pinto, for their continuous support during my undergraduate years; to Javier Figueroa for being the light that illuminated the path after my bachelor's degree; to Bernard Batson, for providing continuous advice and help at every single step during my doctoral journey; to Sylvia Thomas, for mentoring, advising, encouraging, and supporting all the research ideas I generated; to Noel Blackburn and Terrence Buck who acted as a catalyst for my collaborations at National Laboratories; to the Florida Georgia Louis Stokes Alliance for Minority Participation (FGLSAMP) Bridge to the Doctorate (HDR#1400837), Sloan University Center of Exemplary Mentoring Award (#2014-3-07), the McKnight Doctoral Fellowship from the Florida Education Fund (FEF), NSF EAPSI OISE #1714002, the USF Nexus Initiative – Bio and Electronic Advanced Material Systems (USF BEAMS), LSAMP SciComp Skills Building Program HRD #1836400, and the Fulbright U.S. Singapore Student program, for the academic, professional, and financial resources they provided.

And to my family and dearest friends, for their company, encouragement, and sustaining love during this period.

Table of Contents

List of Tables	iv
List of Figures	v
Abstract	ix
Chapter 1: General Introduction to the Electrospinning Technique and Polymeric Composites.....	1
Chapter 2: Background Research	6
2.1 Nanocomposites for Electronic Applications That Can Be Embedded for Textiles and Wearables	6
2.1.1 Fiber Based Field Effect Transistors	12
2.1.2 Fiber Based Light Emitters	15
2.1.3 Fiber Based Capacitors	17
2.1.4 Fiber Based Nanogenerators	18
2.1.5 Conclusions.....	21
2.2 Electrospinning for Sensing Devices	22
2.2.1 Sensor Response of Electrospun Poly(lactic Acid)/Polyaniline Nanofibers to Aliphatic Alcohol Vapors of Varying Sizes	22
2.2.1.1 Introduction.....	22
2.2.1.2 Experimental	23
2.2.1.3 Results and Discussion	25
2.2.1.4 Conclusions.....	30
2.3 Applications of Poly(3-Hexylthiophene) (P3HT).....	30
2.3.1 Fabrication of P3HT Based Fibers: Electrospun Fibers of Poly(VinylideneFluoride-Trifluoroethylene)/Poly(3-Hexylthiophene) Blends from Tetrahydrofuran	30
2.3.1.1 Introduction.....	30
2.3.1.2 Experimental	31
2.3.1.3 Results and Discussion	33
2.3.1.4 Conclusions.....	39
2.3.2 Poly(lactic Acid)/poly(3-Hexylthiophene) Composite Nanofiber Fabrication for Electronic Applications.....	39
2.3.2.1 Introduction.....	39
2.3.2.2 Experimental	40
2.3.2.3 Results and Discussion	41
2.3.2.4 Conclusions.....	49

2.4	General Details of Poly(benzimidazobenzophenanthroline) (BBL).....	51
2.5	References.....	55
Chapter 3:	Idealization of P3HT/BBL Coaxial Composite	61
3.1	Electrospinning Technique for Coaxial Semiconductive Organic Nanofibers for Flexible Electronic Devices Fabrication	61
3.1.1	Summary	61
3.1.2	Objectives	62
3.1.3	Introduction.....	62
3.1.4	Experimental	66
3.1.5	Conclusion	72
3.2	References.....	73
Chapter 4:	Further Characterizations on P3HT and BBL.....	76
4.1	P3HT Loaded Piezoelectric Electrospun Fibers for Tunable Molecular Adsorption.....	76
4.1.1	Abstract.....	76
4.1.2	Introduction.....	77
4.1.3	Materials and Methods	78
4.1.4	Preparation	78
4.1.5	Morphological Characterization	79
4.1.6	Adsorption Via UV–Vis Spectroscopy.....	80
4.1.7	Results and Discussion	80
4.1.8	Conclusions.....	85
4.2	Sensing Mechanisms of the Ladder Polymer Poly(benzimidazobenzophenanthroline) BBL.....	85
4.2.1	Abstract	85
4.2.2	Introduction.....	85
4.2.3	Experimental	86
4.2.4	Discussion	90
4.2.5	Conclusion	94
4.3	References.....	94
Chapter 5:	Fabrication and Characterization of P3HT/BBL Coaxial Structure	97
5.1	Electrospinning Fabrication of Coaxial Semiconductive Organic Nanofibers for Flexible, Multifunctional Electronic Devices.....	97
5.1.1	Abstract.....	97
5.1.2	Introduction.....	97
5.1.3	Experimental	99
5.1.4	Results and Discussion	102
5.1.5	Future Work.....	106
5.1.6	Conclusions.....	106
5.2	References.....	107

Chapter 6: Conclusions and Future Work.....	110
6.1 Conclusions.....	110
6.2 Future Work.....	111
6.2.1 Electrical Characterizations of Coaxial Structured All-polymer p-n Junctions	111
6.2.2 Morphological and Electrical Characterizations of P3HT-BBL Junction Devices	111
6.2.3 Expectations.....	113
Appendix A: Copyright Permissions	114
About the Author	End Page

List of Tables

Table 2.1 Sensor response and recovery times to the presence and absence of alcohol vapors and the percentage fractional change in sensor resistance	29
--	----

List of Figures

Figure 2.1 Fibers of PLA/PANi-CSA showing the rectification of an input (i/p) voltage of 100Hz with 5 V peak-peak sine wave.	10
Figure 2.2 Single nanofiber of PLA/PANi-CSA for aliphatic alcohol vapor sensing	10
Figure 2.3 P3HT based UV tunable diode	11
Figure 2.4 Sketch of organic semiconducting nanowires (a); transfer curves of the designed devices (b); max drain current as function of the nanowires (c); transmission electron microscopy and its elemental mapping by energy-dispersive X-ray spectroscopy (d); length-directional stretching (e); width-directional stretching (f); illustration of the deformable FET with straight nanowires and dielectric with length and width directional stretching (g)	13
Figure 2.5 (a) Schematic of P3HT coating on the fibers, with pre-patterned source-drain gaps (top-left) and weaving transistors with different fibers (bottom); (b) optical image of two transistors in a woven matrix; (c) optical image with a close-up of a fiber transistor showing the source, gate and drain as well as a visible pre-patterned transistor gap on the right	14
Figure 2.6 Laser confocal microscopy images of 5 wt% poly (fluorene) derivative/PMMA blend electrospun nanofibers with (a) PFO, (b) PFQ, (c) PFBT, (d) PFTP	16
Figure 2.7 (a) Schematic of coaxial electrospinning; (b) schematic of white light emitting porous fiber; (c) SEM image of PLA fiber; (d) TEM image of PLA fiber; (e) diameter distribution of PLA fibers	18
Figure 2.8 (a), (b) TEM images of a single nanofiber from the Co ₃ O ₄ - CNFs ₂ sample; (c), (d) HRTEM images of a single Co ₃ O ₄ hollow NP, and (e) the corresponding SAED pattern	18
Figure 2.9 Working mechanism under pressing releasing mechanical force and textile like mesh	20
Figure 2.10 Basic electrospinning apparatus	24

Figure 2.11 SEM image of a single PLA/PANi-CSA nanofiber lying across two gold electrodes	24
Figure 2.12 UV/VIS absorption spectra of the PLA/PANI-CSA polymers in CHCl ₃	26
Figure 2.13 SEM images of electrospun 3wt% PLA/PANi-CSA nanofibers and the corresponding EDS spectrum.....	26
Figure 2.14 Normalized resistance of individual electrospun HCSA-doped polyaniline nanofibers to various alcohols: (a) methanol, (b) ethanol and (c) 1- propanol	29
Figure 2.15 Schematic of the basic electrospinning apparatus	33
Figure 2.16 UV/VIS spectra of the blend solutions prepared from various PVDF-TrFE concentrations with P3HT in THF	35
Figure 2.17 SEM images of electrospun fibers of (a) 1 wt% PVDF-TrFE; (b) 1 wt% PVDF-TrFE/P3HT; (c) 3 wt% PVDF-TrFE; (d) 3 wt% PVDF-TrFE/P3HT; (e) 5 wt% PVDF-TrFE; (f) 5 wt% PVDF- TrFE/P3HT	36
Figure 2.18 SEM images of electrospun fibers of (a) 7 wt% PVDF-TrFE; (b) 7 wt% PVDF-TrFE/P3HT; (c) 9 wt% PVDF-TrFE; (d) 9 wt% PVDF-TrFE/P3HT; (e) 11 wt% PVDF-TrFE; (f) 11 wt% PVDF- TrFE/P3HT	37
Figure 2.19 SEM images of electrospun fibers of (a) 13 wt% PVDF-TrFE; (b) 13 wt% PVDF- TrFE/P3HT; (c) 15 wt% PVDF-TrFE; (d) 15 wt% PVDF-TrFE/P3HT.....	37
Figure 2.20 Plot of the electrospun fiber diameters (d) taken using an atomic force microscope as a function of wt% of PVDF-TrFE/ P3HT	38
Figure 2.21 UV-visible absorption spectra of a 5 wt% PLA-CHCl ₃ solution with various P3HT concentrations prior to electrospinning; included are the absorption spectra for pure P3HT-CHCl ₃ and pure PLA-CHCl ₃	44
Figure 2.22 SEM images of PLA-CHCl ₃ fibers with various PLA/P3HT ratios: (a) 100/0; (b) 83/17; (c) 72/28; (d) 63/37; (e) 56/44	45
Figure 2.23 (a) Optical microscope image at low magnification of the top surface showing the pre-patterned n-doped Si/SiO ₂ substrate.....	47
Figure 2.24 Current-voltage (I-V) characteristic curves at 300 K of the diode shown in Figure 2.23(a) in vacuum.....	48
Figure 2.25 Schematic energy band diagrams for the P3HT/n-Si interface (a) before and (b) after contact	48

Figure 2.26 Current – voltage (I–V) characteristics at 300 K of the diode in the absence and in the presence of UV light ($\lambda = 365$ nm)	50
Figure 3.1 Electrospinning apparatus	68
Figure 3.2 Molecular structures for (a) P3HT, (b) BBL and (c) Chloroform	68
Figure 3.3 Coaxial needle	68
Figure 3.4 Sketch of (a) Semiconducting coaxial nanofiber and (b) sliced nanofiber forming a nanodisk	69
Figure 3.5 Sketch of the expected Semiconducting Coaxial nanofiber: (a) Shell/Core flow rate [X/Y] = 1, (b) Shell flow rate [0] and (c) sliced nanofiber forming a nanodisk	70
Figure 3.6 Sketch of the coaxial electrospinning technique showing nanofiber-based devices such as diodes	71
Figure 3.7 Circuit for sensing characterization	73
Figure 4.1 Scheme of the homemade system used for the adsorption measurements	81
Figure 4.2 PVDF-TrFE electrospun fibers: Fiber surface and surface topography via SEM/ AFM (a); Comparison of PVDF-TrFE fiber mesh respect to control (CTR) (b); Adsorption curves (c)	82
Figure 4.3 Effect of P3HT in PVDF-TrFE electrospun fibers: A, B) Morphological analysis via SEM (scale bar 5 mm); C) Adsorption curves	83
Figure 4.4 Effect of externally applied voltage on MB adsorption: Comparison of adsorption curves of PVDF-TrFE, P3HT/PVDF-TrFE electrospun fibers	84
Figure 4.5 Device fabrication	87
Figure 4.6 BBL Sensor representation (a)	89
Figure 4.7 Film response for different analytes	89
Figure 4.8 Sensor responses for the different analytes in dark and under light conditions (e-h)	92
Figure 4.9 Sensitivities for dark and light conditions	92
Figure 4.10 Example of sensing cycle for acetone (a)	93

Figure 5.1 Coaxial nanofiber fabricated using P3HT (a) and BBL (b) as the semiconducting polymers	100
Figure 5.2 Coaxial nanofiber with p- and n- type semiconducting polymers.....	101
Figure 5.3 Continuous fabrication of coaxial nanofiber p-n junctions, using the electrospinning technique	101
Figure 5.4 Comparison of the UV/VIS spectra of pure PS (7wt%), pure P3HT (2wt% in CHCl ₃), and the P3HT/PS (0.4wt% / 7wt%) blend indicates that adding polystyrene does not change the physical or optical characteristics of P3HT.....	104
Figure 5.5 TEM image of a coaxial nanofiber with a P3HT/PS (0.4 wt%/7 wt%) core and a BBL (0.39 wt%) shell.....	104
Figure 5.6 TEM images of coaxial nanofibers [P3HT/PS core (white arrow) with BBL shell (black arrow)] created simultaneously within a single run of the electrospinning technique	105
Figure 5.7 Future work, electrical characterizations will be performed by using a small amount of MSA to remove the BBL shell and expose the P3HT core.....	107

Abstract

Electrospinning has become one of the most interesting techniques for fabricating nanofibers for multiple applications. The high surface-to-volume ratio nanofibers offer make the perfect structure for filters, sensors, and fiber-based electronics that could lead to a wide range of flexible electronics applications. This technique makes organic semiconducting polymers a promising alternative for single fiber electronics structures. Indeed, a wide variety of structures can be fabricated using electrostatic techniques for polymer manipulation from droplets, fibers, and coaxial structures. Although techniques such as electrospinning led the use of electrostatic forces to generate fibers of a precursor solution, electrospinning requires large enough polymer chains to enhance entanglement. This leads to the formation of long nanofibers, putting aside polymers with low molecular weight and to the formation of beads by a spraying behavior. Thus, development of a multilayer process for the formation of organic semiconductive coaxial fibers is imperative and the subject of this dissertation. Organic semiconductive polymer such as the p-type P3HT and the n-type BBL were used in this research. Fibers of P3HT were fabricated in conjunction with an auxiliary polymer to mechanically help the formation of fibers. P3HT has been shown to form fibers that can be embedded for the fabrication of diodes, sensors, and as a negatively charges molecule adsorbent. BBL thin films were studied as a gas sensor for volatile organic compounds (VOC's). Most importantly, for the first time, a nanofiber comprising P3HT core / BBL shell coaxial structure was fabricated and morphologically characterized.

These coaxial nanofibers were fabricated using the electrospinning technique by taking advantage of their solvent orthogonality. Fast and abrupt production resulted in a wide population of nanofibers in the nanoscale. Previous electrical characterization was performed to the P3HT fibers in different embodiments showing tunable behavior under UV radiation. Gas sensing on BBL thin films were related to the known concentration for different analytes. Coaxial nanofibers were characterized using transmission electron microscopy (TEM), demonstrating the formation of semiconductive nanofibers coaxial arrangements using the electrospinning technique. These advancements demonstrate the ability of forming a single nanofiber junction, the possibility of a cylindrical p-n junction, and create the ability to fabricate single fiber devices increasing the surface-to-volume ratio, ultimately improving the sensing response under a sensing embodiment.

Chapter 1: General Introduction to the Electrospinning Technique and Polymeric Composites

Nanofibers have been presented as one of the most versatile structure for various applications leading the fabrication of filters, drug delivery systems, and more importantly, electronic devices, including sensors, transistors, and photosensors. The functionalities nanofibers offer to the research field are still increasing with more researchers adding the electrospinning technique to their laboratory toolbox. The Covid-19 pandemic saw electrospinning become the to-go technique to manufacture application-focused nanofibers such as air filtration with enhanced antibacterial and antiviral properties. While organic polymers lead to an easy fabrication of this high surface area-to-ratio structures such as the nanofibers mats, other materials that are not usually able to be spun as fibers can be embedded with polymers for the creation of composite nanofibers with extended functionalities. For example, insulating polymers, epoxies, and blends can be spun into nanofibers for the fabrication of gas, liquids, and chemical filters. These insulating polymers can be functionalized or mixed with other electroactive polymers for active sensing while performing the main task of filtration. Drug delivery research has been based in this process due to the ability of some polymers like poly (caprolactone) to be biocompatible and biodegradable to encapsulate drugs, particles, and other materials. Nanofiber technology has significant impact in these and other important areas within energy, sensing, and communication.

For the fabrication of these fibers, the electrospinning technique is used to ensure sub-micron diameters. This process is an electrostatic deposition technique where fibers are formed by means of an electrostatic force sufficiently high to overcome the surface tension of a polymeric solution (organic or inorganic) leading to the formation of charged jets that dries as fibers. To date, it is the most reliable technique for the fabrication of fibers in the nanoscopic scale with lengths over passing the meter scale. Electrostatic theory governs the electrospinning principle for fiber fabrication and the working principle is the same as electrospraying. When producing nanoparticles, dots, or sprays, the solutions tend to be characterized by low molecular weights and therefore, usually have low viscosities, therefore called electrospraying. However, when the molecular weights of the polymer are large enough to promote entanglement between molecules in the solution, the final products lead to the formation of fibers as random nonwoven meshes or aligned fibers, after the evaporation of the solvent. This is called electrospinning. Fibers produced this way can have diameters below 30nm and up to 10ths of a micrometer. The versatility of this technique has made electrospinning an important and indispensable laboratory technique. While the most used and well-known set-up is based on three important parts (power supply, a needle, and a collector), only a power supply with 1kV up to 30kV is required for most solutions. The most common variables for this technique are electric field (voltage and separation of the collector), pump rate, temperature, and humidity. There is a vast number of set-ups and forms to perform the electrospinning process; however, there are three modes that can cover the whole field: needle-based, needle-less, and point-to-point. Needle-based electrospinning is the archetypical process for nanofiber fabrication and the one used in this research where the solution is inserted into the electric field using a needle. Needleless electrospinning has the same fundamental behavior as conventional electrospinning but is oriented to mass production of nanofibers using different

arrangements of electrodes such as disks, cylinders, blades, wires, gas bubbles, or spheres covered by the solution in a container. “Point-to-Point” electrospinning has shown to be extremely helpful for the fabrication of single fibers in the micro scale where two needles in front of each other creates a point-to-point electric field forming standing fibers. While forming fibers down to the nanometer scale is difficult in this mode, fibers in the micrometer scale can be easily performed, ideally for single fiber devices. In principle, for the electrospinning, a critical molecular weight and viscosity of solution is required to achieve the nanofibers, depending on the fundamental structure of the molecules. For example, on an inorganic polymer, silica nanofibers can be produced when mixing silica nanoparticles or TEOS with a supportive polymer, such as Polyvinylpyrrolidone (PVP) or Polyvinyl alcohol (PVA), which promotes the nanofiber formation. This varies depending on whether the polymer is organic or inorganic. In a specific case for inorganic polymers such as silica nanofibers, two fundamental steps are required when blending with a polymer: 1) the electrospinning that led to the formation of the fiber structure and 2) a calcination process to remove the polymer and fuse the nanoparticles together forming the fiber. On the other hand, aging TEOS solutions in this sol-gel mechanism, a solution (sol) can lead to silica chains long enough to form pure silica nanofibers without the need of a supporting organic polymer or a calcination process. The achievement of linear molecular structures in the sol-gel method can be achieved by the growth and linkage of silica repetitive units formed from a hydrolysis and condensation process that has been explained elsewhere.

Polymers used for nanofiber fabrication can be divided into three common groups from an electrical point of view: insulators, semiconductors, and conductive. Insulators are widely used for the fabrication of filters, biocompatible and biodegradable meshes for wound healing scaffolds, as well as for drug delivery applications. It is also used as a supporting material to bring mechanical

stability (to ensure or enhance fiber formation) for materials such as oxides, particles, clusters, metals, and other materials unable to form fibers due to low molecular weight which can agglomerate in the form of particles, crystals, and clusters due to low covalent interaction between the structures. The most common polymers include PS, PCL, PLA, PEO, PMMA, and PVDF, just to name a few.

Semiconducting polymers are extensively studied as diodes and field effect transistors for organic solar cells, light emitting diodes (LED's), and sensors applications. Some of those polymers have also been studied for drug delivery and cell cultures due their ability to be biocompatible and promote cell proliferation. These polymers, usually due to the small molecular weight, are unable to form fibers; an insulating polymer is often used to provide the mechanical stability the fiber formation requires. It is also valid from another point of view, where the insulating polymer is not able to form nanometric fibers and adding a small amount of a semiconducting or conducting polymer promotes the formation of nanofibers at lower weight-percent by increasing the charge at the solution and also making the insulating polymer structure an electroactive nanofiber. In most cases, the semiconducting polymer increases the conductivity of the solution, leading to thinner nanofibers that cannot be achieved with the nonconductive polymer alone. Common polymers of this type include the archetypical p-type polymer sulfur based P3HT and the n-type ladder polymer BBL.

Conducting polymer (conjugated polymers) require a doping process to make them conductive. The most common polymers include the doped polyacetylene (PA), polypyrrole (PPy), the salt based semi-flexible rod polymer Polyaniline (PANI), the branched poly (3,4-ethylenedioxythiophene) polystyrene sulfonate (PEDOT:PSS), and the rigid-rod Poly(p-phenylene vinylene) (PPV). In general, semiconducting, and conducting polymers can be classified as

electroactive polymers. However, in this case, we define an electroactive system as a fiber or composite fiber that can conduct electricity by means of the semiconductive or conducting polymer into the fiber.

Poly (3-hexylthiophene) (P3HT) is one of the most used p-type polymers. It is a member of the P3AT group. The molecular weight of P3HT tends to be too low in order to form fibers by the electrospinning process. To promote fiber formation, a high molecular weight polymer is used, giving the p-type polymer the required mechanical stability to form fibers. For this reason, the secondary polymer is carefully selected to form an electroactive interface for sensing and rectifying characterizations, as will be discussed in the next chapters.

This dissertation work discusses three major processes:

1. Characterization of P3HT composite nanofibers to absorb the negatively charged molecule Methylene blue,
2. Characterization of BBL thin films for volatile compounds vapor sensing,
3. Fabrication of P3HT/BBL coaxial nanofibers structures.

Chapter 2: Background Research

2.1 Nanocomposites for Electronic Applications That Can Be Embedded for Textiles and Wearables

Clothes and jewelry have been used since time immemorial; however, since ancient times, the usage of metals as gold, silver, and copper can be seen not only in jewelry but also in the process of textile decorations. As our technological skills evolved, the aim to use smaller technologies on our bodies has been continuously researched and developed. The 1947 invention of the transistor greatly changed society by increasing our ability to create fast and reliable communications ^[1-4]. Today, technology is closer to our bodies than ever in the forms of electronic based jewelry including near field communication (NFC) rings and smart watches. Since the discovery of conductive and semiconductive polymers ^[5-7], new trends and possibilities have been idealized and studied for the fabrication of intelligent textiles. Because we are approaching an era where biodegradable, biocompatible, and compostable polymers are preferred materials ^[8,9], adding electroconductive characteristics makes these technologies available for use in wearables. For wearables applications, fibers have been shown to be totally malleable and stretchable ^[10-12]; these are preferred characteristics for intelligent textiles. Electrospinning has been the leading technique in the fabrication of nanofibers in the research field, generating fibers in the submicron scale able to conduct electricity and proven to be of use in diodes, field effect transistors, and sensors. Polymers and their composites can bring a durable, bendable, and light weight technology to be even closer to our lifestyles. Their ability to rely on super circuits that can fit not only in the palm of your hand but that can also be embedded, woven, or tethered into the clothes, either as a

textile or as a single fiber, make these fibers indispensable. These electronic/intelligent textiles will be able to sense, communicate, and generate their own energy; sooner rather than later as a single nanofiber.

Electrospun nanofibers can be formed from pure polymer solutions. Fiber of poly (ethylene oxides) (PEO), poly (vinylidene fluoride) (PVDF), and poly (lactic acid) (PLA) have been fabricated and used for different applications including scaffolds, cell proliferation substrates, and filters. Long chain polymers (organic and inorganic) have the ability, however, not only to form fibers but also to mechanically support materials that may have low molecular weights or are not polymers. This advantage lets us create composite nanofibers with unique characteristics down to the nanoscale. These other materials can be and are not limited to polymers like the p-type semiconductor poly(3-hexylthiophene) (P3HT) and the n-type ladder polymer Poly(benzimidazobenzophenanthroline) (BBL).

When blended with polymers such as poly (vinylidene fluoride-co-trifluoro ethylene) [P(VDF-TrFE)], the formation of thinner fibers in comparison with the pure PVDF-TrFE electrospun is promoted. This addition not only makes the nanofibers thinner but also includes as an electronically active material forming a nanofiber that conducts electrical charges within the structure. In some cases, pairing polymers and composites can lead to a chemical change in the solution and therefore, in the morphology. For the case of the composite fibers of PVDF-TrFE/P3HT, UV-VIS spectra were performed and showed that P3HT was uniformly incorporated as a blend in the solution that is not chemically affected by the ferroelectric polymer. The presence of P3HT enabled the formation of fibers at low PVDF-TrFE concentrations in tetrahydrofuran (THF) with reduced beads due to the extra charge present in the solution. This increases the capability of transferring charges from the tip of the needle to the drop of the solution, promoting

the formation of the Taylor cone by forming a jet towards the collector. Indeed, the general ability to fabricate PVDF-TrFE/P3HT fibers enhances the prospects of making quasi-1D ferroelectric based devices ^[13].

Poly(3,4-ethylenedioxythiophene) polystyrene sulfonic acid (PEDOT-PSSA) and PVDF-TrFE composite nanofibers were successfully prepared and used as a Schottky diode. For the process of this composite, the addition of PEDOT-PSSA increases the charge in solution and assists in fiber formation, making it possible to electrospin uniform nanofibers of PVDF-TrFE at low polymer concentrations in DMF and without the beading effect in PVDF-TrFE solutions with high polymer concentrations. These nanofiber composites of PEDOT-PSSA/PVDF-TrFE are promising candidates for use in a variety of applications requiring the ferroelectric and/or conducting properties of the composite fibers. The large aspect ratio and even larger surface-to-volume ratio of the fibers make them ideal candidates in the fabrication of miniaturized, low power consumption devices and super-sensitive sensors as well ^[14].

Other conductive polymers have also been used for fiber fabrication as active materials. Nanofibers of low concentrations (1 wt% in CHCl_3) of PLA and poly(aniline- camphor sulfonic acid) (PANi-CSA) were successfully prepared via electrospinning. Since PLA and PANi-CSA were soluble in a common solvent, UV-VIS analysis shows the polymers were uniformly incorporated into the blend with no phase separation or chemical reaction between the two polymers. For the 3 wt% solution, the fibers had a diameter in the range of 10–300 nm and were conducting. Using an n-doped silicon wafer (Si/SiO_2) as a substrate, a diode was fabricated with these electrospun fibers. This device presented a low turn-on voltage a fairly high rectification ratio with an ideality parameter of 1.6, and a barrier height of 0.49 eV. These fibers structured as diodes were used in half wave rectifier circuit and were able to rectify low frequency ac signals as

seen in Figure 2.1. As demonstrated with this circuit, composites show the ability to make polymers that usually are insulators, into carriers of conducting and semiconducting polymers. This ultimately makes them electroactive, extending the range of applications of biocompatible and biodegradable polyester to include fabrication of electronic devices ^[15].

Composite's fibers have the ability to perform different tasks depending on the fiber arrangement and circuitry; an example can be seen with PLA/PANi-CSA fiber in Figure 2.2. A single composite fiber was able to detect various aliphatic alcohol vapors of varying sizes. While pure 3 wt% PLA/ CHCl₃ solutions did not yield any fibers, the addition of PANi-CSA increased the solution charge density did lead to fiber formation at such low PLA concentrations. This fiber was able to relate the alcohols expressing longer time response for the larger molecules and reusable after every characterization. Furthermore, the ability to selectively deposit isolated nanofibers via electrospinning on a variety of substrates. These abilities make this technique very attractive for the fabrication of low cost and low power consumption rapid response sensors ^[16].

PLA/P3HT composite nanofibers were successfully prepared for the first time via electrospinning with low PLA concentration. UV-VIS analysis shows the polymers were uniformly incorporated into the blend with no phase separation or chemical reactions between them. Pure PLA fibers could not be formed via electrospinning at 5 wt% in CHCl₃; however, the presence of P3HT in the solution made it possible to form composite fibers that were electrically conducting. Increasing the amount of P3HT in the solution increased the formation of well-formed fibers. The fibers had diameters in the range of 100 nm - 4 μm and were electroactive. Using a n-doped Si/SiO₂ substrate with pre-patterned Au electrodes, four p-n diodes were fabricated and successfully tested using these electrospun fibers. These diodes were also able to sense UV radiation and remain operable with an increase in the on/off ratio and a lowering of the turn- on voltage, as illustrated

in Figure 2.3. The ability to make insulating PLA into electroactive nanofibers extends the range of applications of this biocompatible and biodegradable polyester to include electronic devices like diodes and sensors with reduced toxicity [17].

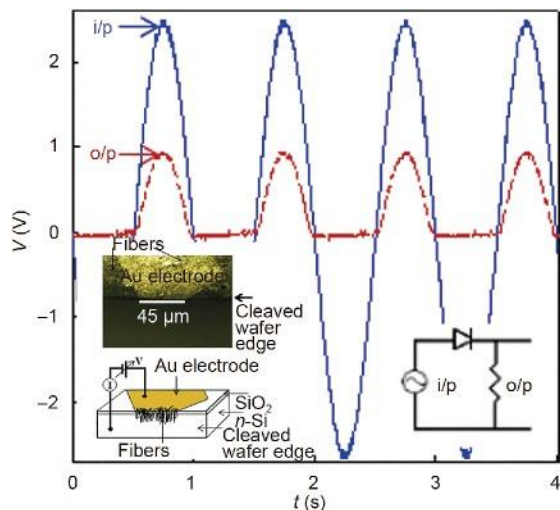


Figure 2.1 Fibers of PLA/PANi-CSA showing the rectification of an input (i/p) voltage of 100 Hz with 5 V peak-peak sine wave. The output (o/p) voltage shows the clipped negative cycle as part of the rectification. Inset: (left) representation of the PLA/PANi-CSA nanofibers device for the diode characterization; (right) electric circuit in series for the dual trace oscilloscope (i/p), the diode and the resistor (o/p) [15].

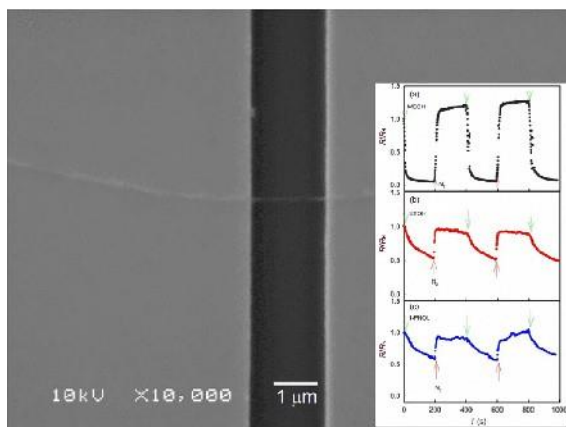


Figure 2.2 Single nanofiber of PLA/PANi-CSA for aliphatic alcohol vapor sensing. Inset: sensing plots for methanol (top), ethanol (middle) and iso-propanol (bottom) [16].

Another P3HT composite fiber, used as a fluorescent phase with PEO and cadmium sulfide (CdS) nanoparticles (with diameters lower than 10 nm) was prepared and studied for optoelectronic applications. These fibers, with diameters above 1 μm , promoted a good dispersion of CdS material for 3.8 wt% and less in the volume of the fiber; however, a direct dependence on the porosity of the fiber was observed with the increment of the amount of CdS, leading to an increased roughness and porous surface. As expected, higher amounts of CdS, on the 6.3 wt% range, formed clusters inside the fibers but promoted a higher fluorescence intensity ^[18]. We envision these fibers, with self-standing containing CdS, to be used in sensors or optoelectronic devices.

Composites of P3HT with gold nanoparticles were prepared to create nonvolatile memory devices. This fiber-based device was able to store and erase charges in the Au nanoparticles by simple charges in gate voltages. With operational voltages around ± 5 V, a threshold voltage shift of 3.5–10.6 V, charge retention up to 104 s and a stress endurance of at least 100 cycles, strongly show that this material and structure can be used on textiles ^[19].

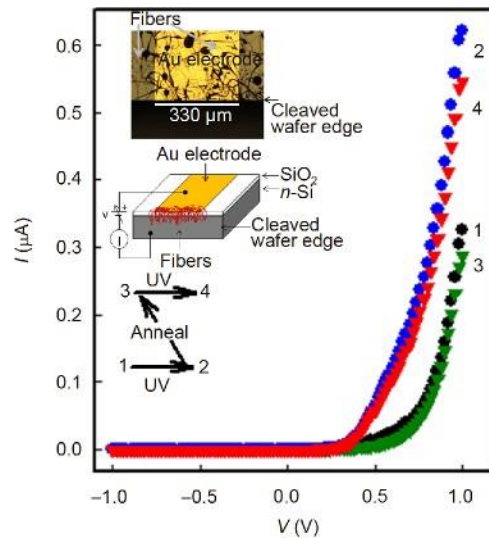


Figure 2.3 P3HT based UV tunable diode. Inset: device structure for characterization (top). Characterization sequence of UV radiation and annealing process (bottom) ^[17].

2.1.1 Fiber Based Field Effect Transistors

Great opportunities for embedding composite electronics on textiles and bendable surfaces are increasing in the scientific community. A highly stretchable field effect transistor using organic semiconducting (OSC) nanowires (NW's) has been reported using a fused thiophene diketopyrrolopyrrole (FT4- DDP) and PEO polymer blend with a 7:3 (w:w) ratio, as shown in Figure 2.4. This fiber-based transistor has been fabricated in a straight and serpentine structure, demonstrating small changes in the electrical transport. While straight fibers presented a minor reduction on the electrical transport properties after tensile strain and release due NW's deformation, a serpentine structure was able to retain the conductive pathway and electrical transport properties after 100% tensile strain and release. The device structure was also characterized in the surface of a balloon, which is a mechanically dynamic surface with a volume expansion reaching 1700%; this suggests the structure can be easily transferred into any stretching surface and envisioned for more specific applications in the medicine field ^[20].

In another experiment, ultra-long zinc oxide (ZnO) nanofibers with diameters down to ~70 nm and a length of several hundred micrometers were able to show an intrinsic n- type semiconductor behavior in a single fiber field effect transistor model. The nanofiber transistors should be useful in building low-cost logic and switching circuits, as well as highly sensitive chemical and biological sensors with reduced device dimensions ^[21].

Specific research on embedding p-channel enhancement- mode electrolyte-gated OTFT transistors on textile micro- fibers and digital devices has been successfully performed using P3HT and imidazolium ionic liquids with a dip-coating technique, as illustrated in Figure 2.5. This transistor, in the micrometers range, works with voltages below 1V but also delivers large current densities. This may improve the creation of embedded complementary digital logics ^[22].

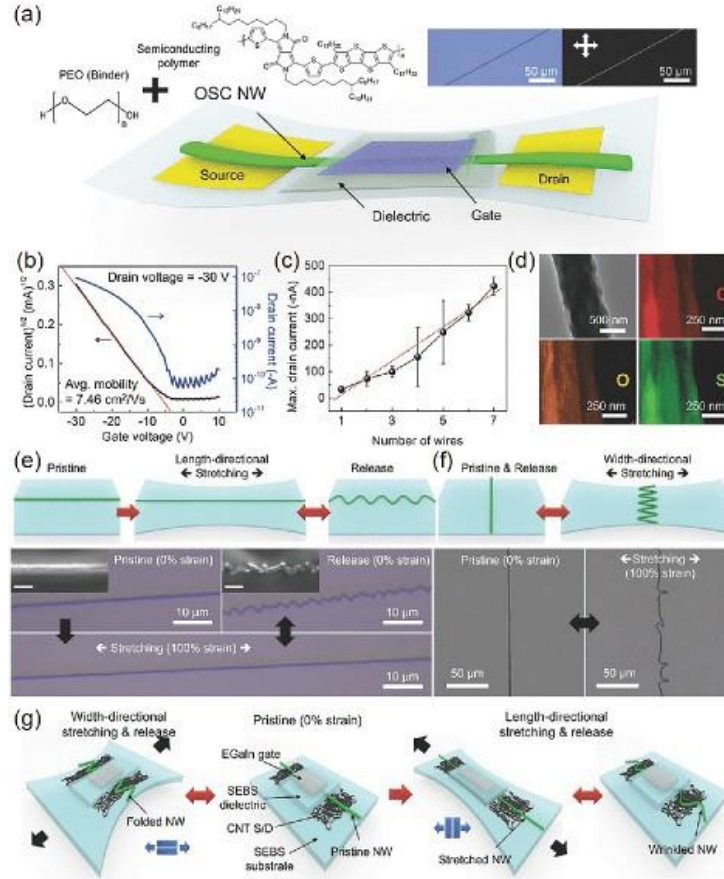


Figure 2.4 Sketch of organic semiconducting nanowires (a); transfer curves of the designed devices (b); max drain current as function of the nanowires (c); transmission electron microscopy and its elemental mapping by energy-dispersive X-ray spectroscopy (d); length-directional stretching (e); width-directional stretching (f); illustration of the deformable FET with straight nanowires and dielectric with length and width directional stretching (g) [20].

Other materials include poly (2-methoxy-5(2'-ethyl) hexoxy-phenylenevinylene) (MEH-PPV), poly (9,9'-dihexyl fluorenyl-2,7-diyl) (PFO), and P3HT. These materials have been processed as blends to perform phase-separated nanofibers fabrication. The blends of MEH-PPV/PHT and MEH-PPV/PFO were able to produce fibers in the scale of 100–500 nm containing tunable optical and charge transport properties. As for the difference between the blends, nanofibers of MEH-PPV/P3HT contained phase separated domains of 30–50 nm and showed efficient energy transfer and enhanced red emission from P3HT.

While compared with nanofibers of MEH-PPV/PFO, which presented a phase, separation in a continuous or core-shell structures, there was no significant energy transfer that showed a broad white light emission contributed from both components. No woven mats of MEH-PPV/P3HT blend showed a p-channel transistor behavior with hole mobility of $(0.05-1)\times 10^{-4} \text{ cm}^2/(\text{V s})$ and an effective field effect mobility of $(0.05-1)\times 10^{-3} \text{ cm}^2/(\text{V s})$, which is 1 order of magnitude higher and only 10% of the FET channel area, were covered by the fibers [23]. However, for our purposes, field effect transistors have been fabricated producing devices with single P3HT nanofibers using single and coaxial spinnerets have also been presented [24,25].

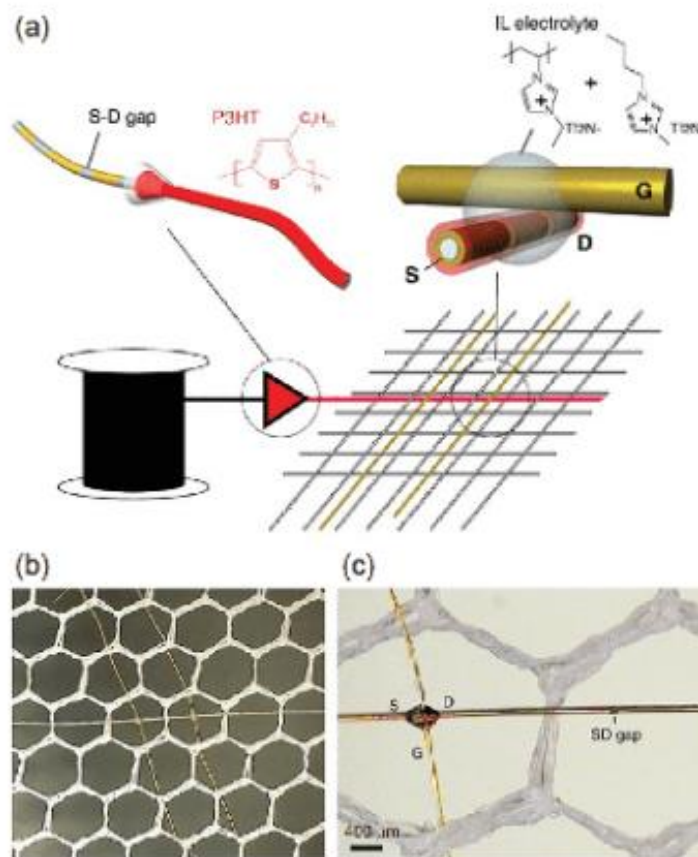


Figure 2.5 (a) Schematic of P3HT coating on the fibers, with pre-patterned source-drain gaps (top-left) and weaving transistors with different fibers (bottom); (b) optical image of two transistors in a woven matrix; (c) optical image with a close-up of a fiber transistor showing the source, gate and drain as well as a visible pre-patterned transistor gap [22].

2.1.2 Fiber Based Light Emitters

Another structure we can find in literature is the ribbon-like nanofibers, in the case for light emitting applications. This typically smooth structure has been made with materials as the electro-luminescent polymer poly(9,9-dioctylfluorene-alt-benzothiadiazole) (F8BT), with PEO to help in the fiber formation and then partially removed, increasing the amount of the electroactive material, performing as organic light emitting diodes (OLED's). These nanofibers have shown to provide a brightness of 2300 cd/m² at 6 V [26].

Alternative light-emitting electrospun nanofibers (LEN) with the diameters of 250–750nm were successfully prepared through the poly (fluorene) derivative (PFO) and poly- (methyl methacrylate) (PMMA) blends using a single-capillary spinneret. The transmission electron microscopy (TEM) results showed that non-continuous fiber-like structure was obtained at the low PFO/PMMA blend ratio but became core-shell structure at a high PFO blend ratio. It also was found that porous surface structure on the PFO/PMMA blend higher luminescence efficiency. This uniform electrospun fiber emitted a full color range, produced from PFO/PMMA, PFQ/PMMA, PFBT/PMMA, and PFTP/PMMA composites. It exhibited the luminescence colors of blue, green, yellow, and red, respectively, as can be seen in Figure 2.6 [27].

Other light-emitting fibers were prepared from ruthenium (II) tris (bipyridine) ([Ru(bpy)₃]²⁺(PF₆⁻)) and PEO mixtures with dimensions in the 150 nm to 5 μm range. Fibers down to 500 nm were readily detectable with a CCD camera with voltages as low as 3.2 V and visible to the naked eye at 4 V, approaching the band gap limit for the organic semi-conductor. These fibers, envisioned for micro and nano-fluidic devices for on chip illumination, could be functional not only for lab-on-a-chip systems but also for the integration in wearable light-based communication [28].

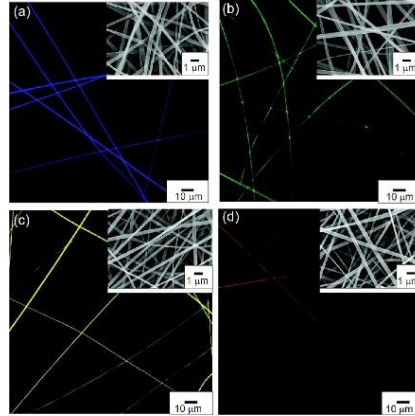


Figure 2.6 Laser confocal microscopy images of 5 wt% poly (fluorene) derivative/PMMA blend electrospun nanofibers with (a) PFO, (b) PFQ, (c) PFBT, (d) PFTP [27].

A coaxial nanofiber structure made of ionic transition-metal complex has also been studied. The structure containing the Galistan liquid metal core and surrounded by a polymer composite with ionic transition-metal complex (iTMC) based organic electroluminescent material drawn from a mixture of ruthenium (II) tris(bipyridine) ($[\text{Ru}(\text{bpy})_3]^{2+}-(\text{PF}^-)$) and PEO were electrospun. This light emitting fiber has a turn-on voltage of 4.2 V, visible with a CCD camera, and can be seen by naked eyes at 5.6 V in N_2 . This light-weight can be used for optoelectronic textiles, bioimaging, chemical and biological sensing, high-resolution microscopy, and flexible panel displays, particularly as iTMCs with emission at different wavelengths [29].

Flexible white-light-emitting fibrous membranes have been also studied by isolating donor and acceptor dyes in the fibers using a coaxial electrospinning method. By controlling the concentration ratio of those dyes, a broad band of emission in the visible spectrum was achieved. In addition, the light emission of the membrane is completely uniform, and all microscopically sized individual fibers emit white light. Moreover, PLA was used as a porous and mechanical support decreasing the blocking effect between the polymer matrix and dye molecules. These fibers mesh with great uniformity, portability, tailor ability, and durability are envisioned for display lighting (Figure 2.7) [30].

2.1.3 Fiber Based Capacitors

The ability to produce nanofibers in a simple and reliable way has also impacted the research of the fabrication of capacitors. Electrospun of electrochemical capacitors using CNFs and cobalt oxide (Co_3O_4) hollow nanoparticles have been studied showing the ability to fabricate binder-free electrodes. The nanoparticles were directly applied as integrated electrodes. This arrangement of materials has shown to deliver a specific capacitance (SC) of 556 and 403 F g^{-1} at a current density of 1 and 12 A g^{-1} , respectively. This flexible and tunable capacitor has shown almost no decay in SC after continuous charge/discharge cycling for 2000 cycles at 4 A g^{-1} . With these characteristics and the ability to incorporate electroactive metal oxides, high-performance electrochemical capacitors and Li-ion batteries can be benefited and improved (Figure 2.8) ^[31].

Electrodes of manganese oxide (MnO_2) based coaxial carbon nanofibers cables have been performed achieving a SC of 311 F g^{-1} for the total area of the electrode and 900 F g^{-1} for the MnO_2 surface. The carbon nanofibers are produced from an iron acetylacetonate (AAI) precursor. This coaxial structure showed high energy densities of 80.2 W h kg^{-1} and high-power densities of 57.7 kW kg^{-1} . It was also shown that the iron compound facilitated the charge transfer between the metal oxide and the carbon nanofibers at higher concentrations of MnO_2 , decreasing the internal resistance of the electrode. These characteristics comply for energy storage devices based on nanofibers ^[32]. Nickel-embedded carbon nanofibers were also tested and have an enhanced specific capacitance of 164 F g^{-1} when compared with the carbon nanofibers without the presence of Ni (50 F g^{-1}) ^[33]. In a comparable work, poly(acrylonitrile) composites containing zinc chloride were successfully prepared and carbonized leading to a specific capacitance as high as 140 F g^{-1} ^[34].

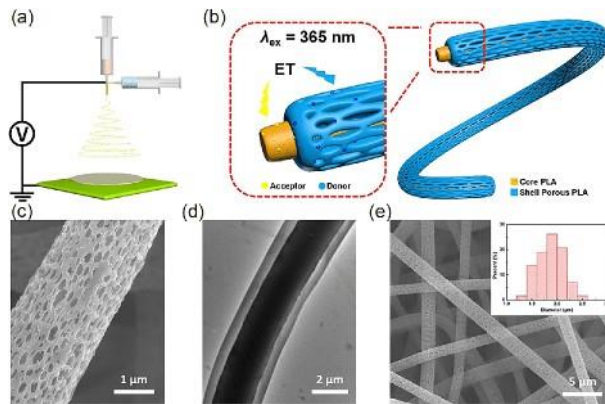


Figure 2.7 (a) Schematic of coaxial electrospinning; (b) schematic of white light emitting porous fiber; (c) SEM image of PLA fiber; (d) TEM image of PLA fiber; (e) diameter distribution of PLA fibers ^[30].

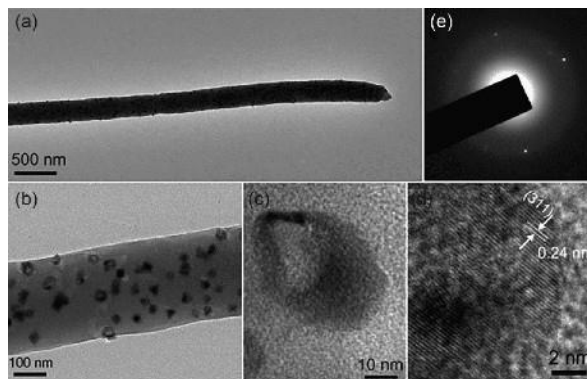


Figure 2.8 (a), (b) TEM images of a single nanofiber from the $\text{Co}_3\text{O}_4\text{-CNFs}_2$ sample; (c), (d) HRTEM images of a single Co_3O_4 hollow NP, and (e) the corresponding SAED pattern ^[31].

2.1.4 Fiber Based Nanogenerators

PVDF has been widely used as a support material for fiber fabrication containing piezoelectric characteristics. While randomly oriented PVDF membranes have been used for power generation^[35], multilayer structures of PVDF nanofibers mats with PEDOT coatings have been used to design organic piezoelectric nanogenerator (OPNG) with high performances such as V_{oc} of 48 V under the normal stress of 8.3 kPa. Vapor phase polymerization (VPP) successfully ensures the coating of PVDF nanofibers. Ultra-sensitivity toward human movements such as walking and foot strikes and highly durable output performance and lasting over 6 months,

broadens its applicability. The collective results suggest the utility of designing OPNG as a weight measurement sensor as well as its applications in the field of self-powered, wearable, and portable electronics [36].

Core-shell nanofiber mats of poly(dimethylsiloxane) (PDMS) ion gel and poly (vinylidene fluoride-co-hexa- fluoropropylene) (PVDF-HFP) for tactile pressure sensor detecting static and dynamic pressure have been fabricated. A capacitive sensor of this mat has been demonstrated to offer higher sensitivity of 0.43 kPa^{-1} in the low-pressure regime ranges up to 1.5 kPa, performing as a wearable heart- rate monitor. When a high dynamic mechanical pressure is applied to this mesh, it can be used in a triboelectric sensor and self-powered energy generating device able to turn on hundreds of LED's. The core-shell PDMS ion gel/PVDF-HFP nanofiber mat, based triboelectric dynamic pressure sensor, exhibits high sensitivity of 0.102 and 0.068 V kPa^{-1} at higher pressure from 40 to 100 kPa and 100 to 700 kPa, respectively [37].

Sensors and generators have been studied with highly porous carbon nanofibers/poly(etherimide) (CNF/PEI) aerogel, paired with electrospun PVDF nanofiber mats, demonstrating an excellent performance as an energy harvesting device and a self-powered sensor. In this case, an amidization process was used to modify the CNF with PEI, leading to a CNF/PEI aerogel with enhanced mechanical properties and tribopositivity, ultimately leading to an enhanced triboelectric output of the TENG. Indeed, as exposed, this TENG demonstrated high sensitivity as a self-powered sensor. It was not only able to detect general human motion, but it also exhibited high sensitivity in detecting lightweight forces such as water droplets and the vibration of the substrate where the device was attached. It is capable of detecting forces within 0.2 mN and pressure within 1 Pa, an open-circuit voltage of 106.2 V and a short-circuit current of $9.2 \mu\text{A}$ was demonstrated with a TENG (2 cm^2 contact area) under a small force ($\sim 6 \text{ N}$) [38]. Some

other nanofiber-based pressure sensors had also used oxides like ZnO and SiO₂ when assembled, to be flexible. These showed good performance for flexible electronic devices comprising smart clothing, low-cost artificial skin, adsorption, and photoelectric devices. These flexible hybrid stress sensors were prepared in a two-step technique where the first step comprises the electrospinning, followed by high temperature annealing technique. This pressure sensor presented sensitivities up to 3.35 and 20.12 when the pressure varied from 1.63 to 32.6 kPa [39].

On the other hand, stretchable nanogenerators of PVDF- HFP/Co-ZnO nanofibers, as shown in Figure 2.9, were performed by electro-spinning method. In this approach, the incorporation of Co-doped ZnO nanofillers enhances the nucleation and stabilization of the piezoelectric polar beta- phase. It was hypothesized that the electrospinning method and Co-doped ZnO nanoparticles has a strong effect on structural and morphological properties of the nanocomposites, which reveals a significant effect on piezoelectric properties giving output voltages as high as 2.8 V, observed for 2 wt% Co-ZnO/ PVDF-HFP nanofibers. An increasing output voltage was observed due the co-doped ZnO nanofiller on the electroactive beta-phase of PVDF-HFP, in addition to the influence of modified ZnO. This enhanced piezoelectric efficiency suggests the use of these nanofibers for electronics and bio- medical fields [40].

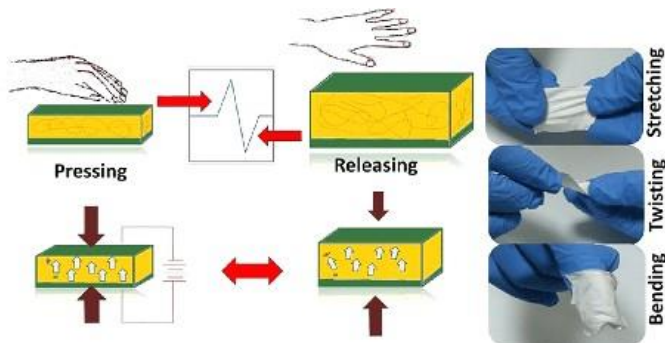


Figure 2.9 Working mechanism under pressing releasing mechanical force and textile like mesh^[40].

In another experiment, PVDF have demonstrated a strain sensor with a good response to the bending and joint angle measurement. For this application, a smart glove made of the stretchable strain sensors assembled in each finger was fabricated and finger motions were detected in real-time. Also, the strain sensors were able to detect posture position and to directly control a robotic hand, leading to possible applications in flexible, stretchable, and wearable electronics due to their excellent performance ^[41].

Highly stretchable transparent triboelectric tactile sensor based on the single-electrode triboelectric nanogenerator for the tactile mapping has been demonstrated. Large-scale patterned Ag NFs electrodes as the key part of the device were fabricated by using a three-step process of electrospinning, photolithography technique, and wet etching. This device made of multioriented Ag NFs, showed the stretchability of the electrodes can be extremely enhanced for the extra conductive paths, with only 10% increase in resistance at 100% strain. Therefore, it is theorized that it could promote tactile sensing platforms for touchpads, robotics, and wear- able electronics applications ^[42].

Furthermore, soft, flexible, and lightweight soles of PVDF fibers with rough surfaces have shown to increase the friction areas and enhance the output voltage and current increasing the performance, when the voltage direction of the piezoelectricity match the direction of the triboelectricity. This all-fiber wearable could light up 214 LED's in series by stepping force ^[43].

2.1.5 Conclusions

Composite fibers and nanofibers have been shown to be effective as an active material for electronic devices. Devices as diodes, transistors, sensors, capacitors, and generators have been discussed in this section. The ability to electrospun these materials into fibers are leading us to the fabrication of actual electroactive threads that can be tethered, embedded, or woven in textiles for

communication, energy, and sensing. As it was presented, these fiber composites are being used as the active material in the devices; however, the envisioned idea is in the fabrication of single fibers self-containing the electronic and electrical properties of the diodes, FETs, and sensors with the ability of generating their own required energy.

2.2 Electrospinning for Sensing Devices

2.2.1 Sensor Response of Electrospun Poly(lactic Acid)/Polyaniline Nanofibers to Aliphatic Alcohol Vapors of Varying Sizes.

2.2.1.1 Introduction

Poly (lactic acid) (PLA) is a biodegradable and biocompatible thermoplastic polyester, with lactic acid being a typical harmless byproduct of decomposition. PLA is mechanically robust and environmentally stable and has therefore attracted interest as biomedical implants ^[44]. Commercial PLA is readily soluble in organic solvents and can be cast into thin films, fibers, foams, or other forms. Of the different forms mentioned, a fiber typically has a larger surface area to volume ratio compared to films and is thus technologically advantageous for sensor applications -if it can be made electrically conducting. Electrospinning is a common method of making PLA fibers. In the past, the PLA solutions required for the formation of fibers were typically very viscous (>8wt%) ^[45]. By using a conducting polymer in a blend with PLA, this high PLA concentration can be reduced, and the fibers obtained became conducting in the process. We have used the electrospinning technique to fabricate nanofibers of PLA, blended with the conducting polymer polyaniline doped with camphor-sulfonic acid (PANi-CSA) at 3wt% of PLA in CHCl₃. Fabrication of nanofibers of PLA at such low concentrations has not been reported before. By controlling the evaporation of the solvent in the blend solution prior to electrospinning, extremely fine and electrically conducting fibers were produced. Sensors were fabricated using *single*

nanofibers of the 3wt% PLA blended with PANi-CSA. They were used to detect aliphatic alcohol vapors of varying sizes. Our results show the response times get longer for larger alcohol molecules, but the recovery time is much faster. The sensitivity was also reduced for the larger alcohol molecules. The ability to engineer insulating PLA into nanofibers that are electroactive extends the range of applications of this biocompatible and biodegradable polyester to now include gas sensors capable of detecting toxic alcohol vapors at potentially low concentrations and in other electronic devices like diodes.

2.2.1.2 Experimental

PLA (MW 60,000) was purchased from Sigma-Aldrich and used as received. The PLA was then dissolved in CHCl_3 to form a 3wt% solution. In a separate synthesis, polyaniline was prepared using standard techniques and doped with camphor sulfonic acid (PANi-CSA) and also dissolved in CHCl_3 [46]. The following technique was used for preparing the solution to obtain PLA nanofibers at lower concentrations than previously studied: 0.45 g of the PLA solution (as prepared above) was mixed with 0.50 g of the PANi-CSA solution (as prepared above) in a vial. With the vial uncapped and then placed on a balance, 0.5 g of the blend solution was evaporated. This resulted in a large fraction of the solution containing PANi-CSA. Since the two polymers were dissolved in a common solvent after evaporation of 0.5 g, the solution was still homogenous with no polymer precipitation. Electrospinning was then used for preparing polymer nanofibers of this blend solution at room temperature under ambient conditions. The basic apparatus used is shown in Figure 2.10 and consists of a hypodermic syringe ($\frac{1}{2}$ cc tuberculin syringe), a high voltage power supply (Gamma Research), a grounded cathode (Al foil) and a syringe pump (Cole Parmer). Approximately 0.4 ml of the solution prepared as indicated above was placed in the hypodermic syringe and connected to the power supply, with the cathode grounded and situated about 20 cm

from the tip of the needle as shown in Figure 2.10. The flow rate was ~ 0.5 mL/hr. As the voltage applied to the needle is increased to about 8-10 kV, the electric force on the polymer droplet at the end of the needle overcomes the surface tension and a jet is issued forth in the form of a very fine spiral. As the solvent evaporates, fibers of the polymer deposit themselves on the cathode. Individual fibers were also captured by passing a pre-patterned Si/SiO₂ wafer with gold electrodes perpendicular to the path of the jet in a downward sweeping action. The fibers that land on the substrate adhere to it and some make firm contact with the gold leads as seen in Figure 2.11 below. The sensors used in this work are made of such individual nanofibers. All fiber samples were dried in air at 80 °C before surface and electrical characterization.

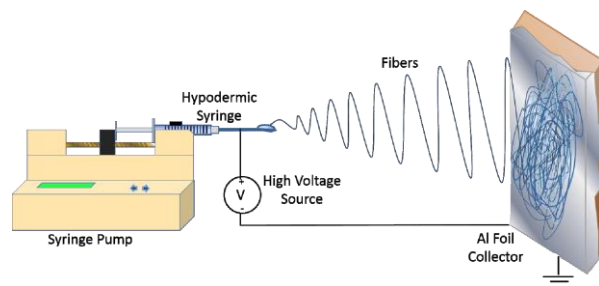


Figure 2.10 Basic electrospinning apparatus

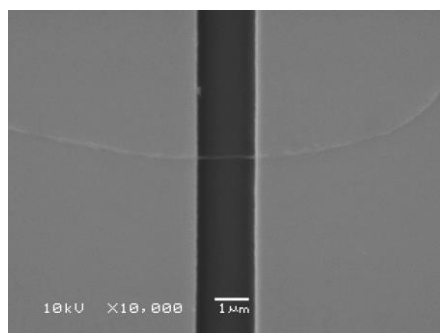


Figure 2.11 SEM image of a single PLA/PANi-CSA nanofiber lying across two gold electrodes.

The ratio of PLA to PANi-CSA was calculated to be 1.57 in the electrospun fibers. After capturing the fibers on pre-patterned substrates, external electrical contacts were made to the fibers

using gold wire and silver paint. In all of the measurements, the current in the sensor was monitored as a function of time at a fixed applied voltage, while a constant flow of dry N₂ gas (control) was passed over it in a homebuilt gas chamber. Once the current stabilized, the control gas was then bubbled at the same rate (350±5 ml/min) into the alcohol at room temperature and allowed to flow into the gas chamber. After the sample resistance stabilized in the presence of the alcohol vapor, the gas flow was then switched between N₂ and alcohol vapor in time intervals of 200 s for three complete cycles after which the experiment was terminated. The currents and voltages were supplied and measured using a Keithley Model 6517A electrometer.

2.2.1.3 Results and Discussion

Since the two polymers used in this experiment were soluble in a common solvent (i.e. CHCl₃), it is important they did not interact with each other chemically. One way to verify this was to measure the UV/VIS spectra of the blends in solution prior to electrospinning and compare it to solutions of pure PANi-CSA and pure PLA. Figure 2.12 shows the UV/VIS spectra of the 3wt% PLA/PANi-CSA blend solution prior to electrospinning. The UV/VIS spectra of pure PANi-CSA and pure PLA in CHCl₃ are also measured and included for comparison in Figure 2.12. The spectrum for PLA is constant in the frequency range studied since this solution was transparent in the visible light range. From Figure 2.12 we see that in the blend, the spectra of the composite PLA/PANi-CSA solution is similar to that of pure PANi-CSA and include a broad absorption valley in the range 450-650 nm that is usually assigned to the π - π^* transition and a relatively sharp absorption peak at about 800 nm, which is typically due to the localized polaron band in doped PANi^[47]. The absorption amplitude is reduced in the blend since the PANi-CSA fraction is now reduced as compared to the PANi-CSA solution. This result implies PANi-CSA is uniformly incorporated as a blend in the solution and does not phase separate or chemically react with PLA.

Visual inspection of the blend solution in a vial after several days did not show any polymer segregation or precipitation, suggesting the blend was stable with no chemical degradation.

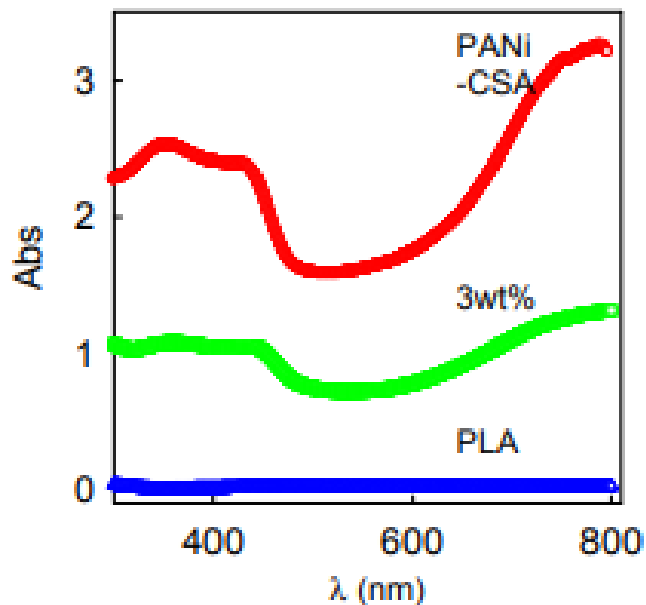


Figure 2.12 UV/VIS absorption spectra of the PLA/PANi-CSA polymers in CHCl_3 .

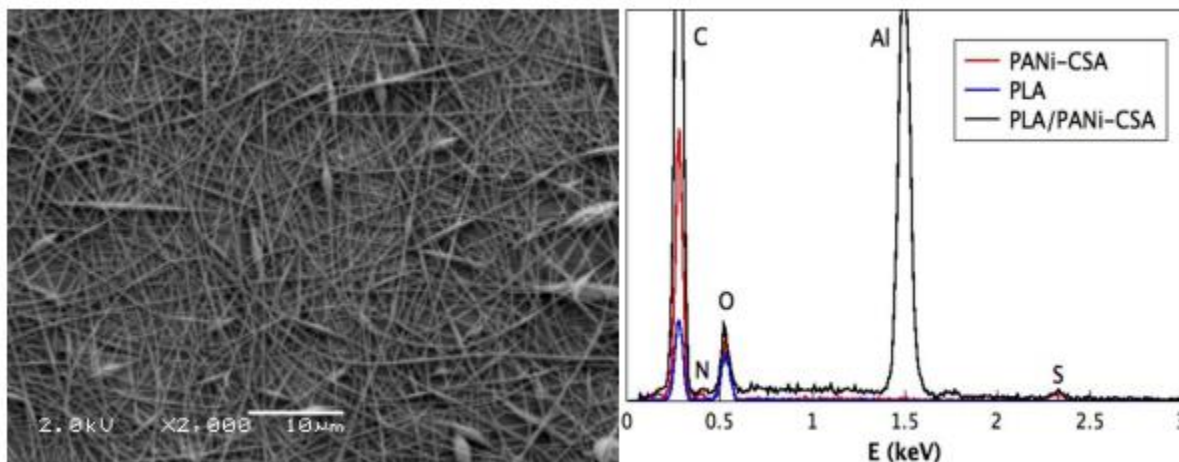


Figure 2.13 SEM images of electrospun 3wt% PLA/PANi-CSA nanofibers and the corresponding EDS spectrum. The EDS spectra of pure PANi-CSA and PLA are also included for comparison.

Figure 2.13 shows an SEM image of the electrospun PLA/PANi-CSA nanofibers. These fibers had diameters in the range 10-300 nm. Without PANi-CSA, no PLA fibers could be formed at this concentration since the solution is not viscous enough; thus, PANi-CSA in the right proportion actively assists in the formation of nanofibers by increasing the solution charge density and also in the elimination of the beading effect commonly seen in electrospun fibers. PANi-CSA also makes the fibers conducting. The fibers formed were long (several cm) and could easily be captured on substrates for device fabrication and subsequent electrical characterization as seen in Figure 2.10. Figure 2.13 also shows the EDS spectrum of the fibers together with the EDS spectra of pure PLA and pure PANi- CSA. Here, the fibers contain the same peaks seen in the individual polymers; thus, they retain the properties of both polymers with no chemical change and are consistent with the results of Figure 2.12. The large peak is from the Al foil used to collect the fibers.

Figures 2.14 (a), (b) and (c) show the time dependence of the change in the normalized resistance for individual isolated electrospun 3wt% PLA/PANI-CSA nanofibers as seen in Figure 2 upon exposure to methanol, ethanol, and 1-propanol vapors respectively, where R_{N_2} is the resistance of the fiber under a flow of dry N_2 gas. In all three figures, in the presence of the sensing alcohol gas, the sensor resistance decreases while the carrier gas increases the resistance. Two other features are also notable. The change in the sensor resistance (sensitivity) gets smaller and the response time gets longer as the size of the alcohol molecule gets larger. These observations are discussed in detail in the next paragraph.

The response of the electrospun nanofiber gas sensors can be explained as follows: The initial flow of N_2 gas for several minutes before exposure to the sensing gas leaves the fiber relatively free of absorbed moisture. The polymer chains are in their relaxed positions and the flow

of current is governed by the usual mechanism of variable range hopping typical in conducting polymers. The moment the sensing gas is introduced into the chamber, the current in the fiber increases due to reduced fiber resistance. The decrease in the resistance upon exposure to alcohol is believed to be caused by an interaction via hydrogen bonding of the alcohol with the nitrogen atoms of polyaniline, leading to an extended coil formation that facilitates charge transport ^[48,49]. Once equilibrium with the sensing vapor is established, subsequent flow of N₂ gas will displace the sensing gas and bring the polymer chains to their original conformation. This process is seen to be reproducible in subsequent cycles of the sensing and the carrier gas. As the size of the alcohol molecule increases from methanol to ethanol to propanol, it takes a longer time for the polymer chains to respond to the sensing gas; the recovery time, however, is relatively rapid. Larger alcohols are seen to have a slower response due to their reduced polarity and the inability to easily penetrate the fiber. The change in the resistance is also smaller for larger alcohol molecules. The response and recovery times of the nanofibers are defined as the time taken for the current in the fiber to reach 90% of the saturated current. In the case of ethanol and 1-propanol, there is no current saturation observed (in the 200 s window) when the sensing gas is introduced. We have extrapolated the data to simulate the saturation regime outside the 200 s time interval used in our experiment. Table 2.1 gives the response and the recovery times of the nanofibers for the different alcohol vapors used in this study and the sensitivity.

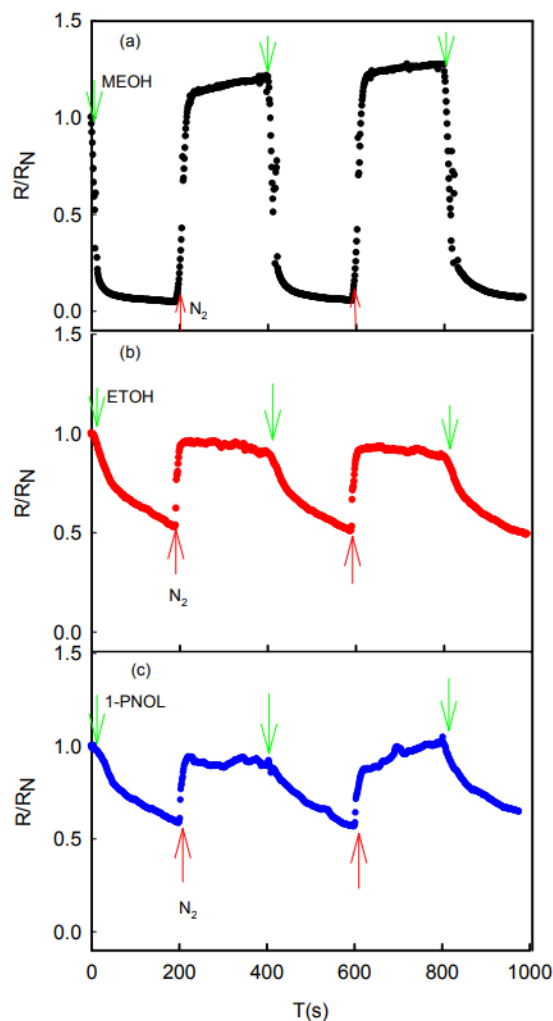


Figure 2.14 Normalized resistance of individual electrospun HCSA-doped polyaniline nanofibers to various alcohols: (a) methanol, (b) ethanol and (c) 1- propanol. The arrows indicate the time when the carrier gas (N₂) or the sensing gas was introduced into the chamber. The period of one cycle was 400 s.

Table 2.1 Sensor response and recovery times to the presence and absence of alcohol vapors and the percentage fractional change in sensor resistance.

Alcohol	Size (Å)	T_{response} (s)	T_{recovery} (s)	ΔR/R_{N2} (%)
Methanol	3.5	46	26	120
Ethanol	4.5	460	20	43
1-Propanol	5.5	550	5	34

2.2.1.4 Conclusions

Sensors fabricated from isolated electrospun 3wt% PLA/PANi-CSA nanofibers were tested in the presence of various aliphatic alcohol vapors of varying sizes. Pure 3wt% PLA/CHCl₃ solutions did not yield any fibers. PANi-CSA was important for obtaining fibers at such low PLA concentrations by increasing the solution charge density. The response times were longer for the larger molecules. This is due to their reduced polarity and the inability to easily penetrate the fiber, which also explains the faster recovery times for the larger alcohol molecules. For methanol vapor, the sensor response was the fastest. The rapid response time suggests that electronic changes also influence the sensing mechanism. The fiber sensors could be tested on various alcohols without damage and hence, were reusable. Conducting PLA based nanofibers therefore, present yet another means of fabricating gas sensors that are biocompatible. Furthermore, the ability to selectively deposit isolated nanofibers via electrospinning on a variety of substrates makes this technique attractive in the fabrication of low cost and low power consumption rapid response sensors.

2.3 Applications of Poly(3-Hexylthiophene) (P3HT)

2.3.1 Fabrication of P3HT Based Fibers: Electrospun Fibers of Poly(Vinylidene Fluoride-Trifluoroethylene)/Poly(3-Hexylthiophene) Blends from Tetrahydrofuran.

2.3.1.1 Introduction

Poly(vinylidene fluoride-trifluoroethylene) (PVDF-TrFE)) is an electrically insulating ferroelectric (FE) copolymer at room temperature for TrFE content in the range 20–50% [50–54]. The permanent dipole moments that point in a direction perpendicular to the main chain polymer backbone renders this polymer ferroelectric, and the ability to control the polarization allows its use in nonvolatile organic memory devices [55–58]. Capacitors using this material as the dielectric form the basic storage element in such FE based devices and have been fabricated using low-cost

spin coating techniques, typically leading to two dimensional (2-D) devices. Recently, field effect transistors (FET's) have been fabricated that use PVDF-TrFE as the gate dielectric, where the polarization via a gate voltage can affect charge transport across a semiconducting channel in intimate contact with the dielectric^[59-61]. Preparing nanofibers of PVDF-TrFE is difficult due to the high concentrations of the polymer needed in solution to make them^[62]. Using the electrospinning technique, we were able to fabricate true PVDF-TrFE nanofibers by incorporating a small fraction of conducting polymers (CP)^[63, 64]. The main advantage of nanofibers is the potential to fabricate quasi 1-D devices that make use of the ferroelectric or the electrical conducting properties or both, and simultaneously have a large surface to volume ratio that can be used in the fabrication of low power consumption devices and supersensitive sensors. In this chapter, it is reported for the first time the fabrication of PVDF-TrFE fibers blended with the semiconducting polymer poly(3-hexylthiophene)-P3HT in tetrahydrofuran (THF). Blending with P3HT assists in fiber formation at lower PVDF-TrFE concentrations than currently possible, with the fiber diameter monotonically increasing with increasing PVDF-TrFE concentration. P3HT is also seen to suppress the formation of beads due to the presence of charge in the solution. Most importantly, the ability to make PVDF-TrFE/P3HT fibers allows for the fabrication of quasi-1D non-volatile memory devices recently reported in the thin film form^[65].

2.3.1.2 Experimental

99% pure PVDF-TrFE (75/25) was purchased from Kureha, Japan (KF W#2200) and used as received. The polymer molecular weight was 350,000 and was soluble in tetrahydrofuran (THF) via ultra-sonication at 60°C for an hour. The following concentrations of PVDF-TrFE in THF were prepared: 15 wt%, 13 wt%, 11 wt%, 9 wt%, 7 wt%, 5 wt%, 3 wt%, and 1 wt%. Regio-regular

poly(3-hexylthiophene) - P3HT was purchased from Sigma-Aldrich and used as received. A 2 wt% of this polymer in THF was also prepared via ultra-sonication at 60°C for a few minutes.

The two solutions prepared above were mixed in the following fixed mass ratio prior to the fabrication of fibers for each of the samples studied: 0.85 g of the PVDF-TrFE and 0.11 g of the P3HT based solutions above were mixed slowly in a 10 ml glass vial until the resulting solution was uniform and homogenous. The solutions were then electrospun to obtain fibers of the polymer blends.

Electrospinning is a simple technique for preparing polymer nanofibers at room temperature under ambient conditions. The basic elements of the apparatus used is shown in Figure 2.15 and consists of a hypodermic syringe (1 cc tuberculin syringe), a high voltage power supply (Gamma Research), a grounded cathode (Al foil) and a syringe pump (Cole Parmer). About 0.5 ml of the solution prepared as indicated above was placed in the hypodermic syringe and connected to the power supply, with the cathode grounded and situated about 20 cm from the tip of the needle. The flow rate was controlled so that a drop fell out from the needle every 20 seconds. As the voltage applied to the needle is increased to about 8–10 kV, the electric force on the polymer droplet at the end of the needle overcomes the surface tension and a jet is issued forth in the form of a very fine spiral. As the solvent evaporates, fibers of the polymer deposit themselves on the cathode. Individual fibers were also captured by passing a pre-patterned Si/SiO₂ wafer with gold electrodes perpendicular to the path of the jet in a downward sweeping action. The fibers that land on the substrate adhere to it; some make contact with the gold leads. The fiber samples were dried in air at 80°C before characterization.

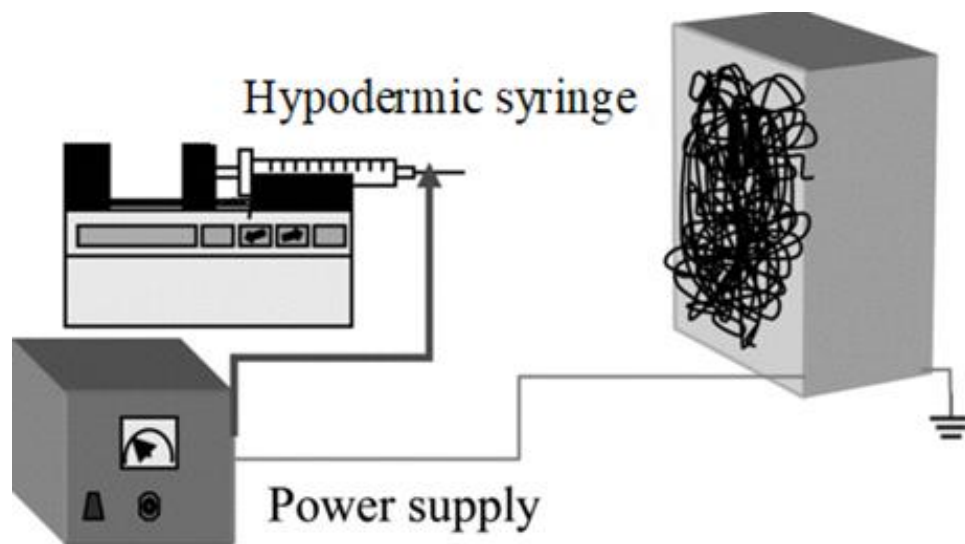


Figure 2.15 Schematic of the basic electrospinning apparatus. The syringe pump was programmed to result in a flow of one drop per 20s to exit the needle.

A JEOL JSM-6360 scanning electron microscope (SEM) was used to observe the fiber morphology. The fiber diameters were determined using an AFM on individual fibers captured on polished Si/SiO₂ substrates. UV/VIS spectra were obtained from polymer solutions before electrospinning using a Perkin-Elmer Lambda 35 spectrometer.

2.3.1.3 Results and Discussion

Figure 2.16 shows the solution UV/VIS spectra of various PVDF-TrFE concentrations with P3HT. The spectra of pure P3HT and pure PVDF-TrFE in THF are also shown for comparison. The P3HT spectrum presents a broad absorption peak at around 440nm resulting from the π - π^* transition of the electronic absorption spectra. A small peak is also seen at around 600nm and implies a long average conjugation length of the polymer chain ^[66]. The spectra for PVDF-TrFE is featureless in the UV/VIS range and consistent with previous results ^[63]. When compared to the spectrum of pure P3HT, regardless of the PVDF-TrFE concentrations in solution, all the UV/VIS absorption spectra exhibit the same general shape. These results imply that P3HT is uniformly incorporated as a blend in the solution and is not chemically affected by the ferroelectric polymer.

Further observations show that once prepared and stored in glass vials, the solutions stayed homogeneous for several weeks with no indication of phase separation of the PVDF-TrFE/THF and P3HT/THF. These results strengthen the claim that the P3HT is well dispersed in the PVDF-TrFE/THF solution.

Figures 2.17(a)-(f) shows the SEM images of electrospun solutions of PVDF-TrFE/P3HT blends in THF at various concentrations of PVDF-TrFE (1, 3 and 5 wt% respectively). As seen in Figures 2.17(a)-(b), at 1wt% without and with P3HT, there were no fibers formed as the solution was not viscous enough and there was a very small amount of the polymer in solution to cause chain entanglement as the solvent evaporated during the electrospinning process. The SEM images show the resulting residue after solvent evaporation. Without P3HT, as one increases the PVDF-TrFE concentration, while the solution gets progressively more viscous, one notices a few scattered fibers emerging as protrusions from the polymer beads.

These results are reasonable, since at such low concentrations, the polymer jet breaks up during electrospinning due to reduced extensional viscosity^[67]. Similar results were seen for other PVDF-TrFE blends electrospun from DMF^[63, 64]. Typically, what was observed at such low concentrations (<5wt%) was a spraying effect that covered the grounded Al foil in the electrospinning apparatus with THF droplets inter dispersed with polymer beads. The addition of P3HT leads to the gradual appearance of fibers as seen in Figures. 2.17(d), (f). Figures 2.18(a)-(f) shows the SEM images of electrospun fibers of PVDF-TrFE/P3HT blends at higher concentrations of PVDF-TrFE (7, 9 and 11wt% respectively). We noticed a clear difference in the formation of fibers when compared to Figures 2.17 (a, c, e) in the absence of P3HT. The addition of PVDF-TrFE in THF increases the viscosity of the solution and fibers are easily formed, although one

notices the formation of beads along the fiber lengths; their shapes appear to change from spherical to oval as the PVDF-TrFE concentration is increased.

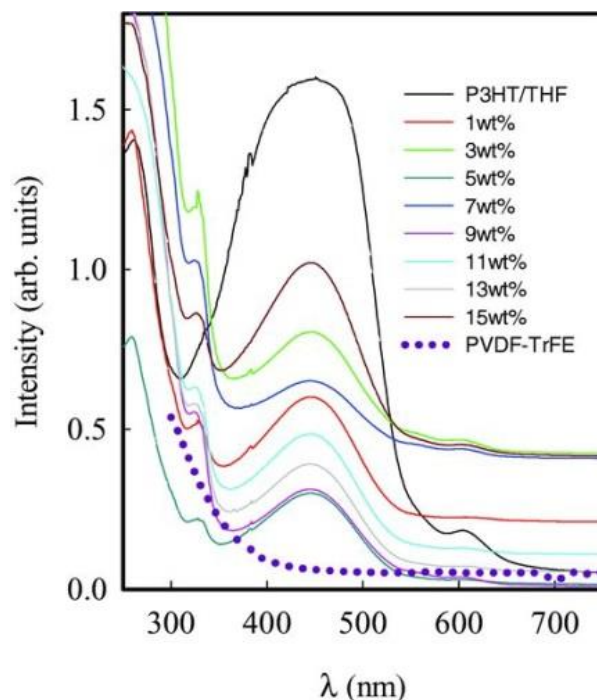


Figure 2.16 UV/VIS spectra of the blend solutions prepared from various PVDF-TrFE concentrations with P3HT in THF. Also included is the spectrum for pure P3HT and PVDF-TrFE. Individual traces have been shifted to avoid overlap.

With the addition of P3HT, there is an increase in the quantity of fibers formed with fewer beads. Figures 2.19(a)-(d) shows the SEM images of electrospun fibers of PVDF-TrFE/P3HT blends at still higher concentrations of PVDF-TrFE (13 and 15 wt% respectively). Here, we notice an abundance of fibers without any beads; they are thicker and the presence of P3HT has very little effect on the fiber morphology. From the left-hand side images in Figures 2.17 and 2.18, we see that while pure PVDF-TrFE fibers are formed at polymer concentrations >7 wt%, the fibers are few and are indiscriminately interrupted by the presence of polymer beads. In order to suppress beading, a small amount of the semiconducting polymer P3HT was added to increase the net charge density in the electrospinning solutions. Such an addition has been known to reduce the surface tension of the solution leading to more uniform fibers without the beading effect [63, 68].

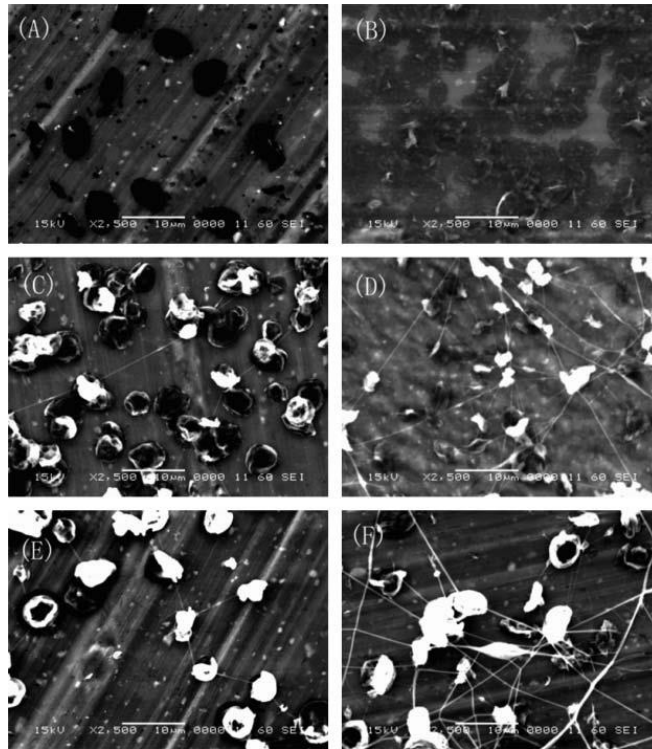


Figure 2.17 SEM images of electrospun fibers of (a) 1 wt% PVDF-TrFE; (b) 1 wt% PVDF-TrFE/P3HT; (c) 3 wt% PVDF-TrFE; (d) 3 wt% PVDF-TrFE/P3HT; (e) 5 wt% PVDF-TrFE; (f) 5 wt% PVDF-TrFE/P3HT. All images have the same magnification and the scale bar in each represents 10 μm .

The right-hand side SEM images in Figures. 2.18 and 2.19 show the result of increasing charge density very clearly when compared to the corresponding left hand side image without P3HT. As the PVDF-TrFE concentrations increase, the presence of small quantities of P3HT allows for the formation of uniform fibers with decreasing beading effects due to the increase in the net charge density carried by the jet^[68]. The fibers are also longer in length and more abundant. Several of these fibers bridged the gap between the needle and the cathode and had to be physically removed in order to allow for a continuous collection of fibers. Electrospinning is therefore a convenient method of fabricating relatively long PVDF-TrFE/P3HT fibers under ambient laboratory conditions.

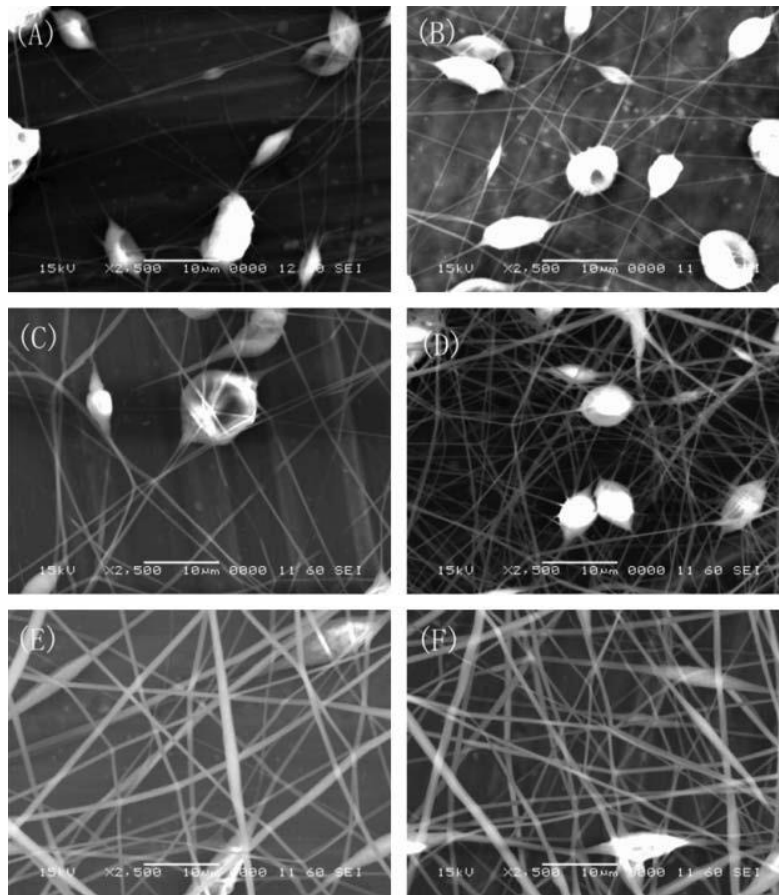


Figure 2.18 SEM images of electrospun fibers of (a) 7 wt% PVDF-TrFE; (b) 7 wt% PVDF-TrFE/P3HT; (c) 9 wt% PVDF-TrFE; (d) 9 wt% PVDF-TrFE/P3HT; (e) 11 wt% PVDF-TrFE; (f) 11 wt% PVDF-TrFE/P3HT. All images have the same magnification and the scale bar in each represents 10 μm .

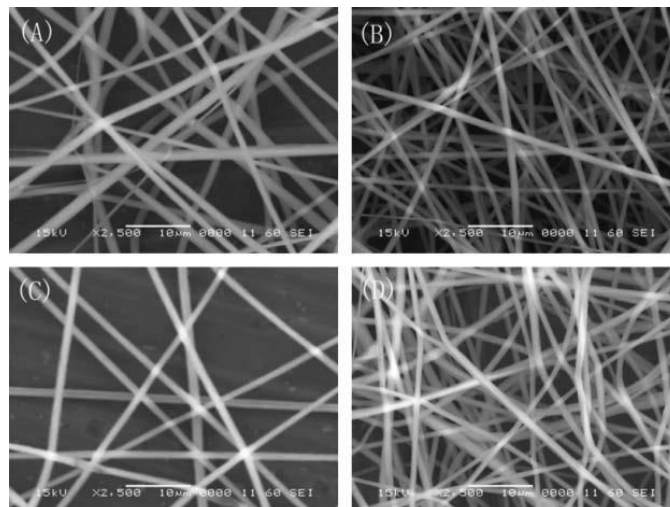


Figure 2.19 SEM images of electrospun fibers of (a) 13 wt% PVDF-TrFE; (b) 13 wt% PVDF-TrFE/P3HT; (c) 15 wt% PVDF-TrFE; (d) 15 wt% PVDF-TrFE/P3HT. All images have the same magnification and the scale bar in each represents 10 μm .

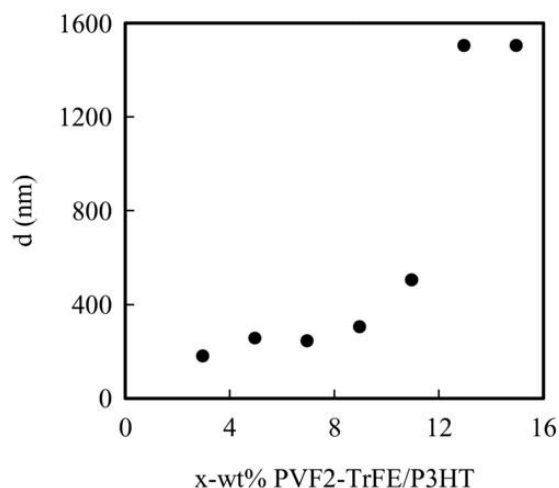


Figure 2.20 Plot of the electrospun fiber diameters (d) taken using an atomic force microscope as a function of wt% of PVDF-TrFE/ P3HT.

Unlike PVDF-TrFE composites with PEDOT-PSSA or PANi-PSSA, PVDF-TrFE and P3HT form blends because they are both soluble in a common solvent and have a larger diameter for similar concentrations. We believe this may be due to the type of solvent used where the polymer prefers a tight coil rather than an expanded coil configuration ^[69]. Typical fiber diameters ranged from a few hundreds of nm for the low PVDF-TrFE concentrations to a few microns for the higher PVDF-TrFE concentrations, as shown in Figure 2.20. The fiber diameters increase linearly as the PVDF-TrFE wt% increases from 3 wt% to 9 wt%, due to the increase in solution viscosity (for a fixed electrospinning voltage), with the smallest diameter measuring 175nm for the 3 wt% sample. Above 9 wt% there is a noticeable increase in the fiber diameters that could be related to the relative reduction in charge density due to the increased amount of PVDF-TrFE in the more viscous solutions. These results are consistent with qualitative observations of the right-hand side images of Figures 2.17, 2.18 and 2.19 where a gradual increase in fiber diameter is observed as the PVDF-TrFE content is increased.

2.3.1.4 Conclusions

Blended fibers of PVDF-TrFE/P3HT have been prepared for the first time via electrospinning for various PVDF-TrFE concentrations in THF. The fiber lengths and diameters increased with increasing PVDF-TrFE concentrations due to increasing solution viscosity. UV/VIS spectra show that P3HT is uniformly incorporated as a blend in the solution and is not chemically affected by the ferroelectric polymer. The presence of P3HT enabled the formation of fibers at low PVDF-TrFE concentrations in THF with reduced beads due to the extra charge present in the solution. The ability to fabricate PVDF-TrFE/P3HT fibers enhances to the prospects of making quasi-1D ferroelectric based devices.

2.3.2 Poly(lactic Acid)/poly(3-hexylthiophene) Composite Nanofiber Fabrication for Electronic Applications

2.3.2.1 Introduction

Poly(lactic acid) (PLA) is compostable and biodegradable thermoplastic plant-derived polyester frequently used in biomedical applications^[70,71]. The intrinsic electrically insulating behavior and malleability make it perfect for use in biomedical implants (muscle tissue engineering), food packaging, passive electrical applications and three-dimensional printing. Different forms, beginning at the nanoscale, can be cast in high surface area/volume ratio structures like fibers, smooth surface structures like thin films, energy absorption structures like foams, and other forms. Recently, a cheap, fast, and reliable electrospinning technique has been used to create PLA fibers.^[72-76] Poly (3-hexylthiophene) (P3HT) is a conjugated p-doped semiconducting polymer widely used in organic electronics especially as a field effect transistor. Electrospinning fibers of pure P3HT^[77] is not easy due to its low molecular weight; however, since both P3HT and PLA are soluble in chloroform (CHCl₃), we have successfully used the electrospinning technique

to fabricate thin fibers of the composite material. The goal is to extend the usage of PLA by making it electroactive^[78] with the integration of the region-regular p-doped P3HT and hence permitting the construction of electronic devices at the lowest PLA concentration where the emergence of fibers begins. Blending these two polymers to fabricate composite nanofibers at low polymer (PLA) concentrations in a common solvent has not been reported before.

In this section, the fabrication of PLA/P3HT composite fibers via electrospinning and the fabrication of a functional elemental electronic device are reported for the first time. PLA used in this work provides mechanical support to the conducting fibers. While fibers of pure PLA cannot be formed at low concentrations due to low solution viscosity, by adding the right amount of P3HT we were able to produce long composite fibers, with the fiber quantity increasing with increasing P3HT concentration. These composite fibers had diameters in the range from 0.1 to 4 μm . As a practical application, a p–n junction diode was fabricated and tested using these composite fibers, thereby extending the use of PLA to include electronic applications. The diode could also be reversibly tuned with UV radiation making it multifunctional as a UV radiation detector, a rectifier of AC signals and possible use as a photovoltaic.

2.3.2.2 Experimental

PLA and regioregular P3HT were acquired from Sigma Aldrich and used as received. PLA, an electrically insulating polymer with a molecular weight of 60 000 g mol⁻¹ is a granular white solid, while P3HT is a stranded dark reddish solid p-doped semiconducting polymer. Both of these polymers are soluble in CHCl₃. In this work, PLA was dissolved in CHCl₃ to form a 5 wt% solution that was colorless. Several compositions of this solution with P3HT were formed in order to make composite fibers. The P3HT fractions in the fibers were 0, 17, 28, 37 and 44%. For example, when 5 mg of P3HT was added to 0.5 g of the 5 wt% PLA – CHCl₃ solution and

electrospun, the fraction of P3HT in the electrospun product was 37 wt%. In a similar manner, the other concentrations were prepared by adding the right amount of P3HT to 0.5 g of the 5 wt% PLA–CHCl₃ solution.

Fibers were fabricated via electrospinning using the apparatus shown previously. A tuberculin syringe was filled with the homogeneous composite solution corresponding to a preselected P3HT concentration prepared as described above and situated on a programmable syringe pump to allow a slow flow (ca 2 mL h⁻¹) of the solution through the needle. The syringe needle worked as the anode and aluminum foil as the grounded cathode. By applying a high voltage to the needle tip (ca 9 kV), the electrical force on a drop formed at the tip of the anode overcomes the superficial tension on the drop. This leads the drop to form a polymer jet in the form of a cone and constantly move towards the Al foil. As the solvent evaporates in air, fine fibers were seen to deposit on the cathode. These fibers were collected on the cathode (Al foil) and used for topological characterization and on an n-doped Si/SiO₂ wafer with pre-patterned Au electrodes for electrical characterization. The fiber samples were dried in an oven for 15 min at 70°C prior to characterization. Images of the fibers were obtained using a scanning electron microscope (JEOL JSM-6360 SEM) and UV-visible spectra were obtained from the pure and blend solutions prior to electrospinning using an Ocean Optics Inc. Jaz spectrometer. The diode was characterized using a Keith-ley model 6517A electrometer while UV illumination ($\lambda = 365$ nm, 4 W) was provided with a UVP model UVGL-25 source.

2.3.2.3 Results and Discussion

Since commercial PLA has a low molecular weight, it is difficult to prepare fibers via electrospinning at low concentrations (<7 wt%) in CHCl₃ due to lack of sufficient solution viscosity.^[77] It is, however, possible to fabricate PLA fibers at these concentrations if the right

amount of a conducting polymer (i.e. P3HT) is dissolved into the solution. Such a method could also make the PLA fiber composite electroactive. PLA and P3HT were dissolved in CHCl_3 and optically characterized to ensure that they do not suffer any phase separation nor chemically interact with one another after electrospinning. UV-VIS spectra of the dissolved polymer composite solutions were measured prior to electrospinning and compared to the spectra of pure P3HT and pure PLA solutions. The spectrum of pure PLA solution does not show any absorption peaks in the range observed. Figure 2.21 shows the UV-VIS spectra of the PLA/P3HT blend solutions prior to electrospinning for different P3HT concentrations in CHCl_3 . The UV-VIS spectra for pure P3HT and pure PLA were also measured; they are plotted for comparison in Figure 2.21. The spectra of PLA/P3HT composite solutions for various P3HT fractions show a wide absorption peak at about 440 nm due the $\pi - \pi^*$ transition.^[79] The similarity of these results with that of pure P3HT shows the polymers are homogeneously integrated as a mixture in the solution, and that phase separation or a chemical reaction with each other does not occur. The blend solution does not show any separation or precipitation even after 30 days, implying that the two polymers are well distributed and constant, without experiencing polymeric structure degradation.

Figure 2.22 shows SEM images of the electrospun solutions of 5 wt% PLA– CHCl_3 with various concentrations of P3HT. All these solutions were thoroughly mixed with a magnetic stirrer until homogeneous blends were achieved based on UV-VIS spectra as described above. PLA at 5 wt% with CHCl_3 does not have the critical amount of PLA needed to form fibers via electrospinning as seen in Figure 2.22(a). Working at that critical concentration, due to the low quantity of PLA, the electrospun jet is transformed into a mist in flight due to reduced solution extensional viscosity.^[80] Because of this, the polymer chains cannot stay entangled in the air, preventing the development of fibers as the CHCl_3 evaporates. SEM images reveal tiny beads form

over the cathode created by the spraying effect of the electrospun mist due to the high amount of solvent in the jet, in comparison to the polymer as is shown in Figure 2.22(a). As is known in the electrospinning method, the development of fibers directly depends on the net charge density and reduced surface tension in the jet^[81]. In this work, the solution charge density is increased by adding the p-type semiconducting polymer P3HT. Figures 2.22(b)–(e) show SEM images of electro-spun PLA/P3HT solutions where the P3HT fractions in the fibers are 17, 28, 37 and 44 wt%, respectively. Figure 2.22(b) shows the 17 wt% P3HT fractions where a small amount of fiber formation is seen to be developing from some of the polymer beads. These fibers are weak and inappropriate for device fabrication. Figure 2.22(c) shows fibers of the 28 wt% P3HT fraction showing an increase in the quantity of fibers and a decrease in the size of beads. Figure 2.22(d) shows fibers of the 37 wt% sample where the quantity of beads is much less and well-defined fibers can be seen, while Figure 2.22(e) depicts the fibers of the 44 wt% sample showing the initial steps of agglomeration. These images show that an increase of P3HT in the blend contributes to an active decrease of bead formation and an enhancement of the quantity of formed fibers with a diameter reduction. The addition of P3HT covers multiple aspects in this process. Primarily, it increases the solution charge density; secondly, it assists the structural formation of nanofibers from dilute PLA polymer solutions; finally, it preserves the conducting properties in the composite nanofibers, thereby extending the functionality of the nanofibers. The fibers developed are several millimeters long, making them easy to capture on Si/SiO₂ substrates for device fabrication. Bead formation can be reduced until elimination by an increase of the PLA content (7 wt%) in the electrospun solution at the expense of making it difficult for the formed fibers to be electroactive due to lack of percolation pathways formed by P3HT.

Once the composite fibers are conducting (for 37 and 44 wt%), several possibilities exist for their use in electronic devices. As a demonstration of a practical application of the composite fibers that makes use of their conducting properties, a p-n diode was fabricated because it forms an important circuit element in signal processing. Figure 2.23(a) shows a top-view image of the formed diode. A schematic of its construction and external electrical connections is shown in Figure 2.23(b). This device was fabricated using 37 wt% P3HT fraction fibers and an n-doped Si wafer ($\langle 111 \rangle$, 0.1-1.0 Ω cm) with a 200 nm layer of thermally grown SiO_2 .

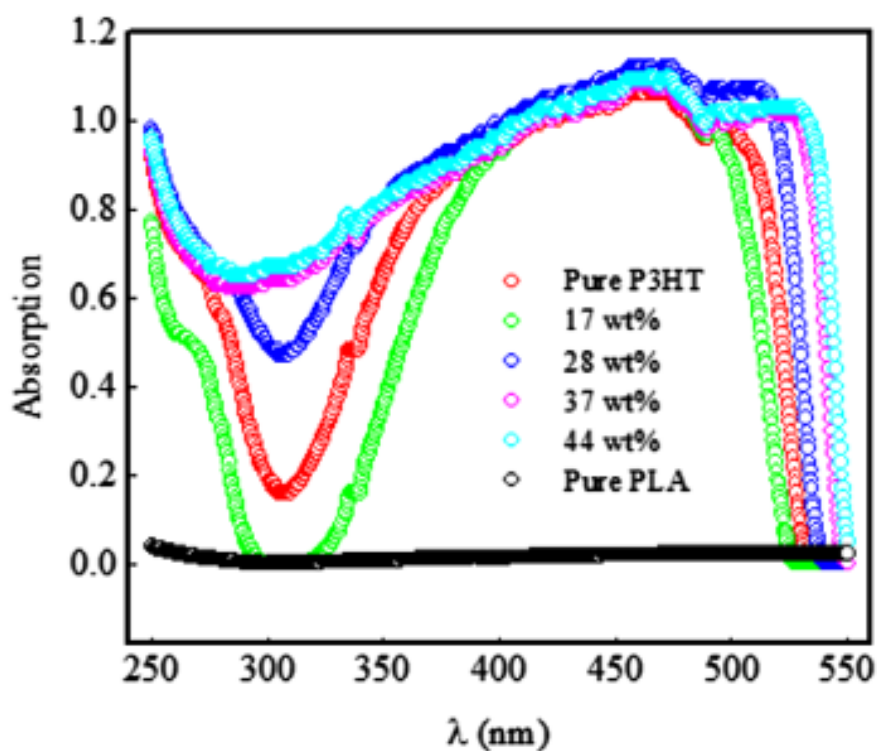


Figure 2.21 UV-VIS absorption spectra of a 5 wt% PLA- CHCl_3 solution with various P3HT concentrations prior to electrospinning; included are the absorption spectra for pure P3HT- CHCl_3 and pure PLA- CHCl_3 .

The Si wafer contains pre-patterned gold electrodes above the oxide that were created via standard lithography and lift-off techniques. Then the substrate was cleaved through the electrodes. In this manner, the gold electrode remains at the edge of the cleaved surface and is separated from the doped Si by an oxide layer that has a thickness of 200 nm. The cleaved edge of the substrate

was then passed up and down between the syringe and Al foil with a weaving movement during the electrospinning process. The nanofibers formed in the air and covered the substrate. Some were long enough to cross over the wafer edge, making a stable contact to the Au electrode above and to the doped Si below the oxide layer as seen in Figure 2.23. The resultant p-n diode was formed along the perpendicular edge of the substrate at the nanofiber/n-doped Si interface. Such diodes were prepared by us in the past using a similar construction technique with different materials.^[82,83]

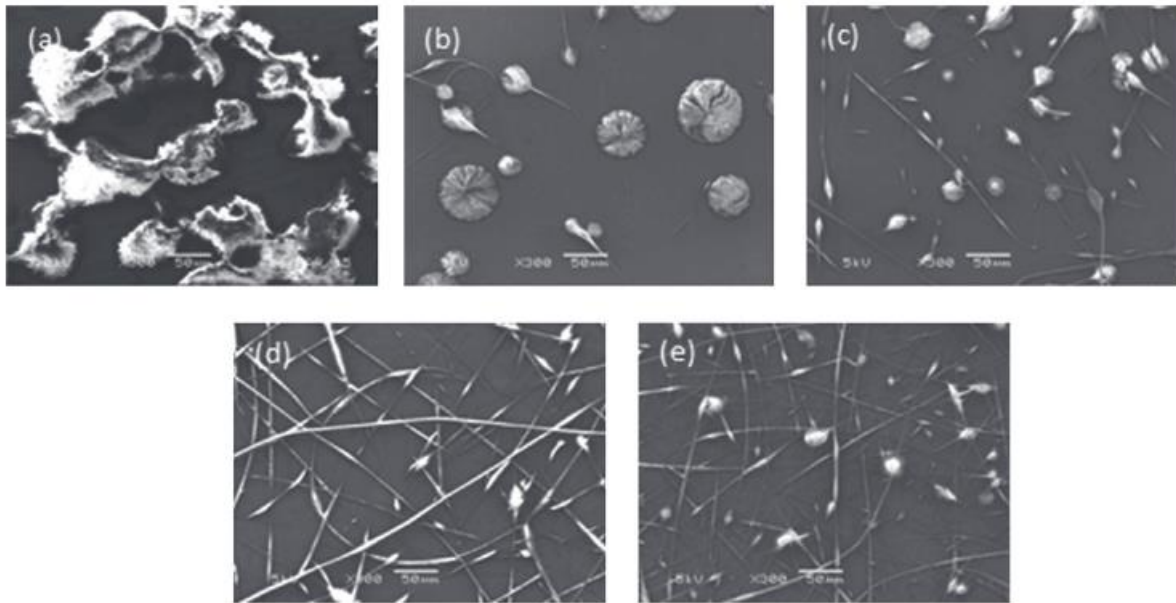


Figure 2.22 SEM images of PLA-CHCl₃ fibers with various PLA/P3HT ratios: (a) 100/0; (b) 83/17; (c) 72/28; (d) 63/37; (e) 56/44. Increasing the P3HT fraction facilitates the formation of fibers. All the images have the same magnification and the scale bars are 50 μm.

Figure 2.24 shows the I-V characteristic curve at 300 K of the diode shown in Figure 2.23 obtained in vacuum (10^{-2} Torr) to reduce the effects of moisture, where the bias positive terminal is connected to the Au electrode and the negative terminal is connected to the n-Si substrate. Since the fibers make Ohmic contacts with the Au electrodes,^[77] the nonlinear response seen in Figure 2.24 arises from the polymer nanofiber/n-doped Si interface. Due to the small difference in diameter, various diodes were fabricated and tested to verify any variation in the behavior. In

general, the characteristic curves for each device remain asymmetric having a turn-on voltage from 0.7 to 0.8 V and a considerably diminished reverse bias current. Indeed, these diodes present rectifying behavior with a forward to reverse current ratio of ca 400 at a bias voltage of ± 1 V. The inset of Figure 2.24 shows the diode I-V curves when the external contact leads are in reverse mode, confirming the formation of a diode and not due to contact resistance with the electrodes but to the interface between the fiber and n-Si.

The band gaps of P3HT and n-Si are generally 2.2 and 1.2 eV, respectively^[84,85]. The essential features of the asymmetric non-linear I-V curves in Figure 2.24 can thus be understood qualitatively based on the energy band diagram for a planar structure in bulk p-n junctions^[86]. Diffusion of charge carriers (polarons in P3HT and electrons in n-Si) across the junction sets up an electric field of opposite polarity that prevents further diffusion and creates a space charge region depleted of all mobile charge across the interface. Band bending through the space charge region helps establish a constant Fermi level in thermal equilibrium resulting in a built-in potential barrier to the flow of electrons from the conduction band of n-Si moving into the lowest unoccupied molecular orbital level of P3HT as shown in Figures 2.25(a) and (b), which correspond to the situation before and after the P3HT fibers make contact with n-Si respectively. When the n-region is biased positive with respect to the p-region it lowers the Fermi energy in the n-region increasing the barrier height, preventing charge diffusion and hence limiting current flow (reverse bias). Applying a positive potential to the p-region with respect to the n-region lowers the Fermi energy in the p-region, decreasing the barrier height in the p-region and allowing for charge diffusion across the junction that constitutes a current (forward bias) that increases exponentially under bias voltage as governed by the Fermi-Dirac occupancy function. Under such conditions, in an ideal diode, the I-V curve can be described by the equation $I = I_s[\exp(eV/nkBT) - 1]$, where I_s is the

reverse bias saturation current, e is the electronic charge, n is the ideality factor, and k_B and T are the Boltzmann factor and temperature, respectively.^[86] The inset to Figure 2.24 shows a semi-logarithmic plot of the diode current versus applied voltage under forward bias conditions. Extrapolating the linear portion of the semi-log plot to zero bias yields a reverse bias saturation current of 60.0 pA and the diode ideality factor is calculated to be $n \approx 2.4$.

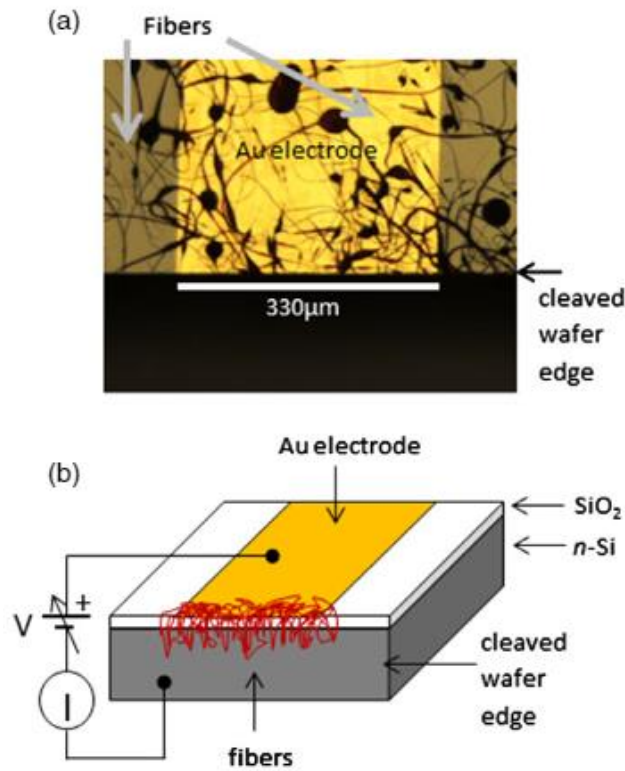


Figure 2.23 (a) Optical microscope image at low magnification of the top surface showing the pre-patterned n-doped Si/SiO₂ substrate. The image shows the side where the Si wafer was cleaved, leaving the electrode that was then covered with electrospun fibers where the fraction of P3HT was 37 wt%. Under high magnification, the fibers are similar in appearance to those seen in Figure 2.22(d). The length of the relevant Au electrode that represents the anode terminal of the diode is 330 μm. Many fibers reach over the wafer edge making contact to the n-doped Si below the oxide layer. (b) Schematic of the optical microscope image of (a) showing the relevant section of the fibers and how they make contact to the Au electrode on the substrate surface and to the doped Si below the surface. The external electrical connections used for characterization are also shown, and the current must flow through the fibers to complete the conduction path. The diode is formed at the junction between the fibers and the n-doped Si.

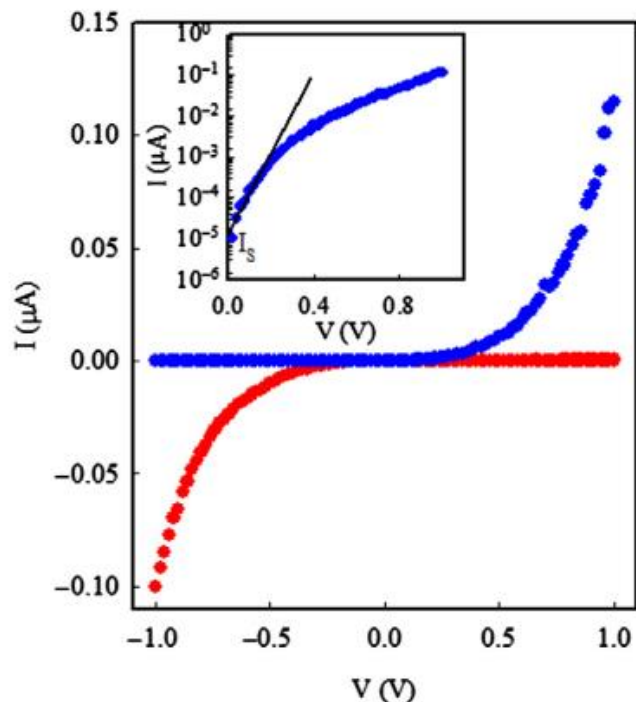


Figure 2.24 Current-voltage (I-V) characteristic curves at 300 K of the diode shown in Figure 2.23(a) in vacuum. The diode conducts current in the first quadrant (blue symbols) of the I-V plot and blocks it in the third quadrant, when the bias positive terminal was connected to the Au electrode and the bias negative connected to the n-doped Si as shown in Figure 2.23(b). When these connections are reversed the diode turns on in the third quadrant (red symbols) confirming the presence of a p–n junction at the fiber/n-Si interface. Inset: semi-log plot of the data taken in the on state of the diode where the intercept is the reverse bias saturation current, and the slope used to calculate the diode ideality parameter.

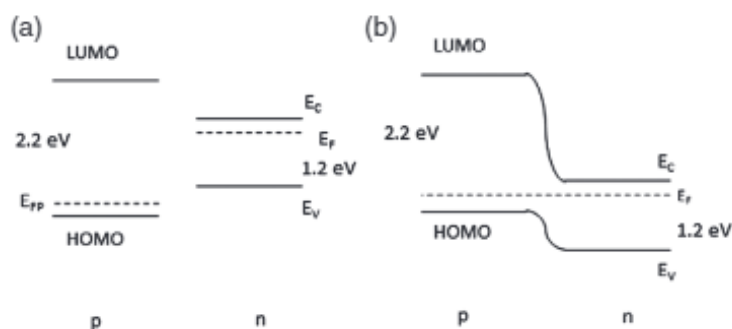


Figure 2.25 Schematic energy band diagrams for the P3HT/n-Si interface (a) before and (b) after contact. E_c and E_v are the conduction and valence band edge energies of n-Si. E_f and E_{fp} are the Fermi levels of Si and P3HT, respectively. The lowest unoccupied molecular orbital (LUMO) and highest occupied molecular orbital (HOMO) levels for P3HT are also indicated. After contact and under thermal equilibrium, the Fermi levels must match, resulting in band bending at the interface of the fibers and n-Si as seen in (b).

A diode whose parameters can be tuned either optically or electrostatically has enhanced versatility by virtue of it being multifunctional. Figure 2.26 shows the I–V characteristic curves of a diode prepared as described earlier when used as a UV sensor. Under UV illumination, the currents increase, and the diode turn-on voltage is lowered from 0.8 to 0.6 V. Analyzing the results under these conditions shows that the ideality parameter decreases from 3.5 to 2.4, and the rectification ratio increases from 1600 to 3100 demonstrating an improvement in the diode performance. We propose that UV radiation generates an electron – hole pair that later dissociates within the P3HT fibers. The hole is attracted to adsorbed electron trapping species (recombination) like H_2O^- and O_2^- (i.e. $\text{h}^+ + \text{O}_2^- \rightarrow \text{O}_2\text{gas}$) on the P3HT fiber liberating it, thereby reducing scattering and donating the electron, which then contributes to the observed current increase. In addition, reducing scattering centers via desorption lowers the series resistance within the fibers and could also contribute to the observed increased currents. The contact resistance of the fiber with the metal electrode is assumed to be relatively small, since the fibers, once stuck to the substrate, cannot be moved without damage. Annealing the device in air at 70°C restores the original condition and the effect is reproducible as seen in Figure 2.26 when the UV lamp is turned on again, making it reusable as a diode and as a UV sensor. Finally, with the presence of holes and electrons on either side of the p–n junction, another possible application envisioned is as a photodiode capable of generating current in the presence of solar energy.

2.3.2.4 Conclusions

PLA/P3HT composite nanofibers were successfully prepared for the first time via electrospinning with low PLA concentration. UV-VIS analysis shows that the polymers were uniformly incorporated into the blend with no phase separation or chemical reactions between them. Pure PLA fibers could not be formed via electrospinning at 5 wt% in CHCl_3 ; however, the

presence of P3HT in the solution made it possible to form composite fibers that were electrically conducting. Increasing the amount of P3HT in the solution increased the formation of well-formed fibers. The fibers had diameters in the range of 100 nm - 4 μm and were electroactive. Using an n-doped Si/SiO₂ substrate with pre-patterned Au electrodes, four p-n diodes were fabricated using these electrospun fibers and successfully tested. These diodes were also able to sense UV radiation and remain operable with an increase in the on/off ratio and a lowering of the turn-on voltage. The ability to make insulating PLA into nanofibers that are electroactive extends the range of applications of this biocompatible and biodegradable polyester to include electronic devices like diodes and sensors with reduced toxicity.

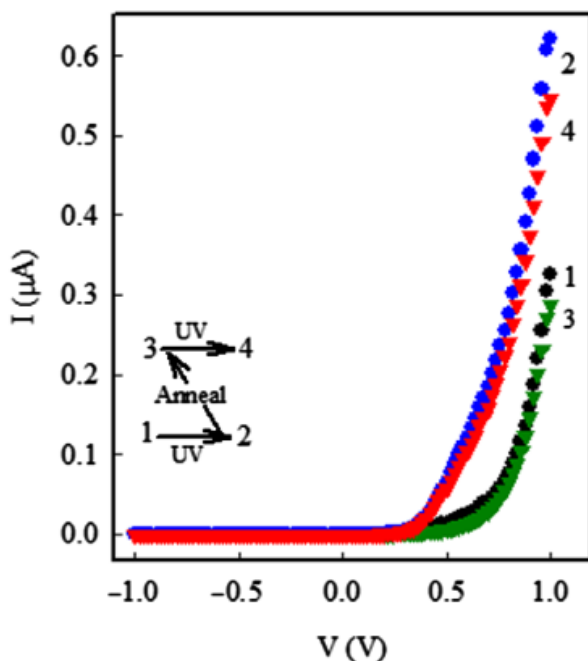


Figure 2.26 Current – voltage (I–V) characteristics at 300 K of the diode in the absence and in the presence of UV light ($\lambda = 365 \text{ nm}$). Inset: process of annealing showing the diode I–V curves of: (1) as-prepared device with UV off; (2) after UV exposure; (3) after turning the UV off, annealing in air at 70°C and placing the device back in vacuum with the UV off; and (4) after UV exposure again. This process demonstrates reversibility and the ability of the fibers to sense UV light.

2.4 General Details of Poly(benzimidazobenzophenanthroline) (BBL)

Poly(benzimidazobenzophenanthroline) is a ladder polymer with interesting n-type semiconducting behavior with coherent π -conjugation and strong π - π stacking interactions. A paper titled “A benzimidazobenzophenanthroline polymer molecular transistor fabricated using club sandwich electrodes” was published in 1987. The objective was to characterize the polymer electronic behavior by using Platinum (Pt) disk (rod) electrodes as source and drain while the BBL was connected with $\sim 100\text{nm}$ of gold as the gate. The gold electrode has been used to adjust the BBL oxidation state (electron sites) by controlling the potential, therefore its conductivity (for solvent wetted film). The procedure for this device consists of a drop casted film over the Pt electrodes, following to dry the polymer at 70°C and a bath in 10% triethylamine + methanol to neutralize the residual acid and re-dried. No annealing process had been discussed until years later. Dried BBL film thicknesses ranged from 30nm to $1\mu\text{m}$ while the distance between electrodes where constant at 200nm . The interelectrode spacing in the gate was at least 30nm (one redox monomer thick) while source (S) and drain (D) was 200nm . Indeed, as the work observes, “the interelectrode spacing is a highly significant property since it controls the device response time in any circumstance where the part of the polymer’s oxidation state is varied.” has been reported Bragg spacings of 0.75 nm and room-temperature electron conductivities as high as $1.1\Omega^{-1}\text{ cm}^{-1}$ when the polymer is “acid doped”. However, here it is shown that a bathing environment of solvent and supporting electrolyte is not necessary for BBL electrical conductivity. For this normal/dry device, the maximal conductivity observed at -0.5 V vs. SSCE (calomel electrode) is $4.0\text{E-}5\ \Omega^{-1}\text{ cm}^{-1}$, about an order of magnitude lower than the evaluated in the bath^[87].

Eight years later (1995), a paper titled “Crystal structure and thin film morphology of BBL ladder polymer” was published. In this work, the authors mention the crystal structure of a BBL

fiber; after extruding it into a film, it lost the anisotropy and resulted in a fiber-like structure. They presented an orthorhombic unit cell with cell parameters of $a=7.87$, $b=3.37$ and $c=11.97\text{\AA}$, determined for the fiber diffraction pattern (c is the periodicity of the molecules in the chain direction). They have shown the chains of the polymer tend to arrange themselves, self-assembling, with the larger molecular plane standing perpendicular on the film surface and the chain axis is lying parallel to the film surface, resulting in an anisotropic layered structure in the polymer films. Thin films were cast from a 0.5% solution of BBL and MSA. The film was extruded from a 10% PPA solution into a thin film by dry-jet wet-spin method. In cast film, it shows a layered structure like other stiff polymers and cracks along the film surface direction indicates the weak interactions between the layers across the film thickness.^[88]

For the cast film, the wide-angle X-ray scattering (WAXD) presented two shapes: First, perpendicular to the surface, the reflection has a ring shape, indicative of an isotropic arrangement of the chain axes on the film surface. The outer reflection, the intensity of which appears stronger than the inner ring, corresponds to the side-to-side interchain packing (100) of a , whereas the inner reflection corresponds to the face-to-face packing (010) of b . Parallel to the surface, the pattern reveals a high degree of orientation across the film thickness. This reflection side-to-side packing (100) appears somewhat stronger in the meridian, while the reflection of face-to-face packing is very intense and highly oriented on the equator. This means (010) planes of the unit cell (a large molecular plane), are lying perpendicular to the film surface with the chain axis (c -axis) being parallel to the film surface in a random manner.

For the extruded film as a fiber, the (WAXD) pattern shows equally strong reflections of (100) and (010), indicating that the film possesses fiber-like symmetry with respect to the extrusion direction. The layered morphology disappeared (SEM) as well as its anisotropy (apparently

destroyed during the extrusion process where the chains or the bundles might have been deformed under the high shear field). (No diameter of the “fiber” has not been provided. However, in the cited paper number 5 for the fabrication of the fiber-like film, they presented a thin film with a thickness of 18 μ m).

In 2000, the “Efficient photovoltaic cells from semiconducting polymer heterojunctions” was published. Here, a heterojunction between PPV (50nm) and BBL (50nm) is characterized having a general structure of ITO/PPV/BBL/Al by spin coating. These are thin films that have been prepared for solar cells and have demonstrated to have a photovoltaic charge collection efficiency as high as 49% while the power conversion efficiency varied from 1.4% under sunlight illumination to 2% at the peak of the wavelength. This heterojunction is proposed and investigated due their complementary electronic structures and optical properties of the conjugated polymers. PPV is recognized as a well p-type polymer while BBL is a robust high-temperature polymer, with stability up to 600°C in air and a promising n-type semiconducting, photoconducting and non-linear optical properties. Under dark conditions the I-V curve revealed excellent rectifying semiconductor diode characteristics with a rectification ratio of 3×10^3 at ± 1.5 V. Also, the PPV/BBL heterojunction photocells had a factor of 2 improvement in the fill factor and over a 45-fold enhancement in power conversion efficiency compared to the PPV Schottky-barrier devices. BBL does not form a Schottky barrier between ITO and Al^[89].

In 2003, the paper “High electron mobility in ladder polymer field-effect transistors” was published. In this work, a bottom gate FET with a thin film of BBL is studied. The device had mobilities as high as 0.1cm²/(Vs) in a solution spin coated BBL. The devices were cleaned in water and dried at 70°C overnight. Further drying and annealing was performed in oven at 100°C

(100°C - 125°C) for 5 min (5 - 30 min). Longer periods for annealing lead to decrease in electron mobility and finally decreasing on/off current ratios as a result of increased off current^[90].

In 2010, “Air-stable ambipolar field effect transistors and complementary logic circuits from solution-processes n/p polymer heterojunctions” was published. Here BBL is used for various sandwiched profiles to form a bottom-gate transistor. However, in terms of P3HT, attempts to prepare BBL-on-P3HT heterojunctions were not successful because BBL solution did not wet films of P3HT, whose surface is highly hydrophobic by virtue of the high-density hexyl side chains. Instead, P3HT-on-BBL heterojunctions were used on a substrate without OTS8 modification. Indeed, in the P3HT-on-BBL devices, the mobilities are rather low and asymmetric compared to the other systems (PBTOT and PSOTT). The electron mobility of $0.002\text{cm}^2/(\text{Vs})$ is similar to previously reported values of BBL on SiO₂. The authors also pointed out that the electron mobility in n-on-p is generally higher than p-on-n, making a p-core n-shell structure promising for ambipolar devices. However, in this work the very low mobility of holes ($\sim 1 \times 10^{-5} \text{cm}^2/(\text{Vs})$) attributed the high thickness (20-30nm), which also is rough ($R_q=5\text{nm}$) acting as a barrier for hole injection and the rough interface scatters the charge carriers in the p-channel, resulting in the much lower hole mobility in P3HT.^[91]

In 2011, “n-Channel polymer thin film transistors with long term air stability and durability and their use in complementary inverters” was published. In this paper, most of the findings already published have been reused since these complementary inverters were prepared with devices already published 4 years before. The air stability (ambient of water and oxygen) is demonstrated. The Charge carrier mobilities of the p- and n- channel transistors are $7.2 \times 10^{-4} \text{cm}^2/(\text{Vs})$ [P3HT] and $6.2 \times 10^4 \text{cm}^2/\text{Vs}$ [BBL].^[92]

In summary, it has been proved that P3HT with BBL are great materials to be studied together due their intrinsic characteristics and good electronic coupling between them (regardless the publication of 2010, which can be improved by using a top gate with mechanical pressing). However, as far as I know, there is a large quantity of papers that deal with the fabrication of P3HT but no research has been published on the study of the nanofiber structure using the electrospinning technique to produce BBL nanofibers. The advantages of nanofibers (and those in the low micrometer regime (1~4 microns), have been used in air and water filtration, muscle mimicking and scaffolds, standalone nonwoven textiles, and electronic devices. Devices as diodes, field effect diodes (FED), field effect transistors (FET), solar cells mats, and sensors have benefited by the intrinsic characteristics of fibers such as flexibility (to certain extent) and a high surface area to volume ratio, perfect for capacitors, ionic batteries electrodes/separators, nonwoven electrodes, gas sensors and electronic nose applications. Devices containing full electroactive mats to a few fibers, even one fiber, have been used efficiently for ionic gates, ambipolar FET and sensors, respectively. To fabricate nanofibers of BBL will expand the range of usage and even overcome past mobilities by the simple fact that a nanofiber (in a polymer perspective) is a very long crystal.

2.5 References

1. Brinkman W F, Haggan D E, Troutman W W. *IEEE J Solid-State Circuits*, 1997, 32: 1858–1865
2. Peercy P S. *Nature*, 2000, 406: 1023– 1026
3. Riordan M, Hoddeson L, Herring C. *Rev Mod Phys*, 1999, 71: S336–S345
4. Farvis W E J. *Electron Power*, 1973, 22: 52–55
5. MacDiarmid A G. *Angew Chem Int Ed*, 2001, 40: 2581–2590
6. Heeger A J. *Rev Mod Phys*, 2001, 73: 681–700

7. Shirakawa H. *Synth Met*, 2002, 125: 3–10
8. Jadhav A H, Mai X T, Appiah-Ntiamoah R, et al. *J Nanosci Nanotechnol*, 2015, 15: 7980–7987
9. Jadhav A H, Kim H. *Adv Mat Res*, 2013, 622- 623: 827–832
10. Coleman J N, Khan U, Blau W J, et al. *Carbon*, 2006, 44: 1624–1652
11. Sun B, Long Y Z, Chen Z J, et al. *J. Mat. Chem. C*, 2014, 2: 1209–1219
12. Kou L, Liu Y, Zhang C, et al. *Nano-Micro Lett.*, 2017, 9: 51
13. Serrano W, Pinto N J. *Ferroelectrics*, 2012, 432: 41–48
14. Serrano W, Pinto N J. *Proceedings of the 15th European Conference on Composite Materials. Venice, 2012. 1–7*
15. Serrano W, Meléndez A, Ramos I, et al. *Polymer*, 2014, 55: 5727–5733
16. Serrano W, Melendez A, Ramos I, et al. *Proceedings of the IEEE 9th IberoAmerican Congress on Sensors. Bogota, 2014. 1–4*
17. Serrano W, Meléndez A, Ramos I, et al. *Polym. Inter.*, 2016, 65: 503–507
18. Hernández-Martínez D, Nicho M E, Hu H, et al. *Sci Semicond Process*, 2017, 61: 50–56
19. Chang H C, Liu C L, Chen W C. *Adv Funct Mater*, 2013, 23: 4960–4968
20. Lee Y, Oh J Y, Kim T R, et al. *Adv Mater*, 2018, 30: 1704401
21. Wu H, Lin D, Zhang R, et al. *J Am Ceramic Soc*, 2008, 91: 656–659
22. Hamedi M, Herlogsson L, Crispin X, et al. *Adv Mater*, 2009, 21: 573–577
23. Babel A, Li D, Xia Y, et al. *Macromolecules*, 2005, 38: 4705–4711
24. Liua H, Reccius C H, Craighead H G. *Appl Phys Lett*, 2005, 87: 253106
25. Chen J Y, Kuo C C, Lai C S, et al. *Macro- molecules*, 2011, 44: 2883–2892
26. Vohra V, Giovanella U, Tubino R, et al. *ACS Nano*, 2011, 5: 5572–5578

27. Kuo C C, Lin C H, Chen W C. *Macromolecules*, 2007, 40: 6959–6966
28. Moran-Mirabal J M, Slinker J D, DeFranco J A, et al. *Nano Lett*, 2007, 7: 458–463
29. Yang H, Lightner C R, Dong L. *ACS Nano*, 2012, 6: 622–628
30. Qin Z, Zhang P, Wu Z, et al. *Mater Des*, 2018, 147: 175–181
31. Zhang F, Yuan C, Zhu J, et al. *Adv Funct Mater*, 2013, 23: 3909–3915
32. Zhi M, Manivannan A, Meng F, et al. *J Power Sources*, 2012, 208: 345–353
33. Li J, Liu E, Li W, et al. *J Alloys Compd*, 2009, 478: 371–374
34. Kim C, Ngoc B, Yang K, et al. *Adv Mater*, 2007, 19: 2341–2346
35. Fang J, Wang X, Lin T. *J Mater Chem*, 2011, 21: 11088–11091
36. Maity K, Mandal D. *ACS Appl Mater Interfaces*, 2018, 10: 18257–18269
37. Lin M F, Xiong J, Wang J, et al. *Nano Energy*, 2018, 44: 248–255
38. Mi H Y, Jing X, Zheng Q, et al. *Nano Energy*, 2018, 48: 327–336
39. Zhang H D, Liu Y J, Zhang J, et al. *J Phys D-Appl Phys*, 2018, 51: 085102
40. Parangusan H, Ponnamma D, Al-Maadeed M A A. *Sci Rep*, 2018, 8: 754
41. Khan H, Razmjou A, Ebrahimi Warkiani M, et al. *Sensors*, 2018, 18: 418
42. Wang X, Zhang Y, Zhang X, et al. *Adv Mater*, 2018, 30: 1706738
43. Huang T, Wang C, Yu H, et al. *Nano Energy*, 2015, 14: 226–235
44. B.Guo, I. Glavas, et al., *Progress in Polymer Science*; vol. 38, pp.1263–1286, 2013.
45. P.H.S. Picciani, E.S. Medeiros, et al, *J. Appl. Polym. Sci.*, vol. 122, pp. 744- 753, 2009.
46. Y. Cao, P. Smith, A.J. Heeger, *Synthetic Metals*, vol. 48, pp. 91-97, 1992.
- 47 Y. Min, Y. Xia, A.G. MacDiarmid, A.J. Epstein, *Synthetic Metals*, vol. 69, pp. 159- 160, 1995.
- 48 S. Virji, J. Huang, R.B. Kaner, B.H.Weiller, *Nano Lett.* vol. 4, pp. 491–496, 2004.

49. C.K. Tan, D.J. Blackwood, *Sens. Actuator B: Chem.* vol. 71, pp. 184–191, 2000.
50. T. Yamada, and T. Kitayama, *J. Appl. Phys.* 52, 6859–6863 (1981).
51. J. Lovinger, G. T. Davis, T. Furukawa, and M. G. Broadhurst, *Macromolecules* 15, 323–328 (1982).
52. J. Lovinger, T. Furukawa, G. T. Davis, and M. G. Broadhurst, *Polymer* 24, 1225–1232 (1983).
53. N. Koizumi, N. Haikawa, and H. Habuka, *Ferroelectrics* 57, 99–102 (1984).
54. V. Bune, V. M. Fridkin, K. A. Verkhovskaya, and G. Taylor. *Polymer J.* 22, 7–11 (1990).
55. Y. J. Park, S. J. Kang, B. Lotz, M. Brinkmann, A. Thierry, K. J. Kim, and C. Park, *Macromolecules* 41, 8648–8654 (2008).
56. S. H. Lim, A. C. Rastogi, and S. B. Desu, *J. Appl. Phys.* 96, 5673–5682 (2004).
57. R. Schroeder, L. A. Majewski, M. Voigt, and M. Grell, *IEEE Electron Device Lett.* 26, 69–71 (2005).
58. T. J. Reece, S. Ducharme, A. V. Sorokin, and M. Poulsen, *Appl. Phys. Lett.* 82, 142–144 (2003).
59. G. H. Gelinck, A. W. Marsman, F. J. Touwslager, S. Setayesh, and D. M. de Leeuw, R. C. G. Naber, and P. W. M. Blom, *Appl. Phys. Lett.* 87, 092903 (2005).
60. R. C. G. , Naber, C. Tanase, P. W. M. Blom, G. H. Gelinck, A. W. Marsman, F. J. Touwslager, S. Setayesh, and D. M. De Leeuw, *Nature Mat.* 4, 243–248 (2005).
61. S. J. Kang, Y.J. Park, J. Sung, P. S. Jo, C. Park, K. J. Kim, and B. O. Cho, *Appl. Phys. Lett.* 92, 012921 (2008).
62. S. Koombhongse, W. Liu, and D. H. Reneker, *J. Poly. Sci. B: Poly. Phys.* 39, 2598–2606 (2001).

63. O. Martinez, A. G. Bravo, and N. J. Pinto, *Macromolecules*, 42, 7924–7929 (2009).
64. M. Abreu, S. Montanez, and N.J. Pinto, *J. Appl. Poly. Sci.* 119, 3640-3644 (2011)
65. R. McNeil, K. Asadi, B. Watts, P. W. M. Blom, et al., *small* 6, 508–512 (2010).
66. G. Xu, Z. Bao, and J. T. Groves, *Langmuir* 16, 1834–1841 (2000).
67. J. H. Yu, S. V. Fridrikh, and G. C. Rutledge, *Polymer* 47, 4789–4797 (2006).
68. H. Reneker, and L. Y. Yarin, *Polymer* 49, 2387–2425 (2008).
69. Y. Xia, A. G. MacDiarmid, and A. J. Epstein, *Macromolecules* 27, 7212–7214 (1994).
70. Guo B, Glavas L and Albertsson A-C, *Prog Polym Sci* 38:1263 (2013).
71. Lim JY, Kim SH, Lim S and Kim YH, *Macromol Mater Eng* 288:50 (2003).
72. Hou H, Jun Z, Reuning A, Schaper A, Wendorff JH and Greiner A, *Macromolecules* 35:2429 (2002).
73. Kim K, Yu M, Zong X, Chiu J, Fang D, Seo Y *et al.*, *Biomaterials* 24:4977 (2003).
74. Mo XM, Xu CY, Kotaki M and Ramakrishna S, *Biomaterials* 25:1883 (2004).
75. Kwon IK, Kidoaki S and Matsuda T, *Biomaterials* 26:3929 (2005).
76. Tsuji H, Nakano M, Hashimoto M, Takashima K, Katsura S and Mizuno A, *Biomacromolecules* 7:3316 (2006).
77. Gonzalez R and Pinto NJ, *Synth Met* 151:275 (2005).
78. Serrano W, Meléndez A, Ramos I and Pinto NJ, *Polymer* 55:5727 (2014).
79. Serrano W and Pinto N, *Ferroelectrics* 432:41 (2012).
80. Yu JH, Fridrikh SV and Rutledge GC, *Polymer* 47:4789 (2006).
81. Reneker DH and Yarin LY, *Polymer* 49:2387 (2008).
82. Pinto NJ, González R, Johnson AT and MacDiarmid AG, *Appl Phys Lett* 89:033505 (2006).

83. Serrano W, Pinto NJ, Naylor CH, Kybert NJ and Johnson AT, *Appl Phys Lett* 106:193504 (2015).
84. Sun Q, Park K and Dai LJ, *Phys Chem C* 113:7892 (2009).
85. Martinez O, Bravo AG and Pinto NJ, *Macromolecules* 42:7924 (2009).
86. Neamen AD, *Semiconductor Physics and Devices*, 3rd edition. McGraw-Hill, New York, chaps 7 and 8 (2003).
87. J.C.Jernigan, K.O.Wilbourn, R.W.Murray, *Journal of Electroanalytical Chemistry and Interfacial Electrochemistry*. 222, Issues 1–2, Pages 193-200. (1987)
88. H.H.Song, A.V.Fratini, M.Chabinye, *Synthetic Metals*. 69, Issues 1–3, Pages 533-535. (1995)
89. Samson A. Jenekhe, Shujian Yi. *Appl. Phys. Lett.*, 77, 2635. (2000)
90. Amit Babel, Samson A. Jenekhe. *J. Am. Chem. Soc.*, 125, 45, 13656–13657.(2003)
91. Felix Sunjoo Kim, Eilaf Ahmed, Selvam Subramaniyan, Samson A. Jenekhe. *ACS Appl. Mater. Interfaces*, 2, 11, 2974–2977. (2010)
92. Alejandro L. Briseno, Felix Sunjoo Kim, Amit Babel, Younan Xia and Samson A. Jenekhe. *J. Mater. Chem.*,21, 16461-16466.(2011)

Chapter 3: Idealization of P3HT/BBL Coaxial Composite

3.1 Electrospinning Technique for Coaxial Semiconductive Organic Nanofibers for Flexible Electronic Devices Fabrication

3.1.1 Summary

The electrospinning technique is a reliable and low-cost method that has been broadly used in the fabrication of nanofibers, down to the 5 nm in diameter range, which includes intelligent textiles, filters, and bone scaffolds, just to mention some of its practical applications. One of the most important utilizations for this research resides in the applications for electrical and electronic devices. In particular, this work is intended to use organic semiconductor polymers for electronic device fabrication that would be innovative for diode, field effect transistor, solar cell, and sensor nano technology development. Organic polymers have been noted to have excellent thermal stability, electrical conductivity, mechanical flexibility, and chemical/biological functionality. This proposed work will use the regioregular p-doped polymer Poly(3-hexylthiophene-2,5-diyl) (P3HT) and the n-doped ladder polymer Poly(benzimidazobenzophenanthroline) (BBL) as the organic semiconductor materials for nanofiber device fabrication. Forming a coaxial structure, P3HT as the core and BBL as the sheath, the nanofibers are expected to form cylindrical p – n junctions. This research looks forward to expanding the knowledge in organic polymeric semiconductors for efficient flexible arrays with better performance and lower power requirements. Moreover, this work hopes to establish a reliable procedure for a predictable formation of the coaxial electrospinning set up for organic semiconductors.

3.1.2 Objectives

The overall research goal of this work is to fabricate a fully functional organic polymer nano device. The primary research objectives of this work include the following:

1. To investigate the conditions under which selected semiconducting polymers form 1 dimension (1D) coaxial nanofiber p-n junctions and
2. To characterize the nano device behavior in the presence of light and organic gases.

First, electrospinning variables for P3HT and BBL fiber formation will be determined. After the fabrication, topological characterization will be realized using SEM technology to determine and prove the nanofiber formation and coaxial structure. Also, electrical characterizations will be performed in different arrangements. This characterization includes dark and light conditions for solar cell applications, field effect transistors, and organic gas sensors. With the formation of fiber coaxial arrangements, there will be investigations of dimensionality crossovers e.g., from one-dimensional (1D) to two-dimensional (2D) and one-dimensional (1D) to three-dimensional (3D). To date, no reported studies regarding organic semiconducting coaxial p-n junction nanofibers have been conducted. Thus, this study will be fundamental and essential for organic semiconducting nanodevices for flexible electronics and multi-dimensional integrated circuits.

3.1.3 Introduction

A study from Sandler Research concluded the nanofiber market will grow at 24.12% Compounded Annual Rate of Growth (CAGR) driven by the technical industry in 2020 ^[1]. Part of this critical growth is driven by the need for new nanometric structures for organic flexible electronic devices that do not depend on silicon (Si). Semiconductive nanoparticles have been used to create p-n junctions in an electrospun poly-vinyl pyrrolidone (PVP) nanofiber using a

hydrothermal method^[2]. In other approaches, oxide nanofibers formed tapered and twisted p-n junction yarn;^[3] metallic and polymers formed coaxial nanofibers^[4] as well. High fabrication costs, oxide charging, large fiber diameters, non-biodegradability, and rigidity limit these p-n junctions. To our knowledge, there has never been a fundamental study conducted on the use of two organic semiconductive polymers to form a coaxial p-n junction for basic electronic devices. Organic semiconductive materials electrospun into high surface area nanofibers can offer several advantages to the semiconductor industry in terms of reliability, flexibility, and tuning. This work proposes the fabrication and characterization of an organic semiconductive coaxial nanofiber p-n junction for flexible organic semiconducting devices, such as diodes, field effect transistors, sensors and p-n junction based solar cells.

The basic behavior of electrospinning was observed in the 17th century, with the observation of liquid (water drops) being attracted by an electrostatic force^[5]. In the mid 1920's, with photography technology, extensive research was done to understand the bursting of soap bubbles under a uniform electric field^[6]. This initial work from Taylor, including further research, was the foundation of a mathematical model that describes the cone formed by the surface tension in a drop due the strength of an electric field^[7]. Later, this conical shape behavior became known as the Taylor's Cone^[8]. The electrospinning apparatus and the technique were patented by Cooley in the 1900's and is still relevant today^[9]. In that same year, fundamental studies showing the formation of polymer-based nanofibers performed by Reneker were published, with this extensive research the name of "electrospinning" was coined for the technique^[10]. In general, the high electric field stretches the polymeric solution while the solvent evaporates from the solution leaving behind the solute as nanofibers, which are typically polymer based. As published elsewhere, the basic electrospinning technique is formed using a High Voltage Power Supply (10

to 30kV), a tuberculin syringe or a coaxial needle, Electronic Pump and Aluminum foil as an anode with a distance of 20cm apart from the needle^[11].

With the understanding of nanofiber fabrication and later on the discovery of conducting polymers, the electrospinning technique started to be used for electrical applications. In 1977, three scientists, including Alan MacDiarmid, reported an increased conductivity in oxidized iodine-doped polyacetylene; this work was part of the awarded Nobel Prize in Chemistry “for the discovery and development of conductive polymers”^[12]. This novel discovery opened the door to the direct application of the Electrospinning technique and the emergent conductive polymers for nanoelectronic devices fabrication^[13]. Electrospun polyaniline-based Field Effect Transistors,^[14,15] as well as Poly (3, 4-ethylenedioxythiophene) polystyrene sulfonate (PEDOT:PSS) based^[16] were studied and published. Furthermore, PEDOT:PSS^[17], Polyaniline (PANI)^[18] and Poly (3-hexylthiophene) (P3HT) diodes^[19], solar cloths for solar cells^[20] as well as nanofiber organic vapor sensors,^[21] have been fabricated and characterized to demonstrate electro active behavior.

BBL is a well-known conjugated ladder polymer where the monomers are unified by four bonds and used for Field Effect Transistors^[22] and organic solar cells^[23]. The intrinsic electrically n-type semiconductor behavior and flexibility make it perfect for flexible sensors, devices, and solar cells in the nanofiber form. In addition, the proposed coaxial nanostructures will assist in reducing device weight production costs, and size. Organic semiconductive polymers have been noted to have excellent thermal stability^[24], electrical conductivity^[25], mechanical flexibility^[26], and chemical/biological functionality,^[27] showing high electron transport in one dimensional nanobelts created by solvent dispersion self-assembly technique^[28].

The other material of choice, P3HT, is a conjugated *p*-doped semiconducting polymer extensively used in organic electronics including field effect transistors (FET's). Electrospinning

fibers of pure P3HT^[29] is not easy due to its low molecular weight; however, by blending the P3HT with another polymer (i.e. PLA) under the same solvent, thin fibers can be fabricated of the composite material^[19].

The formation of coaxial structures has been around since the 1930's. The purpose of the technique was to add a gas stream to the surface of the core fiber to help the formation^[9] or ultimately to add mineral oil as the core and polymers as the shell for “nanotube” fabrication^[30]. Electrospinning for coaxial structures^[31] has been studied for antibacterial applications^[32], nanochannels for single molecule detection^[33], encapsulation and controlled release^[34], and drug delivery applications^[35]. More recently, a coaxial fiber was fabricated making a functional light emitting coaxial strand^[36]. The work exposes a non-polymer based ionic transition-metal complex at the core of the fiber while the shell is a passive polymer-based material where the overall nanofiber is coated using an ITO thin film. This fiber is not formed by organic semiconductive polymers. Therefore, making a coaxial nanofiber with two polymers is a new approach to nanofiber device fabrication. No reported studies have been conducted regarding organic semiconducting coaxial p-n junction nanofibers, making this study foundational and essential for organic semiconducting nanodevices for flexible electronics and multi-dimensional integrated circuits.

Using organic semiconductive coaxial nanofibers will produce p-n junctions with enhanced electronic properties and reliability are candidates for flexible electronics, receptive to crosslinking, and are cost effective. These novel organic semiconductive p-n junctions have the potential to demonstrate high I_{on}/I_{off} ratios, a reduction in leakage current, and a tunable depletion region in diode mode can be achieved.

To verify this, the formation of the depletion region by the core or shell diameter will be determined as well as by applying UV radiation to study the behavior of the junction in diode mode. Also, due to the large surface area that can be generated by nanofibers in a small region, a coaxial p-n junction matrix should excel in sensing capability for sensor technology. The surface of the nanofibers can be functionalized for specific sensing and higher selectivity.

3.1.4 Experimental

The electrospinning technique consist of a DC high voltage Power Supply, a syringe pump, coaxial needle, and a collector surface as shown in Figure 3.1. The formation of the Taylor cone and the nanofibers occurs between the needle and the collector in this case an Aluminum (Al) foil. A voltage that can range from 10 kV to 30 kV can be used to form an electric field that goes from the needle to the collector, cathode, and anode, respectively. A separation of 20 cm between the cathode and anode is used. The electric field deforms the polymer drop, forming Tylor's cone that forms a jet of the solution. At the jet, the surface tension is overcome by the electric field forming the nanofibers. Is after the surface tension breakdown that the solvent in the jet evaporates and nanofibers formed in the air land over the collector. The Al foil collector is sufficient for nonwoven textile fabrication recollection and Topological Characterization in the Scanning Electron Microscope (SEM). For diameter measurements, a small piece of 1 cm² Silicon wafer can be collocated over the collector surface. For electrical characterizations, where single nanofibers will be studied, 1 cm² Silicon wafer with pre-patterned electrodes is waved near the collector so the nanofibers can land over the electrodes in the wafer.

Electronic grade p-doped Poly (3-hexylthiophene) (P3HT) and n-doped Poly(benzimidazobenzophenanthroline) (BBL) will be prepared with anhydrous chloroform (CHCl₃) to form the precursor solutions for the coaxial nanofibers. Figure 3.2 shows the molecular

structures, respectively. The solutions will be prepared based in weight percent (wt%). For example, a P3HT solution of 3wt% will be comprised of 1g of CHCl_3 and 0.03g of P3HT. UV-VIS spectra of pure and blended solutions will be realized before electrospinning to determine the energy gap of the polymers and verify if any segregation occurs in the solution that leads to variations in the physical properties. The absorption spectra of the blended solution (p-type and n-type in CHCl_3) will show the variation and possible balancing of charge due the difference charges (doping) in the blend. For coaxial fibers, the polymers, in the core/shell junction must have limited chemical interaction to help maintain characteristic p- and n- material properties and desired performance. Figure 3.3 shows the coaxial needle from Ramé-Hart that will be used. Chemical changes shown in spectra will lead to additional characterization to determine if any extended reaction has occurred that will impact the expected material properties. Coaxial nanofibers will be prepared using the electrospinning technique with a coaxial needle with a sheath gauge of 18G and the core gauge of 23G. The coaxial needle promotes the formation of the coaxial arrangement from the solution. The sheath polymer will cover the core in the middle of the syringe and be stretched at the Taylor's Cone. A syringe pump will be used to maintain a constant output rate of the polymeric solutions. Fibers are formed when a critical voltage (electric field times the distance from syringe) is enough to overcome the polymer surface tension and solvent evaporation occurs, as explained above. Two substrates will be used as collectors: Si wafer for electrical characterization and device fabrication and Al foil for morphological characterization (SEM).

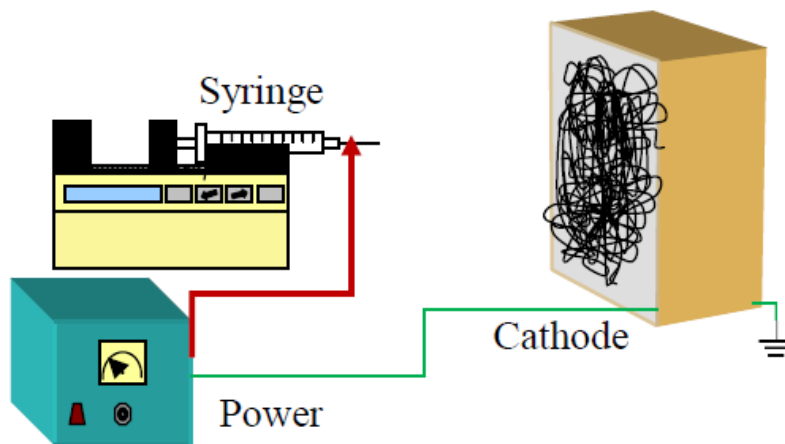


Figure 3.1 Electrospinning apparatus

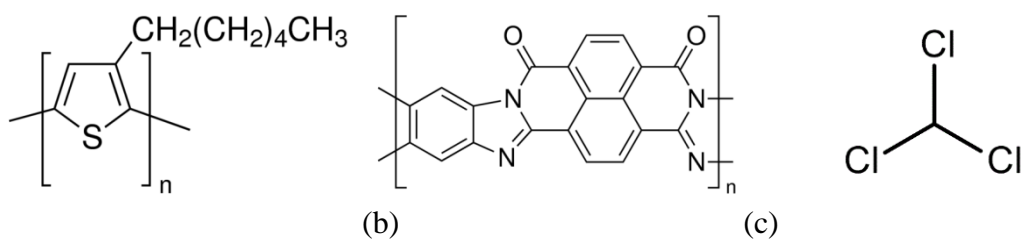


Figure 3.2 Molecular structures for (a) P3HT, (b) BBL and (c) Chloroform

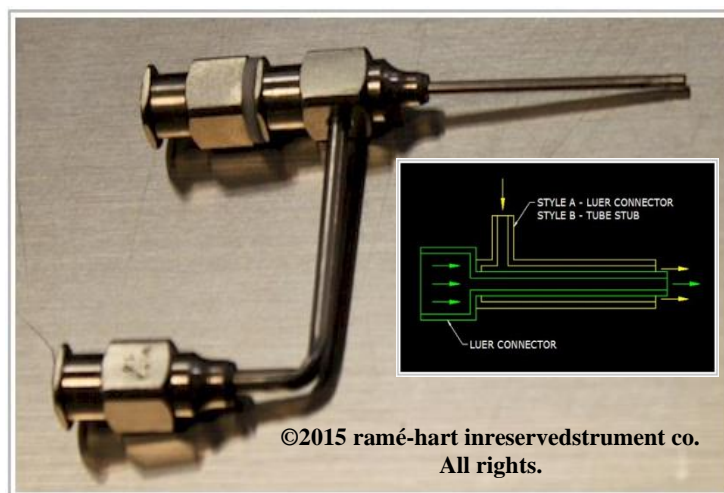


Figure 3.3 Coaxial needle

Figure 3.3 shows the expected array of the coaxial nanofiber. Controlled characteristics of the fibers will include inner and outer diameter, alignment, and porosity, which will be studied using SEM and atomic force microscopy (AFM). This project will lead to new applications for organic semiconductor electronics that are not heavily dependent upon silicon (Si) as an active material.

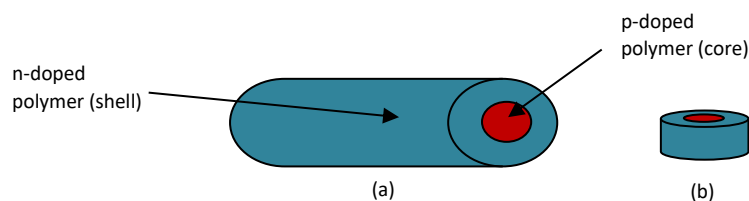


Figure 3.4 Sketch of (a) Semiconducting coaxial nanofiber and (b) sliced nanofiber forming a nanodisk.

Average diameters in the range of 100 nm – 100 μ m is expected for different concentrations and will be verified with AFM and SEM. Average coaxial nanofibers can range in the 5 nm scale and can be achieved with further studied and fine-tuned variables including humidity, separation, electric field, and viscosity, among others. Changes in morphology due to an increment in solute will be observed in the SEM and will determine the critical concentration where well-formed fibers are formed. Fibers from 1wt% to 5wt% of P3HT and BBL may not form fibers due to a lack of solute. 7wt% to 11wt% should present the small fibers with beading. 13wt% to 17wt% should form very well as symmetrically formed fibers with no bead formation. 19wt% to 21wt% will produce bigger diameter fibers and possible agglomeration of the polymer, where single fiber formation will be decreased due the excess of solute^[11]. Electrical characterization is expected to show rectification behavior with an ideal parameter between 1 and 2 due to the formed p-n junction. Diffusion of electrons from n-type to p-type and further combination of electron/hole pairs creates a depleted region that results in band bending^[18]. The turn-on voltage will depend on

the inner (core) diameter exerting a direct effect in the depletion region. Gold electrodes, of a thickness less than 100 nm, will be used to ensure an ohmic contact between the fiber and the electrode. Low power ($\pm 1V$) forward and reverse bias, first quadrant and third quadrant respectively, should show the independence of the diode formed in the fibers to the Au electrodes. This same approach will be performed for p-n junction based solar cell including initial characterizations on light spectrum response as DC current – voltage (I-V) Measurements^[37]. Field Effect Transistor (FET) characterization will be performed in the same basis as the diode, where here the gate electrode in the Si wafer and the separation between the fiber and the Si is 200nm of silicon dioxide (SiO_2).

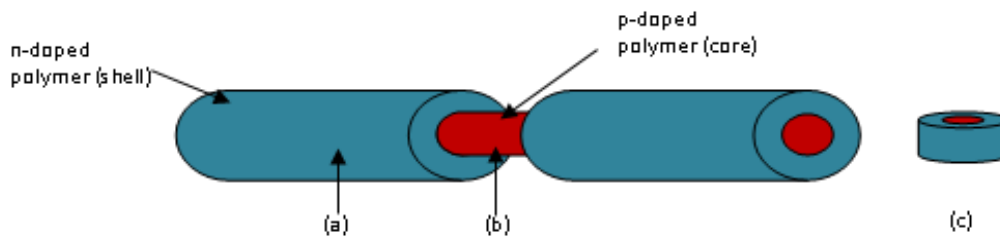


Figure 3.5 Sketch of the expected Semiconducting Coaxial nanofiber: (a) Shell/Core flow rate $[X/Y] = 1$, (b) Shell flow rate $[0]$ and (c) sliced nanofiber forming a nanodisk.

Figure 3.5 shows the expected formation of the coaxial nanofiber with a pulsed variation of the pump for the sheath or the core syringe. As can be seen above, assuming the flow rate of the core and shell is constant and every particular time the shell flow rate converges to zero, a coaxial nanofiber forms multiple devices in the same strand. This formation extends the applications of the technology, opening the possibilities for mass production of devices. Figure 3.6 shows an interpretation of the idea.

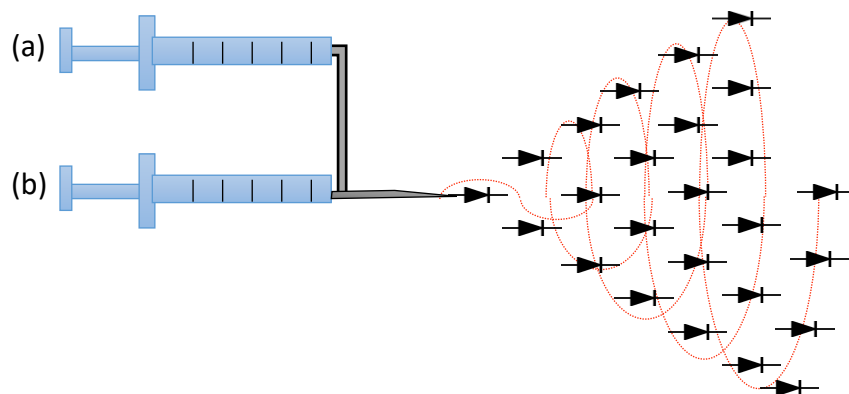


Figure 3.6 Sketch of the coaxial electrospinning technique showing nanofiber-based devices such as diodes. (a) core and (b) sheath syringes.

For the sensor characterization, hydrogen (H_2), carbon monoxide (CO), volatile organic compounds (VOC's) (i.e. acetone, ethanol, methanol, etc.), and an inert gas will be used. With the device fabricated and with a constant voltage of 0.1V applied to it, flow of nitrogen or argon (inert gas) will be applied to neutralize the device for several minutes. Then, a periodical change between the inert gas and the organic gas (ethanol, methanol, and propanol) will be applied. The expected sensor response by the fiber is due to molecule relaxation when the ambient reacts with an organic gas^[21]. Figure 3.7 shows a schematic of the circuit for gas flow that will be used for the characterization for the organic gases. In the circuit, two valves are present: valve A and B for inert gas and organic gas, respectively. When A is open and B closed, inert gas flows from A to the interior of liquid methanol. Bubbles of the inert gas forms when the flows get in contact with the organic compound and leaves the alcohol taking molecules (as vapors) to the sensor. B is closed. When A is closed, and B opened, inert gas flows from B to the interior of the flask keeping the organic compound vapors inside it. Pure and clean inert gas moves to the sensor. A is closed. The molecules in the fiber tend to be packed between each other. In the presence of the organic gas the molecules stretch, allowing a less randomized path for electrons. Time response, saturation, accuracy, and precision measuring the variations will be calculated. Also, changes in resistance,

when UV is irradiated to the coaxial fiber surface, will be measured. It is expected that the device will show a turn on voltage from .1V to .5V that decreases when the device is exposed to UV light, being perfect for low power electronics.

3.1.5 Conclusion

For the first time, two organic semiconductor polymers will form a p-n junction, a critical building block of electronics in a coaxial structure. We are expecting functional p-n junction diodes of approximately 100 nm in diameter that can be tethered to any surface shape or active device layers. We anticipate global interest from engineers and scientists to advance the current state-of-the-art through our novel, single step, efficient, cost effective electrospinning process to fabricate organic semiconductive coaxially structured nanofibers. The fabrication of a 1D semiconducting coaxial nanofiber configuration with a large outer surface area can promote sensing characteristics, rectification due to core/shell junction, and low threshold voltage limitations due to the dimensions of the coaxial nanofiber. The devices can be spun or patterned on insulating substrates or plates to produce field effect transistors, sensors, and solar cells to extend the research beyond p-n junctions. The outcomes will include the characterization of organic semiconductive polymers under laboratory conditions; formation of p-n coaxial nanofiber with a diameter range of 100 nm – 1 μ m from different concentrations and electroactivity; morphological, chemical and electrical characterization data for coaxial p-n junction nanofibers that will rectify signals with low constant power consumptions and have an ideality factor between 1 and 2; and fabrication of final flexible p-n junction membranes to be used as high surface density area sensors and test database of organic semiconductive coaxial nanofiber p-n junction device reliability, IV response and stability.

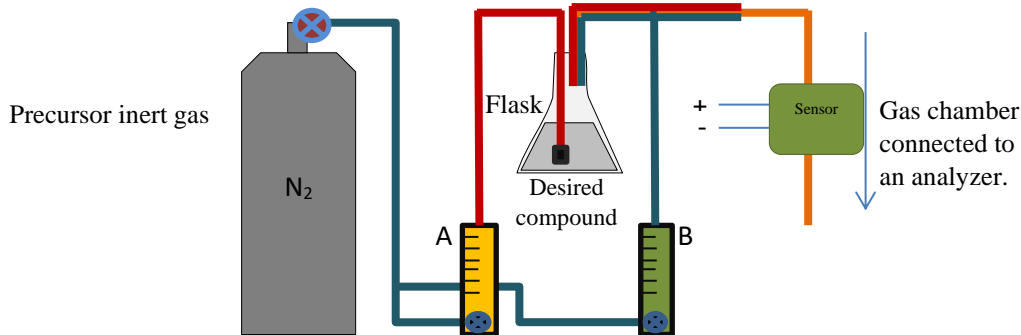


Figure 3.7 Circuit for sensing characterization.

3.2 References

1. Sandler Research Global Nanofiber Market 2016-2020 (<http://www.sandlerresearch.org/global-nanofiber-market-2016-2020.html>) Retrieved on 10/01/2016.
2. C. Yang et. al, RSC Adv., 4, 31941. (2014).
3. A.F Lotus, S. Bhargava, E.T. Bender, E.A. Evans, R.D Ramsier. *Journal of Applied Physics*, 106, 014303 (2009).
4. H.Yang, C.R. Lightner, Liang Dong. *ACS NANO*, vol.6, No.1, 622-628 (2012).
5. De Magnete Magnetcisque Corporibus, et de Magno Magnete Tellure (On the Magnet, Magnetic Bodies also, and on the Great Magnet the Earth. London: The Chiswick Press; (1600).
6. C.T.R. Wilson and G.I. Taylor, Trinity College. *Phil.Soc.Proc.* Vol.22 Pt.5, 728-730, (1924).
7. G.I. Taylor. *Proceedings of the Riyal Society of London Series A Mathematical and Physical Sciences*, 280, 383-397. (1964).
8. G.I. Taylor. *Proc. Roy. Soc. Lond. A.* 313, 453-475, (1969).
9. J.F. Cooley. United Kingdom Patent 6385, (1900).

10. J. Doshi and D.H. Reneker. *Journal of Electrostatics*, 35, 151-160, (1995).
11. W. Serrano and N.J. Pinto, Taylor & Francis (Taylor & Francis Group) *Ferroelectrics*, 432:41 – 48, (2012).
12. A.J Heeger, A.G. MacDiarmid and H. Shirakawa. The Royal Swedish Academy of Sciences. The Nobel Prize in Chemistry. (2000).
13. J. Fang, H. Niu and T.Lin. *Handbook of Smart Textiles*. Chap 24, 618-652. (2015).
14. N.J. Pinto, A.T. Johnson, A.G. MacDiarmid et al. *Applied Physics Letters*, Vol 83, Issue 20, (2003).
15. Y. Zhou, M. Freitag, J. Hone, C. Staii, A.T. Johnson Jr., N. J. Pinto and A.G. MacDiarmid. *Applied Physics Letters*, Vol 83, No. 18, (2003).
16. J. Lu, N.J. Pinto, A.G. MacDiarmid. *Journal of Applied Physics*, Vol 92, No. 10, (2002).
17. N.J. Pinto and W. Serrano. ECCM15, Venice, Italy, (2012).
18. W. Serrano, A. Melendez, I. Ramos, N.J. Pinto, *Polymer*, 55, 5727-5733, (2014).
19. W. Serrano, A. Meléndez, I. Ramos and N.J. Pinto, *Polymer International*, (2016).
20. S. Sundarrajan, R. Murugan, A. Sreekumaran Nair, S. Ramakrishna. *Materials Letters*, 64, 2369-2372, (2010).
21. W. Serrano, A. Meléndez, I. Ramos and N.J. Pinto, *Sensors (IBERSENSOR)*, 2014 IEEE 9th Ibero-American Congress on Sensors, (2014).
22. Babel. A.; Jenekhe, S. *J. Am. Chem. Soc.*, 125, 13656, (2003).
23. Alam, M.; Jenekhe, S. *Chem. Mater.*, 16, 4647, (2004).
24. S.S. Dalal, D. M. Walters, I. Lyubimov, J.J. de Pablo, M.D. Ediger, *PNAS*, vol. 112, no. 14, 4227-4232, (2015).

25. K. Fukuda, Y. Takeda, M. Mizukami, D. Kumaki, Shizuo Tokito, *Scientific Reports*, 4, 3947, (2014).
26. Organic Electronics for a Better Tomorrow: Innovation, Accessibility, Sustainability, *White paper from the Chemical Sciences and Society Summit*, San Francisco, California, US, (2012).
27. Mihai Irimia-Vladu, *Chem. Soc. Rev.*, 43, 588-610, (2014).
28. A.L. Briseno, S.C.B. Mannsfeld, P.J. Shamberger, F.S. Ohuchi, Z. Bao, S.A. Jenekhe and Y. Xia. *Chem. Mater.* 20, 4712-4719. (2008).
29. R. Gonzales, N.J. Pinto. *Synthetic Metals*, Vol 151, Issue 3, 275-278. (2005).
30. J.T. McCann, D. Li and Y. Xia. *Journal of Materials Chemistry*, 15, 735-738. (2005).
31. A. K. Moghe & Professor B. S. Gupta, *Polymer Reviews*, 48:2, 353-377, (2008).
32. T.T.T. Nguyen, O.H. Chung and J.S. Park. *Carbohydrate Polymers*, 86, 1799-1806. (2011).
33. M. Wang, N. Jing, C.B. Su and Jun Kameoka. *Applied Physics Letters*, 88, 033106. (2006).
34. H. Jiang, L. Wang, K. Zhu. *Journal of Controlled Release*, 193, 296-303. (2014).
35. X. Hu, S. Liu, G. Zhou, Y. Huang, Z. Xie, X. Jing. *Journal of Controlled Release*, 185, 12-21. (2014).
36. H. Yang, C.R. Lightner, Liang Dong. *ACS NANO*, vol.6, No.1, 622-628, (2012).
37. Electrical Characterization of Photovoltaic Materials and Solar Cells with the Model 4200-SCS Semiconductor Characterization System. Keithley, Application Note Series, No. 3026. (2011).

Chapter 4: Further Characterizations on P3HT and BBL

4.1 P3HT Loaded Piezoelectric Electrospun Fibers for Tunable Molecular Adsorption

4.1.1 Abstract

Electrospinning is a compelling technique for the fabrication of fibrous platforms for a wide range of applications such as electronic devices, electroactive wearables, and wound healing scaffolds. This versatile, reliable, and low-cost technique has been recently investigated using a wide selection of active materials to fabricate nonwoven meshes for use as smart filters to control the adsorption/delivery of small molecules. In this chapter, electrospinning is proposed for the fabrication of polyvinylidene fluoride (PVDF)-based fibers able to control the adsorption of negatively charged molecules such as Methylene Blue (MB). We demonstrate that PVDF fibers with pronounced surface roughness (from 126 nm to 1983 nm) are able to adsorb a higher amount of MB than smooth fibers made of PCL, used as a control. Moreover, the integration of a p-type conjugated polymer such as Poly (3-hexylthiophene) (P3HT), con-curs influencing the adsorption mechanism of MB, mediated by the microscopic interactions among dipolar β phases in PVDF. In addition, an increase of MB absorption was measured in the presence of an externally applied voltage (10 kV), ascribable to the P3HT oxidation change that influences microscopic dipole interactions. Hence, we suggest the use of P3HT/Polyvinylidene fluoride-trifluoroethylene (PVDF- TrFE) fibers to design new filtering systems able to tune the absorption of negatively charged molecules for environmental and biomedical applications.

4.1.2 Introduction

One of the main challenges of improving the quality of life in overpopulated cities today is the plight to define innovative fouling mitigation strategies to support water reuse processes able to safeguard water quality levels for ever increasing urbanization ^[1]. The use of commercialized membranes is compatible with the use of fouling mitigation techniques, but this requires energy and intensive cost resources ^[2]. In recent years, electrospinning has shown to be an elective technology to fabricate nanofibrous membranes with low production costs and lower capital investments, as compared to conventional manufacturing techniques ^[3]. High surface area to volume ratio of nanofibers, however, still represents a relevant limitation for the fabrication of systems suitable in microfiltration due to the ability to form a fouling better than available commercial one's membrane ^[4]. In the last years, piezoelectric polymers used to fabricate innovative nanofibers have been able to control fouling mechanisms for more sustainable operations, with lower energy consumption and significant cost savings ^[5]. Recent studies demonstrate the piezoelectric properties of fibers can assure more accurate control of in-situ fouling, preventing initial deposition of foulants on the membrane surface via active deformation of the membrane surface ^[6]. Indeed, piezoelectric materials can also be electrically stimulated to produce small vibrations that generate mechanical deformations of the fiber surface, with relevant benefits for waste removal in water filtration ^[7,8]. In this work, piezoelectric polymers, such as PVDF, and its copolymer, PVDF-TrFE, have been selected for their processability in contrast to the intrinsic brittleness of inorganic materials (i.e., oxides). In particular, permanent piezoelectric properties of PVDF-TrFE, defined by high ratios of dipolar β -phases/nonpolar α -phases, are amplified by the use of the electrospinning technique, enabling a more efficient orientation of dipoles in the β -phases namely poling effect ^[9].

In this section, the fabrication of electrospun nanofibers by the blend of PVDF-TrFE and P3HT was investigated for validating their capability to influence absorbent transport. P3HT is a p-type conjugated regioregular polymer, heavily used in organic photovoltaics, diodes, and field effect transistors ^[10–12]. The intrinsic electronic behavior and its chemical processability makes P3HT perfect for industrial scale manufacturing of nanofibers; however, due to the low molecular weight of this conjugated polymer, it is usually blended with other polymers able to provide efficient mechanical support. In this case, a secondary polymer was accurately selected in order to confer additive functionalities to the fibers (i.e., piezoelectricity) for specific applications. Herein, we demonstrate that composites based upon the addition of the conjugate polymer P3HT to PVDF-TrFE can improve the selective adsorption of negatively charged molecules, such as Methylene blue (MB) onto the fiber surface, with relevant benefits in biomedical and environmental filtering applications.

4.1.3 Materials and Methods

Conjugated polymer, the regioregular p-type polymer P3HT (Poly(3-hexylthiophene-2,5-diyl)), acquired from Sigma-Aldrich was used as received. Piezoelectric and ferroelectric Poly(vinylidene fluoride) PVDF-TrFE with average molecular weights of 350,000 from Kureah, Japan (KF W#2200) and the biodegradable polyester Poly(caprolactone) PCL (MW 60kDa, Sigma Aldrich, Milan, Italy) were used as received. For the characterization of the surface adsorption, a 10 wt% of Methylene Blue (MB) in distilled water was prepared.

4.1.4 Preparation

The electrospinning technique is used to fabricate PVDF-TrFE nanofibers (coded as PVDF) as well as their composites with P3HT; PCL nanofibers and their composites were used as a control (coded as CTR). The solutions were prepared in the following concentrations: 13 wt%

PVDF-TrFE/THF, 25 wt% PCL/CHCl₃, and 2 wt% P3HT/THF. The composite solution of PVDF-TrFE/P3HT was prepared by mixing 0.83 g of 13 wt% PVDF-TrFE/THF and 0.11 g of 2 wt% P3HT/THF via continuous stirring. The bi-component polymeric solution (P3HT/PVDF-TrFE) was electrospun by using a 18G blunt needle with a voltage of 12 kV, a pump rate of 0.3 ml/h, and a needle to collector distance of 130 mm to ultimately form fibers. All the fibers were collected over aluminum foil used as ground surface.

4.1.5 Morphological Characterization

Fiber morphology was performed qualitatively by field emission scanning microscopy (FESEM, QUANTA200, FEI, The Netherlands). Prior to the analysis, circularly cut samples were mounted on metal stubs by using a double-sided conducting adhesive tape. They were then sputtered with a gold-palladium coating to form a thin conductive layer (ca. 19 nm) after about 20 s, in order to minimize any artifacts of the images, during the evaluation of the surface roughness. SEM images were taken under high vacuum conditions (10⁻⁷ torr) using the secondary electron detector (SED) at a working voltage equal to 5 kV. On selected SEM images, fiber diameter size and distribution were determined by using image analysis software (ImageJ ver. 1.48, freeware). Morphological analysis was also performed by using an AFM microscope (Innova, Bruker, Germany) equipped with a large area scanner (INSC090, Bruker, Germany) to evaluate fiber roughness of PVDF fibers. The imaging was performed via tapping mode (TM-AFM) on thin scaffold slices, about 150 μm thick, in air at room temperature (25 °C) by using a RTESPA silicon cantilever (Bruker Corporation, Santa Barbara, USA). The images of interest were first captured by AFM raster scanning, processed using the NanoScope Analysis data processing software 1.40 (Bruker Corporation, USA), and then graphically reported in 2D and 3D form. A roughness parameter for the surface R_q, (the root mean-square height of the surface) was also calculated.

Roughness data was acquired by manually applying a rectangular region of interest (ROI) box of (5 x 10) μm^2 to different areas of the scaffold surface.

4.1.6 Adsorption Via UV–VIS Spectroscopy

The measurement setup was schematically reported in Figure 4.1. Samples (i.e fibers onto Aluminum foil) were cut in rectangular strips (0.5 x 2 cm), and the effective weight of the fibers was measured (0.99 mg PVDF/P3HT, 0.68 mg PVDF, and 10.62 mg PCL), respectively. The strips were immersed in 10 ml of MB solution at room temperature. The strips were connected to a positively charged connector holder and a voltage of 10 kV was applied. The adsorbed MB amount was measured at regular time intervals using UV–VIS spectroscopy at $\lambda_{\text{max}} = 663.5 \text{ nm}$, and calculated at time t (q_t, mg^{-1}), as well as removal efficiency, using the following equations:

$$\text{Adsorption capacity } q_t = \frac{C_o - C_t}{m} * V \quad [1]$$

$$\% \text{ removal efficiency} = \frac{C_o - C_t}{C_o} * 100 \quad [2]$$

4.1.7 Results and Discussion

PVDF-TrFE fiber fabrication was preliminary optimized by accurately setting the main process parameters including voltage and flow rate. We verified that a voltage of 12 kV and a flow rate of 0.3 ml/h pump rate converge to promote a reproducible Taylor cone formation, leading to the production of PVDF nanofibers without bead and defects, in agreement with previous experimental evidence ^[13]. The morphology of the optimized electrospun fibers of PVDF-TrFE was reported in Figure 4.2 (a) and (b). SEM image analysis reveals a homogenous distribution of fibers without defects and partially uniform diameters. A remarkable porosity was detected on the fiber surface in contrast with a smooth surface in the PCL control fiber (Figure 4.2b); this is

ascribable to the peculiar properties (i.e., permittivity, boiling point) of the solvent used [14,15]. Quantitative measurements via image analysis indicate an average diameter for PVDF-TrFE fibers to be 1.8 ± 0.2 μm , as compared to the control showing an average diameter of 1.3 ± 0.2 μm . A coarse surface is achieved for all the PVDF-TrFE nanofibers as can be seen from the AFM scan. Pure PVDF-TrFE nanofibers present a R_q of 28.6 nm and up to 357 nm, when P3HT is added to form the fiber structure.

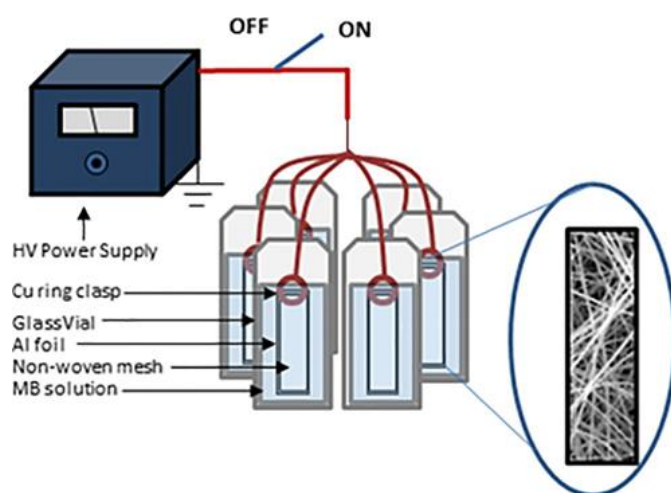


Figure 4.1 Scheme of the homemade system used for the adsorption measurements.

Adsorption curves – i.e., removal efficiency vs. time - were reported for PVDF-TrFE fibers (Figure 4.2). A remarkable increase of the removal efficiency was calculated, due to the higher MB adsorption, with respect to the control (Figure. 4.2c). In this case, MB transport is driven by electrostatic effects. Indeed, the piezoelectric properties of PVDF thin films promote the adsorption of MB molecules as a function of the microscopic interactions (i.e., Van der Waals) between dipolar β -phases and molecular ions [16,17]. At the same time, fiber porosity concurs to facilitate the MB molecular transport, as reported in similar studies in the case of dielectric fibres [18]. Accordingly, in the case of inert PCL fibers, the transport of MB molecules is further inhibited, due to the hydrophobic properties of the polymer. Only a very slight absorption was detected,

probably due to the contribution of extended surface area of thin electrospun fibers, as reported elsewhere ^[19]. This was also confirmed by the MB adsorption values measured in the case of bulk films with very low exposed surface (ca. 1% after 75 min for both systems).

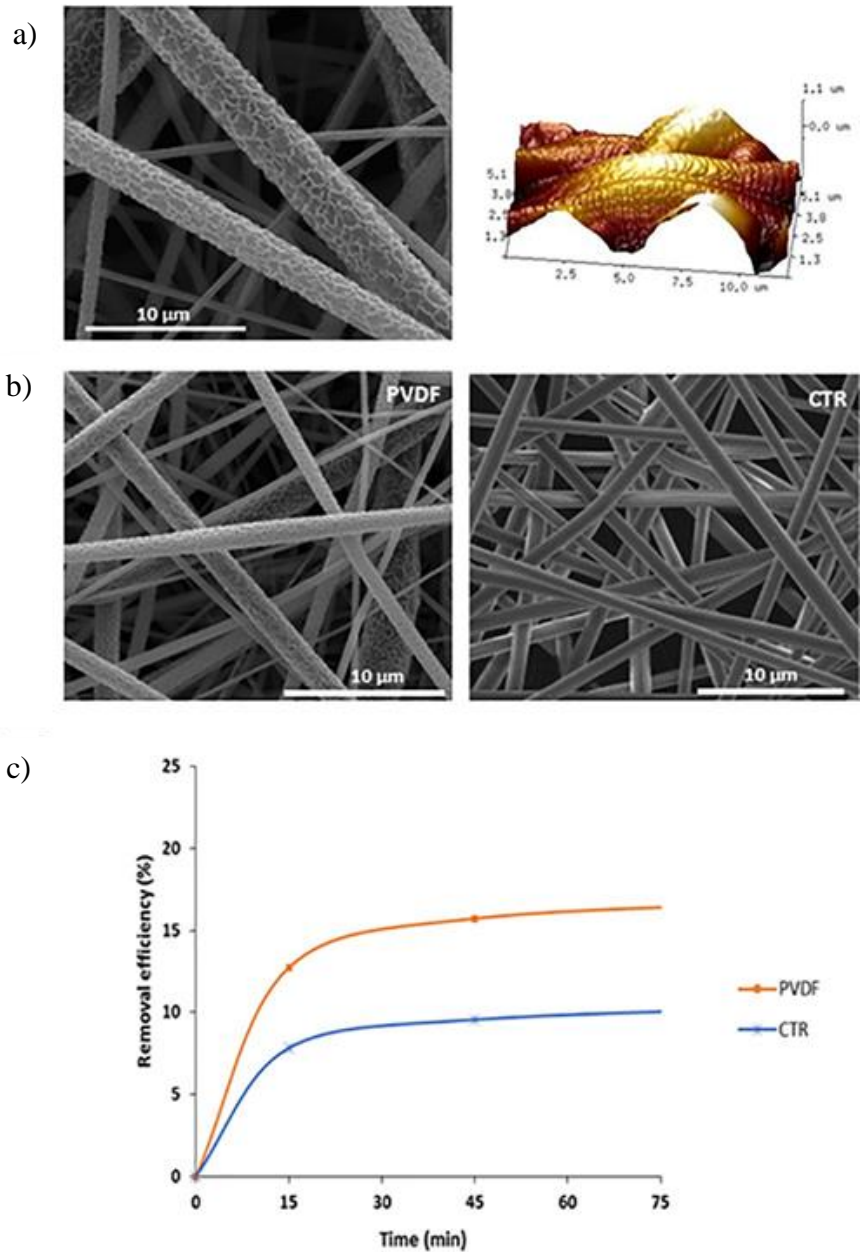


Figure 4.2 PVDF-TrFE electrospun fibers: Fiber surface and surface topography via SEM/ AFM (a); Comparison of PVDF-TrFE fiber mesh respect to control (CTR) (b); Adsorption curves (c).

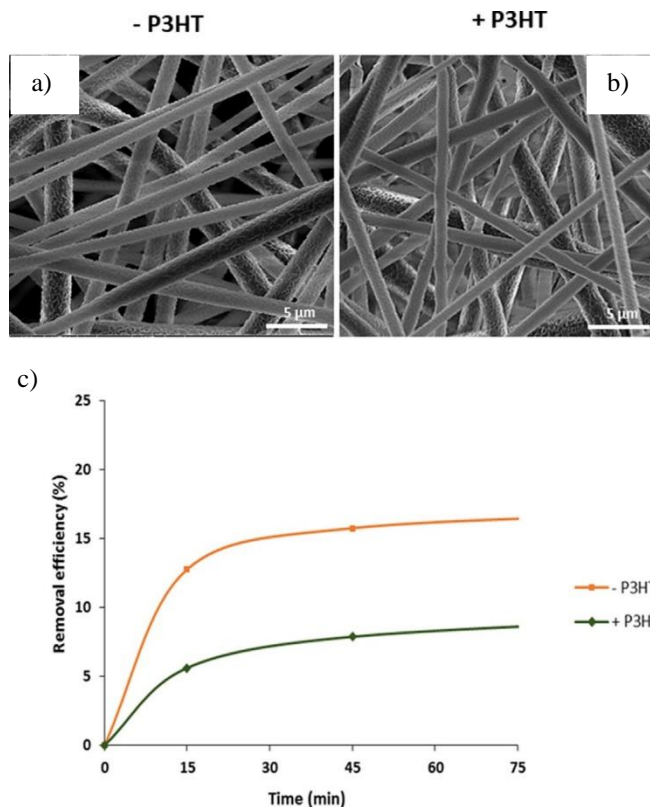


Figure 4.3 Effect of P3HT in PVDF-TrFE electrospun fibers: a, b) Morphological analysis via SEM (scale bar 5 mm); c) Adsorption curves.

In Figure 4.3, the morphology of P3HT/PVDF-TrFE electrospun fibers was reported. No significant differences in the surface (i.e., presence of pores) and fiber size were reported. Thus, we confirmed that the presence of P3HT, homogeneously mixed with the PVDF, does not interfere with evaporation mechanisms occurring during the fiber deposition. This effect was confirmed by image analysis data, showing an average diameter equal to 1.4 ± 0.4 mm; however, UV tests evidenced a mitigation of an adsorption mechanism of MB in the presence of P3HT (Figure 3c) as confirmed by the reduction of adsorption efficiency. It is assumed that P3HT may affect the adsorption of MB molecules, at the level of dipole–dipole interactions. Indeed, it is well known that the piezoelectric moment creates a dipole moment enhanced by the molecular poling generated by the electrospinning process ^[17]. The addition of P3HT domains into the fibers tends to interfere with these interactions, thus reducing the capability of MB molecular attraction.

Herein, it is also demonstrated that the application of an external voltage can contribute to modulate MB molecular adsorption through the fiber mesh. For this purpose, a tailor-made experimental system was realized to apply a positive HV equal to 10 kV to fibrous meshes, as schematically reported in Figure 4.1. Adsorption curves confirm MB interactions are affected by the externally applied electrical forces (Figure 4.4).

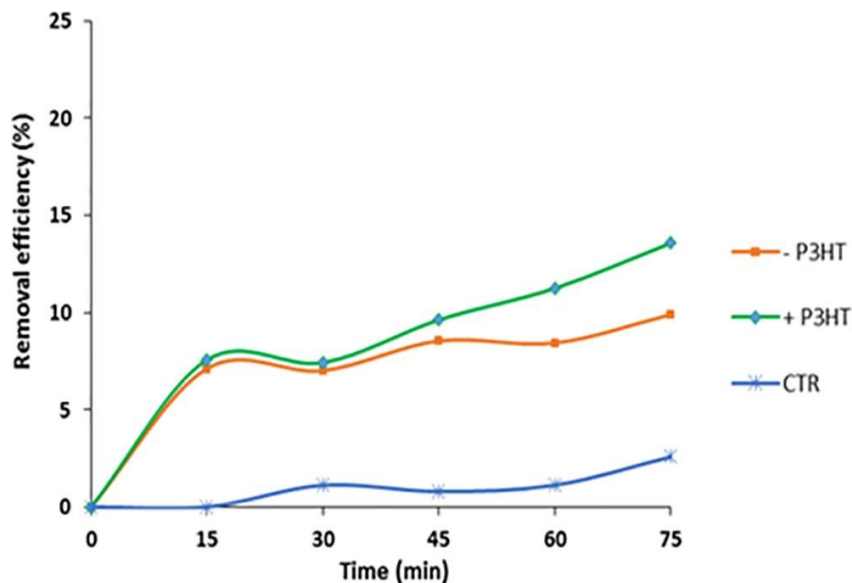


Figure 4.4 Effect of externally applied voltage on MB adsorption: Comparison of adsorption curves of PVDF-TrFE, P3HT/PVDF-TrFE electrospun fibers. PCL fibers (CTR) are reported as negative control.

P3HT is a well known p-type organic semiconductor and is characterized by high oxidation levels with higher p-type characteristics ^[20]. In the presence of externally applied electrical forces – in this case, a positive voltage – the oxidation from O₂ or H₂O increases this oxidation level (also known as doping effect) thus promoting the interaction with negatively charged molecules such as MB. Our result is consistent with recent studies on P3HT and PVDF-TrFE interpenetrating networks ^[21]. It confirms that applied voltage, acting on dipole-dipole interactions, actively contributes to the circulation of ion charges, thus ultimately influencing the adsorption of MB molecules.

4.1.8 Conclusions

In this work, the fabrication of P3HT/PVDF-TrFE electrospun nanofibers with selective adsorption of Methylene Blue from an aqueous solution was optimized. The electrospun nanofibers showed a pronounced surface roughness enhancing the ability of removing MB. The incorporation of the p-type polymer allowed tuning the molecular absorption in the presence of an electric field, changing the P3HT oxidation state. The data suggest fibers can lead to the design of new antibacterial membranes and filtering systems are able to tune the absorption of negatively charged molecules (i.e, MB or others) for environmental and biomedical applications.

4.2 Sensing Mechanisms of the Ladder Polymer Poly(benzimidazobenzophenanthroline) BBL

4.2.1 Abstract

For the first time, we report the sensing response and interaction mechanisms of the ladder polymer Poly(benzimidazobenzophenanthroline) (BBL) for different volatile organic compounds (VOC's). Our findings open a new window for applications involving ladder-like polymers for electronic devices. While this polymer has been previously characterized for field effect transistors (FET's) and solar cells (SC's) applications, sensors and its mechanisms have not been studied, making this work essential for the applications of this robust and electroactive ladder polymer.

4.2.2 Introduction

Poly(benzimidazobenzophenanthroline), or BBL for short, is a ladder polymer with excellent chemical and thermal resistance; it can be dissolved solely under strong acids and can be thermally degraded above 500°C, respectively. BBL thin films are highly organized in the polycrystalline regime and when characterized as an n-type polymer, have electron mobilities as high as 0.1 cm²/Vs. Commercial BBL can be effectively dissolved into methanesulfonic acid

(MSA) and casted or sprayed into thin films or nanoribbons. While no previous study on sensing mechanism have been performed, we have proceeded to characterize the thin film structure as the easiest and most reliable manner for device fabrication. However, other forms including the novel fabrication of pure BBL fibers has been studied for electronic device fabrication. These thin films from BBL/MSA solutions were spin coated at a velocity of 1000 rpm for 30 s. Films that were spin at higher rpm's produced noncontinuous films with pores formations. In past works, BBL solutions required extensive processes for thin film fabrication and removing the acid from the films into water with time frames of 12 to 24 hrs. Indeed, the thin films required vacuum (or hot plate) baking in the same range of time leading to the fabrication of devices ranging from 1 to 2 days. Our devices where immersed in ethanol and water for 5 min each, nitrogen drying for about 1 min, and vacuum oven at 200°C for 30 min.

4.2.3 Experimental

BBL was purchased from Sigma-Aldrich and used without further purification. The BBL was dissolved by using methanesulfonic acid (MSA) to form a 1wt% solution. No continuous films were achieved with solutions down to 0.3wt%. To enhance the “spreadability” of BBL/MSA, the prepatterned gold electrodes and the silicon dioxide (SiO₂) surface were cleaned by oxygen plasma. The interaction between SiO₂ and BBL is extremely poor, and the polymer can be easily removed by dipping the devices in ethanol and water; however, the surface interaction between BBL and gold is distinctively higher than the one mentioned before. Indeed, the BBL films on the gold surface and between the electrodes is not easily removed by ethanol and water, with no delamination during the preparation and characterization period as it shown in the corners of (a) through (c) in Figure 4.5.

For the device fabrication, interdigitated electrodes were evaporated by thermal evaporation of Ti (10nm) for gold (Au) adhesion and Au (90nm) as the main electrode. The interdigitated fingers are separated by 50 μ m (width) and 18.32 mm (length). Thin films thickness range between 50 nm to 200nm (Figure 4.5d).

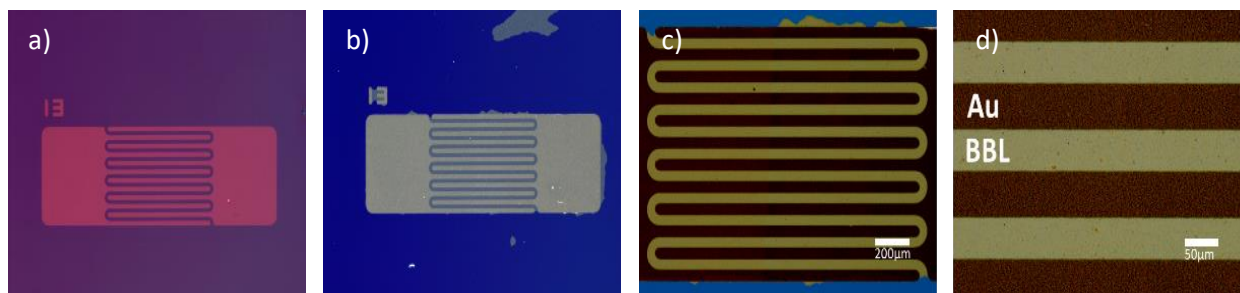


Figure 4.5 Device fabrication. BBL/MSA thin film after spin coating (a); Thin film consolidation after immersion in ethanol and water (b); Close up to the sensor active area after annealing (c) & (d). Scale bar of 200 μ m in (c) and 50 μ m in (d). Lighter stripes in (d) are BBL while darker stripes are the gold electrodes.

The films were consolidated and self-cleaned by immersing the devices into ethanol for 5 min, followed by deionized water for another 5 min, and finalized with blowing the samples with a bold nitrogen stream until a metallic golden luster, characteristic of BBL films, appears. In our approach, immersing the devices in water after spin coating, consolidate the BBL film by removing the acid. After periods above 30 s, the film self-detaches from the surface, however, undoing the devices. On the other hand, dipping the devices in ethanol for as long as 5 min, consolidates the film and those areas separated by gold at distances larger than 80 μ m, permit the film delamination, self-cleaning the devices matrices.

Deep drying and thermal annealing is performed using a vacuum oven at 200 $^{\circ}$ C for 30 min. After this procedure, the films were conductive, photoactive, and able to sense different volatile organic compounds (VOC's). No field effect behavior were characterized, however (i.e. Si wet oxide growth quality and incapability to properly attach to the SiO₂ surface).

To evaluate the VOC's sensing mechanisms, four distinctive analytes were used. This survey was performed using the smallest ketone, acetone; the simplest alcohol, methanol; 6 carbons alkane, n-hexane; and the simplest aromatic hydrocarbon, toluene. Two regions were characterized from the response plots and can be divided into surface and bulk interactions, as shown in Figure 4.6. The surfaces interactions are dominated by hydrogen bond forces between the carboxyl and imine group in BBL, which are hydrogen-bond acceptors, and the functional groups of the analyte molecules. For every analyte, the surface and bulk interactions lead to an increase in the current, by decreasing the film resistance. Indeed, in this case, fast saturating responses can relate solely to surface interactions (i.e. acetone and n-hexane). Therefore, slow saturating responses are due to surface and bulk interactions (i.e., methanol and toluene).

Incident light into the sensors produce photogenerated charges that increase the total current through the device; however, the sensitivity decreases when light is irradiated to the surface. This may be explained since the charge given by the analytes is constant while increasing the background charges with the photogenerated charges decrease the impact of the “partial analyte doping” onto the film.

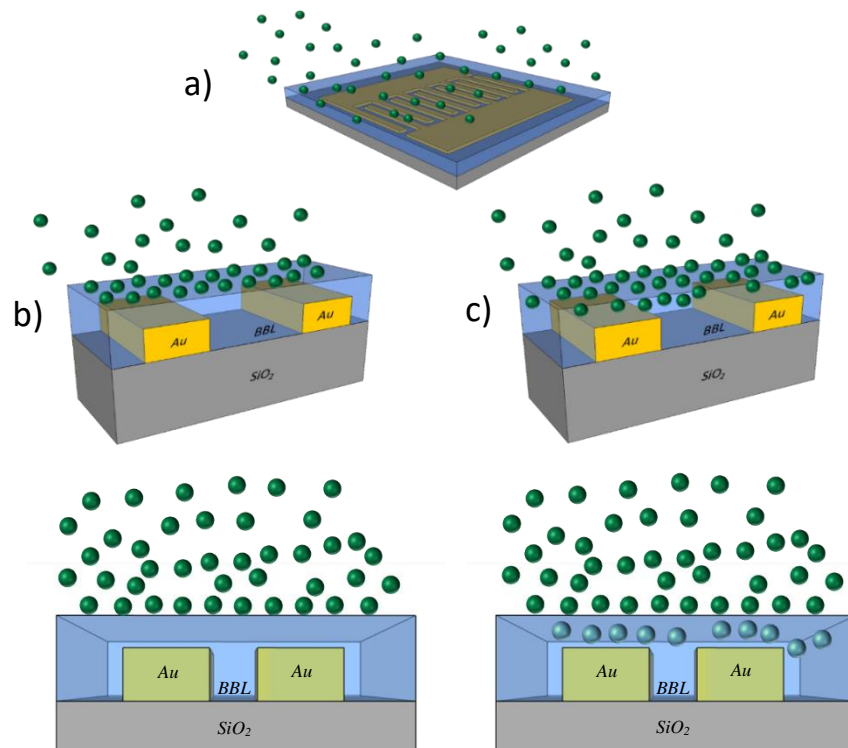


Figure 4.6 Sensor representation (a). Surface (b) and bulk (c) interactions of the analytes with the BBL film.

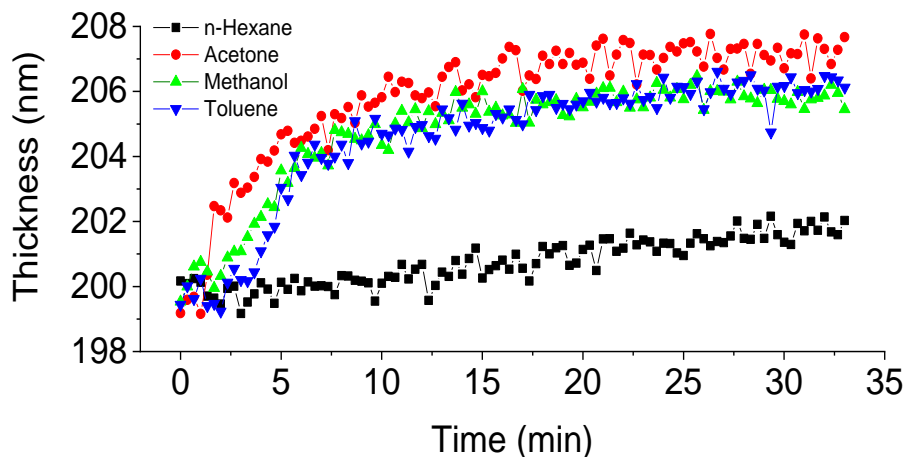


Figure 4.7 Film response for different analytes. The sensor was in the middle of a vapor chamber while the swelling process was measured using an optical thickness reader, recording the increase in thickness when the analytes impregnate the surface, and subsequently the bulk.

4.2.4 Discussion

The four analytes interact with the surface by hydrogen bonding between the analyte and the surface. It is important to denote that acetone, methanol, and toluene physically swells the film (6nm of 200nm) while n-hexane does not swell the film (less than 2nm of 200nm) as characterized in Figure 4.7.

All the analyte molecules lands over the surface, being the first point of contact and quickly doping the BBL film. To understand the absorption mechanism for each analyte, the film was subject to swelling due to exposition of an analyte saturated chamber for 30 min. The swelling response for acetone, methanol, and toluene is around 5 min (6 nm). For n-hexane, no sudden change in film thickness is recorded having a maximum change of 2nm in a ca. 30 min window. The recovery for all the analytes is ca. 20 s.

Acetone (ketone) dopes the film and saturates quickly when compared with Methanol and Toluene. It gets into the bulk by making hydrogen bonding with the carboxyl and N groups in BBL, leading to a film swelling. Indeed, hydrogen bonding between analyte molecules may decrease, therefore preventing analyte-analyte interactions. Since all the hydrogens in acetone are attached to carbons, it leads the BBL molecules to separate slightly (due to film swelling), partially weakening π - π interactions, decreasing the paths available for charge conduction, and therefore, saturating the response quickly.

Methanol (hydroxyl) lands on BBL surface doping the film and slowly saturating it (saturation regime not recorded in the used range). In this case, methanol, smaller than acetone, easily gets into the bulk doping the material (with two electron pairs each molecule). While methanol swells the film, there is a strong a hydrogen bonding interaction between the methanol molecules, which may explain the conductivity enhancement and the slow saturation process.

Toluene (aromatic) demonstrates the highest response in our characterizations. This is due to the aromatic ring, which may interconnect and enhance the π - π interactions increasing the film conductivity. For every aromatic ring, 3 electron pairs may be available for transfer, explaining the notable increase in current.

n-Hexane have shown to exert an interaction with the surface, leading to a charge conductivity in the interface. This is due to the hexane (n-hexane) molecular structure being the largest, with the smallest dipole moment and not swelling the film, leading us to believe that the whole interaction occurs on the surface of the film and only a small portion may interact with the outer part of the bulk. While no other sensing mechanism has been found on the literature regarding hexane and n-type polymers interactions, we suggest the charge transfer occurs in the interface between the analyte and the film.

Due to the increase in current for each sensing mechanism, the sensitivities were calculated using the equation 1:

$$Sensitivity = \frac{R_{N_2} - R_{gas}}{R_{gas}} \quad [1]$$

It can be denoted an increase in response under light conditions (530nm, 10W/cm²), with a decrease in sensitivity. This may be due to no charge interference between the photogenerated charges and the analyte charges. In this model, a constant analyte-related charge (for dark and for light) will be present in the film in comparison with the (3 orders of magnitude) high photogenerated current, therefore decreasing the sensitivity.

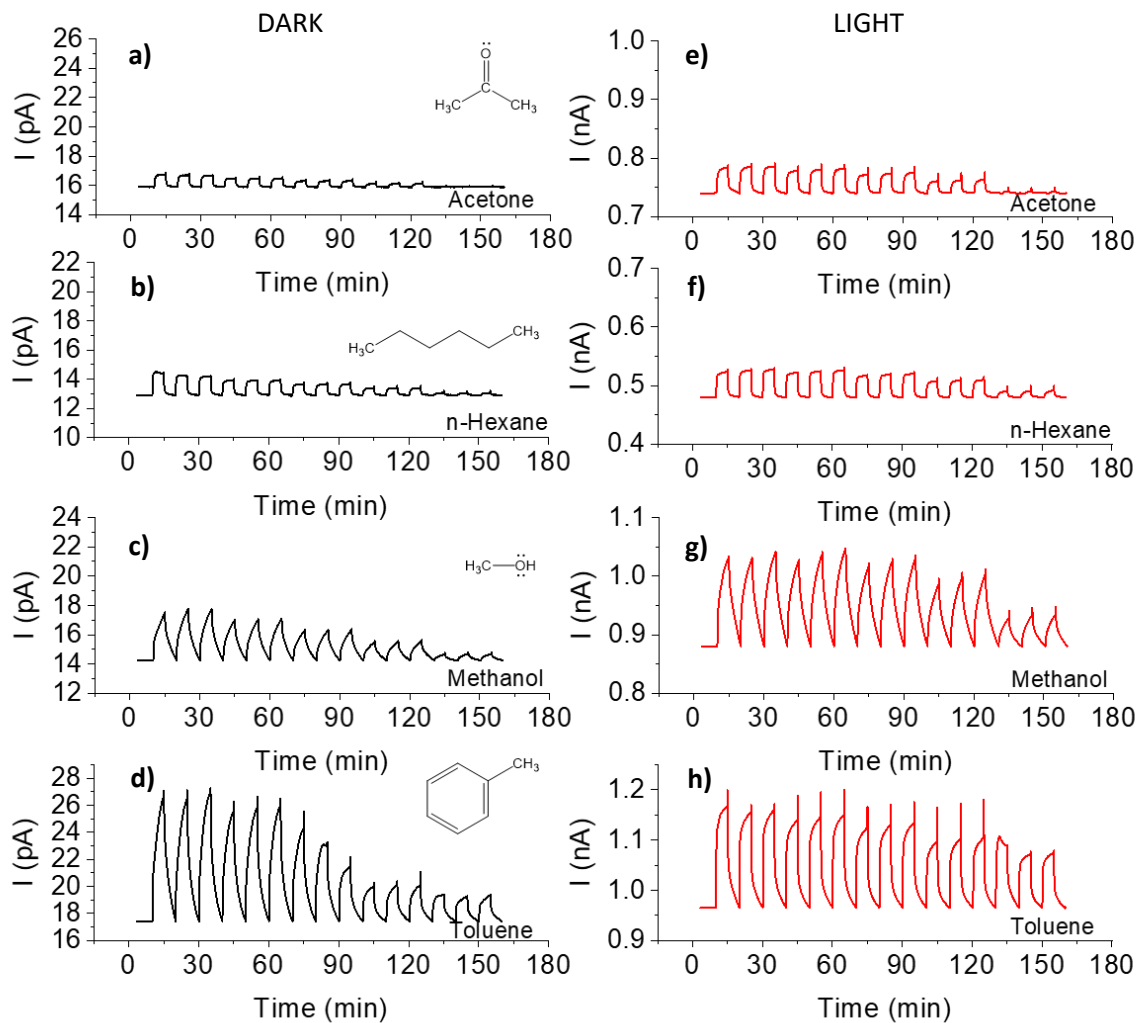


Figure 4.8 Sensor responses for the different analytes in dark (a-d) and under light conditions (e-h). Inset (a-d): molecular structures.

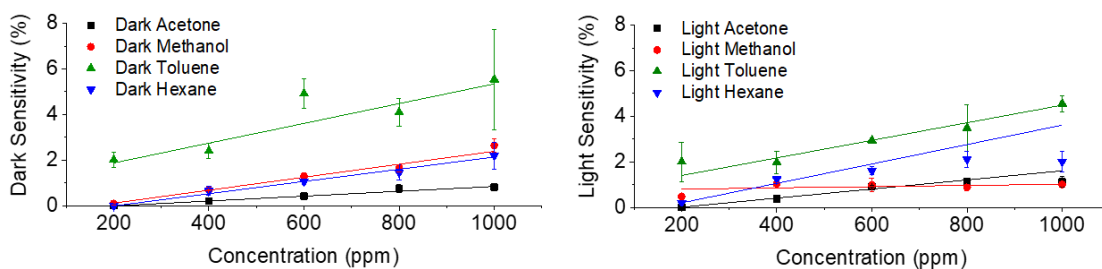


Figure 4.9 Sensitivities for dark and light conditions.

The introduction of the analyte into the chamber leads to a quick response that is almost similar for every volatile organic compound. The slope characterized by the response represents the rate of change in charge due to the analyte interaction with the surface. Positive slope denotes the introduction of charges in the film by the molecule-film interaction. Negative slope represents the molecule rate removal from the film. Saturation and Relaxation are mostly constant for every concentration since no more molecules are added or removed from the film. However, the sensitivity mostly has a linear relationship with the response slope.

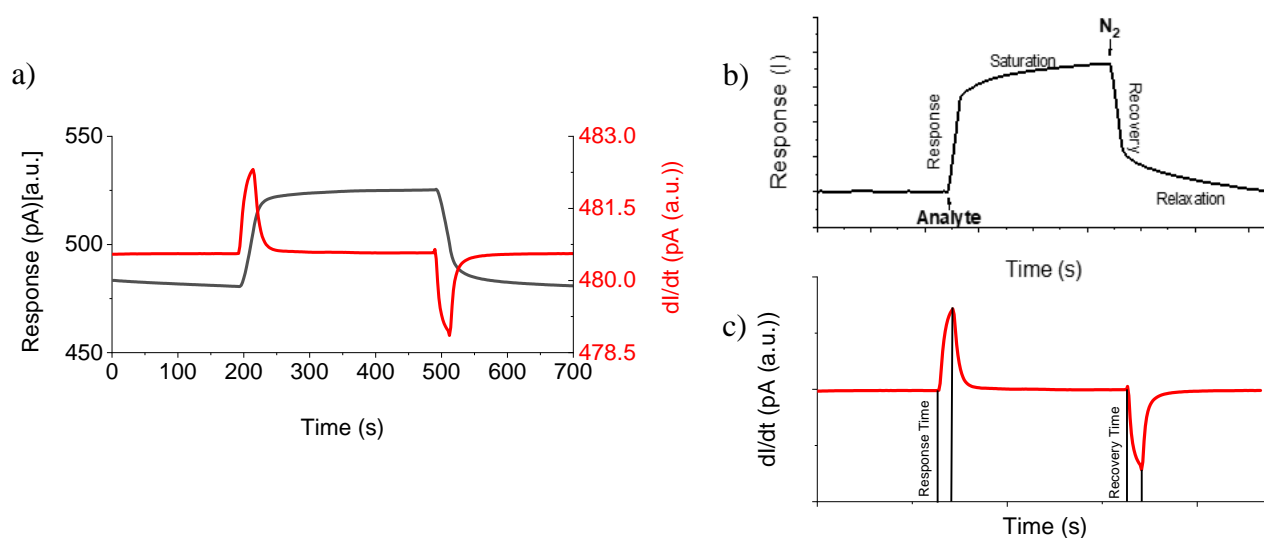


Figure 4.10 Example of sensing cycle for acetone (a). Current vs. time plot with response, saturation, recovery, and relaxation sections (b). Change in current vs. time plot representing the response and recovery time (c).

The analyte response is divided into two mechanisms: surface interaction and bulk absorption. A representation of this analysis can be seen in Figure 4.6. While the surface interaction is dominated by hydrogen bonds interactions and Van der Waals forces, the hydrogen bonds interactions also lead to bulk interactions leading to film swelling. For our response characterization, we have defined it as “the time required for the analytes to interact with the film surface, decreasing the film resistance sufficient to observe a change in conductivity”. More concisely, we can say “the minimum amount of time to sense X analyte”. This behavior is directly

related to the 1st derivative of the sensor response which shows the abrupt change (peak) in charge in the film. This method for characterizing the time responses (which here is the minimum time necessary to denote a change) works for every analyte regardless of the sensing mechanism. In a more general approach, for each cycle, the first derivative has two peaks, one maxima (peak) and one minima (recovery). Time response is the time value at the height of the curve's peak minus the time value just before the analyte interact with the surface. Recovery time is the time value of the minima, minus the time value just before the analyte is removed from the surface.

4.2.5 Conclusion

BBL based vapor sensors have been tested with different analytes reaching concentrations down to 200ppm. The vapors were carefully selected to represent functional groups of common solvents like ketones (i.e Acetone), alcohols (i.e. Methanol), aromatic (i.e. Toluene), and alkane (i.e. Hexane). For all characterizations, the devices showed a decrease in charge distribution while decreasing the incident concentration (from 1000 to 200ppm). We have proposed a sensing mechanism where the analytes increase the carrier concentration of the n-type semiconductor after van der Waals/surface interactions. While dark measurements reveal the sensing mechanism in the picoampere (pA) range, the practicality of the sensor can be enhanced by regenerating photoexcited carriers (by incident light). Counterintuitively, we have also shown that the sensing ability is independent of the total amount of charge carriers. Indeed, photogenerated carriers may be independent of the induced charges by each analyte. This matter has to be carefully studied.

4.3 References

1. J.M. Laine, D. Vial, P. Moulart, *Desalination* 131 (2000) 17–25.
2. P. Le-Clech, V. Chen, T.A. Fane, *J. Membr. Sci.* 284 (1) (2006) 17–53.
3. V. Guarino, A. Varesano, *Filtering Media Electrospinn.* (2018) 1–24.

4. R. Wang, Y. Liu, B. Li, B.S. Hsiao, B. Chua, *J. Membr. Sci.* 392 (2012) 167–174.
5. D. Bjorge et al., *Desalination* 249 (3) (2009) 942–948.
6. J. Bae, I. Baek, H. Choi, *Chem. Eng. J.* 307 (2017) 670–678.
7. J.K. Krinks et al., *J. Membr. Sci.* 494 (2015) 130–135.
8. P.A. Jacobson, L.G. Rosa, K. Kraemer, P. Ducharme, S. Dowben, *Mater. Lett.* 61 (2007) 1137–1141, <https://doi.org/10.1016/j.matlet.2006.06.073>.
9. J.H. Lee, K.Y. Lee, B. Kumar, N.T. Tien, N.E. Lee, S.W. Kim, *Energy Environ. Sci.* 6 (2013) 169–175.
10. S. Ludwigs, *Advances in Polymer Science* 265, Springer, Verlag Berlin Heidelberg, 2014.
11. W. Serrano, A. Meléndez, I. Ramos, N.J. Pinto, *Polym. Int.* 65, 503–507 (2006)
12. P.R. Berger, M. Kim, *J. Renew. Sustain. Energy*, 10, 013508 (2018)
13. W. Serrano, N. Pinto., *Ferroelectrics* 432:1, 41-48, 2012.
14. K. Alexandros, G. Katsogiannis, G.T. Vladislavljevic´, S. Georgiadou, *Eur Polym J* 69 (2015) 284–295.
15. V. Guarino, L. Ambrosio. *Proc Inst Mech Eng H* (2010), 224, 12, 1389-1400.
16. A. Rajjak, S.H. Karkhanechi, T.Yoshioka, H. Matsuyama, H. Takaba, D-M Wang. *J. Phys. Chem. B*, 2018 1226, 1919-1928
17. C. Morel-Salmi, A.J.C. Vigor, J. Vercauteren, A. Hüge, *Chromatographia* 77 (13– 14) (2014) 957–961.
18. J.P. Arenas, J.P. Arenas, M. Crocker, M. Crocker, *Sound Vibrat.* 44 (7) (2010) 12–17.
19. I. Fasolino, V. Guarino, V. Cirillo, L. Ambrosio, *J. Biomed. Mater. Res.* 105A (9) (2007) 2551–2561.

20. X. Chen, X. Han, Q.-D. Shen, *Adv. Electron. Mater.* 3 (2017) 1600460.

21. K. Asadi, D.M. De Leeuw, B. De Boer, P.W.M. Blom, *Nat. Mater.* 7 (2008) 547.

Chapter 5: Fabrication and Characterization of P3HT/BBL Coaxial Nanofibers

5.1 Electrospinning Fabrication of Coaxial Semiconductive Organic Nanofibers for Flexible, Multifunctional Electronic Devices

5.1.1 Abstract

Intelligent textiles, air/water filters, bone scaffolds, and drug delivery applications have all directly benefitted from the development of the reliable and low-cost electrospinning technique for fiber fabrication. This technique has also been successfully used to fabricate fibrous electronic devices. Diodes, field effect transistors, and sensors using organic semiconductive polymers offer unique characteristics found only in such polymers (e.g., excellent thermal stability, tunable electrical conductivity, mechanical flexibility, and chemical/biological functionality). In this work, the electrospinning technique is used to fabricate, for the first time, a polymer-polymer coaxial-structure nanofiber from the p-type regioregular polymer poly(3-hexylthiophene-2,5-diyl) (P3HT) and the n-type conjugated ladder polymer poly(benzimidazobenzophenanthroline) (BBL). The P3HT was successfully used as the core and the BBL as the shell, thus forming a p–n junction that is cylindrical in form. This work expands the current knowledge of organic electroactive polymer structures for efficient coaxial flexible arrays, thus advancing the state-of-the-art for fiber-based devices.

5.1.2 Introduction

Organic semiconductive polymers are known to have well known thermal stability,^[1] electrical conductivity,^[2] mechanical flexibility,^[3] and chemical/biological functionality.^[4] Polymeric coaxial arrangements have been researched for use in drug delivery and hollow fiber

channels. ^[5] Previous work has also been reported on organic semiconducting p-n junction nanofibers in a coaxial core-shell (core-sheath) structure but with a focus on small-molecule (organic–organic) heterojunctions and partial organic (organic/polymer–inorganic) heterojunctions, rather than polymeric heterojunctions. ^[6] Polymer-polymer heterojunctions have not yet been fabricated. ^[7]

Based on this previous work, we expect organic semiconductive coaxial nanofibers will produce p-n junctions with enhanced electronic properties and fabrication reliability, thus making them excellent candidates for use in flexible electronics, crosslinking, and cost-effective nanomanufacturing. ^[8] More specifically, these novel organic semiconductive p-n junctions have the potential to demonstrate high I_{on}/I_{off} ratios, and in field-effect transistor (FET) mode, a reduction in leakage current compared to thin film structures. In diode mode, a tunable depletion region can be achieved by the phase created by the outer covering. Therefore, due to the large surface area that can be generated by nanofibers (non-woven mesh or aligned nanofibers) in a small region, a coaxial p-n junction matrix will be capable of performing as a sensor. As a result, the surface of the nanofibers can be functionalized for specific sensing and higher selectivity, improving the performance for electronic applications. ^[9]

Nanofibers of the semiconductive regioregular polymer poly(3-hexylthiophene-2,5-diyl) (P3HT, with field effect mobilities as high as $0.1 \text{ cm}^2\text{V}^{-1}\text{s}^{-1}$)^[10] and thin films, as well as self-assembled nanobelts, of the ladder polymer poly(benzimidazobenzophenanthroline) (BBL, with electron mobilities of approximately $1 \times 10^{-3} \text{ cm}^2 \text{ V}^{-1} \text{ s}^{-1}$ and $7 \times 10^{-3} \text{ cm}^2 \text{ V}^{-1} \text{ s}^{-1}$, respectively)^[11] have been previously characterized as having morphologies and high-mobility behaviors that make them ideal candidates for organic electronics. ^[12] However, fiber fabrication of pure P3HT is challenging (due its low molecular weight ^[13]), and under laboratory conditions, this material tends

to degrade over time due to oxygen exposure.^[14] BBL, on the other hand, has been shown to exhibit high stability in air over a long period of time, thus improving the shelf life of the formed devices.^[15] Polystyrene (PS) can be used to facilitate the formation of P3HT fibers.

The goal of this work is to investigate the utility of organic semiconductive polymers (specifically, P3HT and BBL) in forming one-dimensional (1D) coaxial p-n junctions that can lead to the miniaturization of organic electronics. The expectation is that devices can directly be tethered in a single functional fiber possibly increasing the efficiency and even lowering power requirements for textile applications. More broadly, this research seeks to address the technological challenges of using nanoelectronics and nanosensors for flexible, low power nanodevices (e.g., tethered and 1D components for chemical, vapor, and gas sensing) by enhancing the nanometric morphology of the coaxial structure.^[16]

The specific aim of this process is to produce a nanofiber with a P3HT/PS core and a protective, electrically active outer shell or sheath of BBL. The novelty of the approach lies in its polymer-polymer structure and its electrospinning-based fabrication process. The present study thereby advances the simplicity regarding the use of organic semiconducting nanodevices for flexible electronics and multi-dimensional integrated circuits.

5.1.3 Experimental

Electronic grade p-type regioregular poly(3-hexylthiophene-2,5-diyl) (P3HT) ($M_w > 45,000$) from Lumtec, n-type polymer poly (benzimidazobenzophenanthroline) (BBL) and polystyrene (PS) ($M_w = 350,000$), both from SigmaAldrich, (Figure 5.1) were used as received. Solutions of anhydrous chloroform (CHCl_3) were used to dissolve the P3HT and PS (and to allow for subsequent optical characterization); methanesulfonic acid (MSA), from SigmaAldrich, was used to dissolve the BBL. Solutions were prepared based on weight percent (wt%). For the core-

material solution of P3HT/PS, 7 wt% PS/CHCl₃ was used to lend mechanical support to the P3HT molecules; the final concentration of P3HT in the P3HT/PS/CHCl₃ blend was 0.4 wt%. For the shell-material solution, 0.39 wt% BBL was dissolved in MSA. Each of the two solutions were thoroughly blended with a magnetic stirrer until homogeneous equilibria was achieved.

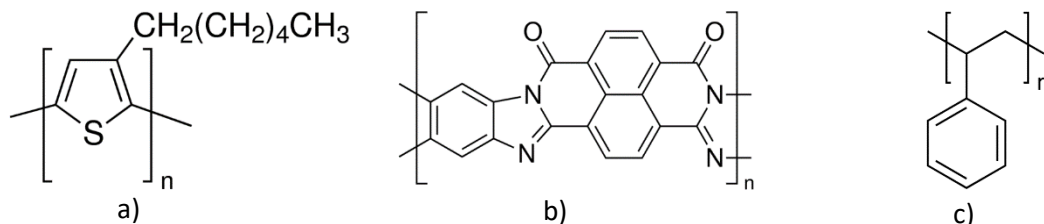


Figure 5.1 Coaxial nanofiber fabricated using P3HT (a) and BBL (b) as the semiconducting polymers. Because pure P3HT is unable to form fibers (due its low molecular weight), PS (c) was added to improve mechanical support for fiber formation.

PS dissolved in chloroform is colorless; adding P3HT, which is red, imparts a red color to the solution blend. Dissolving BBL in MSA yields a dark red solution; with continued processing with CHCl₃, BBL changes to a vivid blue-violet color.^[17] UV-VIS spectra were obtained (using an Evolution 201 PC spectrometer) for the solutions of pure PS, pure P3HT, blended P3HT/PS, and pure BBL, to achieve the optical distinguishable characteristics of the material solutions.

To form the coaxial nanofibers (Figure 5.2) from these solutions, the electrospinning technique was employed (Figure 5.3), using two luer-lock syringes and a coaxial needle (Ramé-Hart Instrument Co.). The gauge sizes were 23G for the core material and 18G for the shell material. The coaxial needle functioned as an anode, and a sheet of aluminum foil served as a grounded cathode. A programmable syringe pump (pump rate = 3000 $\mu\text{L hr}^{-1}$) was used to maintain a slow, steady flow of the polymeric solutions into the electric field. This setup resulted in the polymers forming a Taylor cone jet that continuously moved toward the cathode. Fibers

were formed when a critical voltage of 9 kV overcame the polymer surface tension — stretching the material, enhancing solvent evaporation, and forming the coaxial nanofibers. The fibers were collected (i.e., attracted and deposited) onto the aluminum foil.

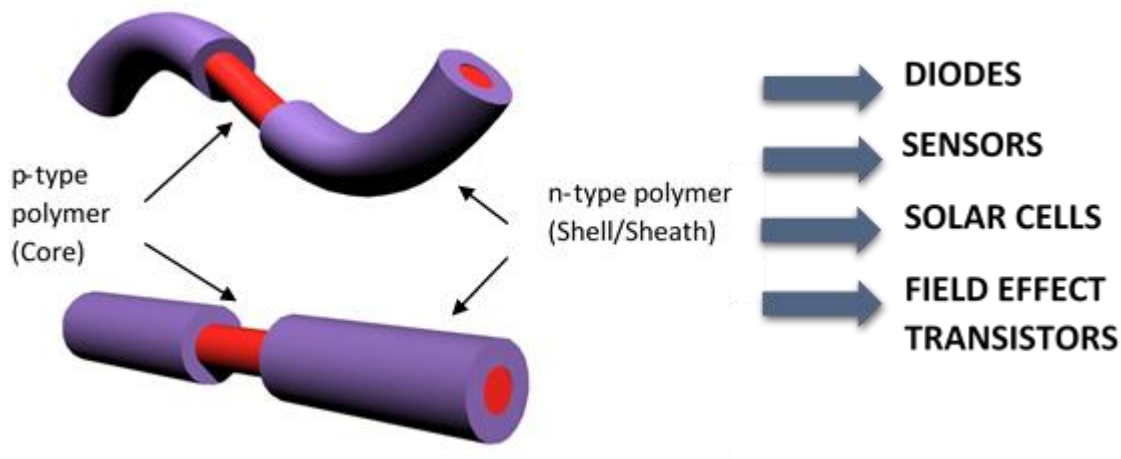


Figure 5.2 Coaxial nanofiber with p- and n- type semiconducting polymers. This nanofiber provides an opportunity to form p-n junctions that can be tethered for electroactive textiles and single-nanofiber devices.

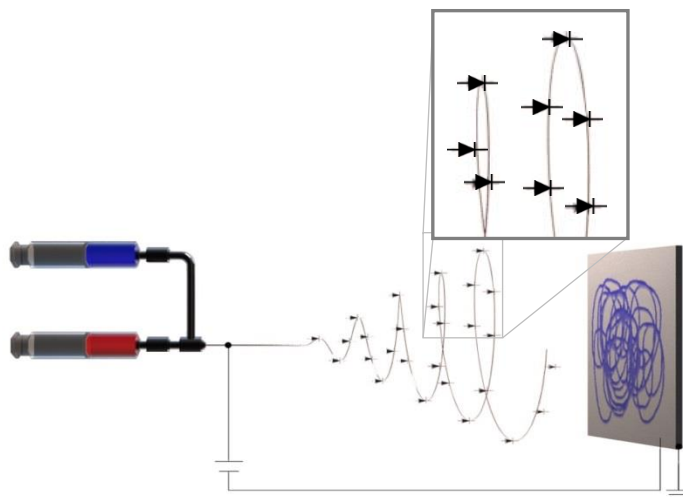


Figure 5.3 Continuous fabrication of coaxial nanofiber p-n junctions, using the electrospinning technique. The BBL solution (a, blue) forms the shell/sheath, and the P3HT/PS solution (b, red) forms the core. An electric field overcomes the surface tension, stretching the solution and forming nanofibers. Inset: magnification (c) after the Taylor cone formation, with the diode symbols representing the continuous heterojunction formed between the core and the shell.

For topological characterization of the nanofibers, transmission electron microscope (TEM) grids with $50 \times 50 \mu\text{m}$ apertures were passed near the cathode in a weaving motion to collect in-air nanofibers. These fiber samples were first rinsed gently with deionized water to remove any residue of MSA from the surface and then dried for 15 min at $70 \text{ }^\circ\text{C}$ prior to characterization. Images were taken with a TEM (Phillips FEI Morgagni M 268).

5.1.4 Results and Discussion

In this process, coaxial semiconductive polymer-polymer nanofibers were, for the first time, fabricated and morphologically characterized. The homogeneous composite P3HT/PS served as the core and the BBL solution formed the shell, thereby achieving the desired structure (Figure 5.2). The p-n junctions thus formed can perform as diodes ^[18], sensors ^[19], and transistors ^[20] as well as photodiodes for solar cell applications ^[21].

At low concentrations of P3HT, it is difficult for the electrospinning technique to generate well-formed fibers. This difficulty is due to low molecular weight hindering the formation of molecular entanglements. This, results in a solution extensional viscosity too low to form fibers. To overcome this impediment, PS was added to the P3HT solution to provide mechanical support for fiber formation without compromising the semiconductive property of P3HT ^[22]. At 7 wt% PS, the solution was sufficiently viscous and electrically charged by the P3HT such that core fibers with a diameter of 200 nm were formed. The BBL solution required no additional polymer for fiber production; the PS in the core-material solution did indirectly help to form and support the final structure. This method could also make the PS fiber composite electroactive as the semiconductor carrier. ^[23] As noted above, the PS and P3HT polymers were dissolved in CHCl_3 . BBL does not dissolve in CHCl_3 , resulting in the extrusion of uniformly coated BBL shell and

P3HT/PS core nanofibers (Figure 5.3) moving from a viscous to a flexible state, to solvent evaporation and stretching to form a polymer-polymer coaxial nanofiber.

The UV/VIS spectrum of the P3HT/PS polymer composite was compared to the spectra of the pure (in CHCl_3) PS and P3HT solution (Figure 5.4). Over the wavelength range examined, the spectrum of the colorless PS solution is featureless. The P3HT solution exhibits an absorption peak at approximately 450 nm, as does the P3HT/PS blend. This peak is attributable to the π - π^* transition of the electronic absorption spectra, as previously documented for pure P3HT^[24]. The coincidence of these peak positions indicates that the PS and P3HT polymers are homogeneously integrated within the blend solution, without phase separation or chemical interaction. Measuring the UV/VIS spectra in this way also enabled the BBL to show the absorption peak defining its optical band gap. The BBL spectrum showed a peak at approximately 380 nm and a wider peak at approximately 540 nm. This is consistent with previous results,^[25] due to the onset of π - π^* transition; this spectrum is characteristic of this ladder polymer^[26]. These π - π^* transitions determine the band gaps of P3HT and BBL, which are generally 2.2 eV and 1.9 eV respectively,^[27] in agreement with the optical band gap cutoff values determined from the UV-VIS spectra shown in Figure 5.4.

While the P3HT/PS blend solution showed no evidence of separation or precipitation, the combined solutions of P3HT/PS and BBL were heterogeneous because BBL is insoluble in CHCl_3 and P3HT is insoluble in MSA. These characteristics led to the successful formation of nanometric coaxial fibers. TEM images of the fibers show well-formed core and shell structures (Figure 5.5). The smallest nanofiber examined had a total diameter of approximately 225 nm, with a core diameter of approximately 194 nm and a stable BBL shell thickness of 31 nm.

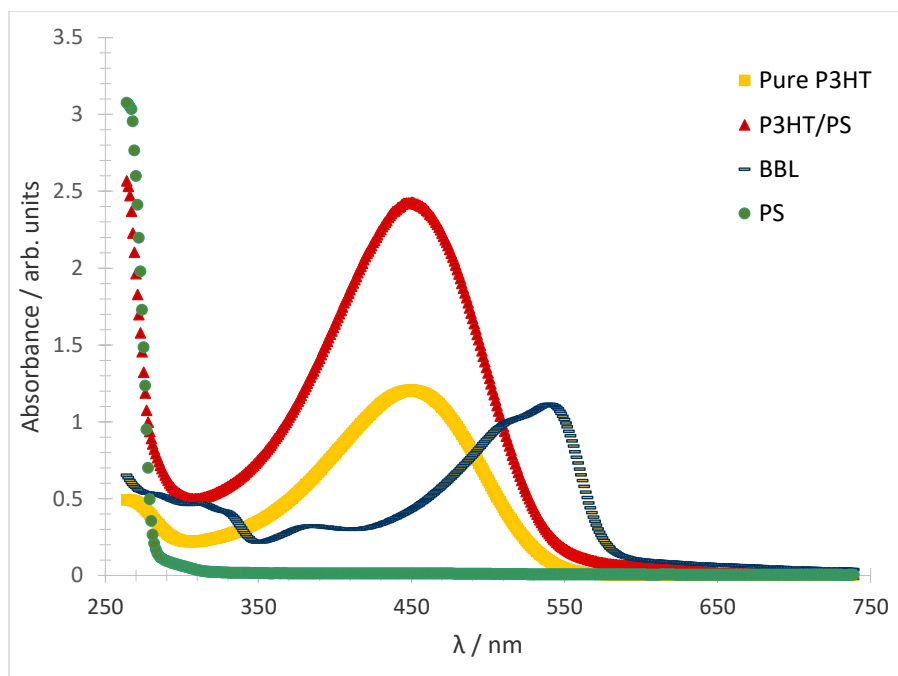


Figure 5.4 Comparison of the UV/VIS spectra of pure PS (7wt%), pure P3HT (2wt% in CHCl_3), and the P3HT/PS (0.4wt% / 7wt%) blend indicates that adding polystyrene does not change the physical or optical characteristics of P3HT. The BBL solution (0.39wt%) exhibits its characteristic broad absorption peak at approximately 540 nm.

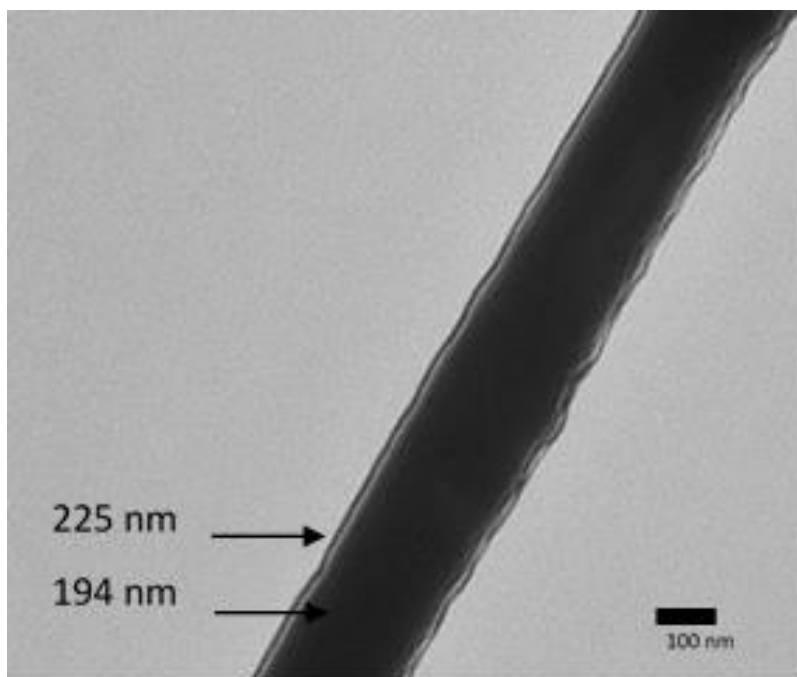


Figure 5.5 TEM image of a coaxial nanofiber with a P3HT/PS (0.4 wt%/7 wt%) core and a BBL (0.39 wt%) shell. This nanofiber was the smallest one examined. The scale bar is 100nm.

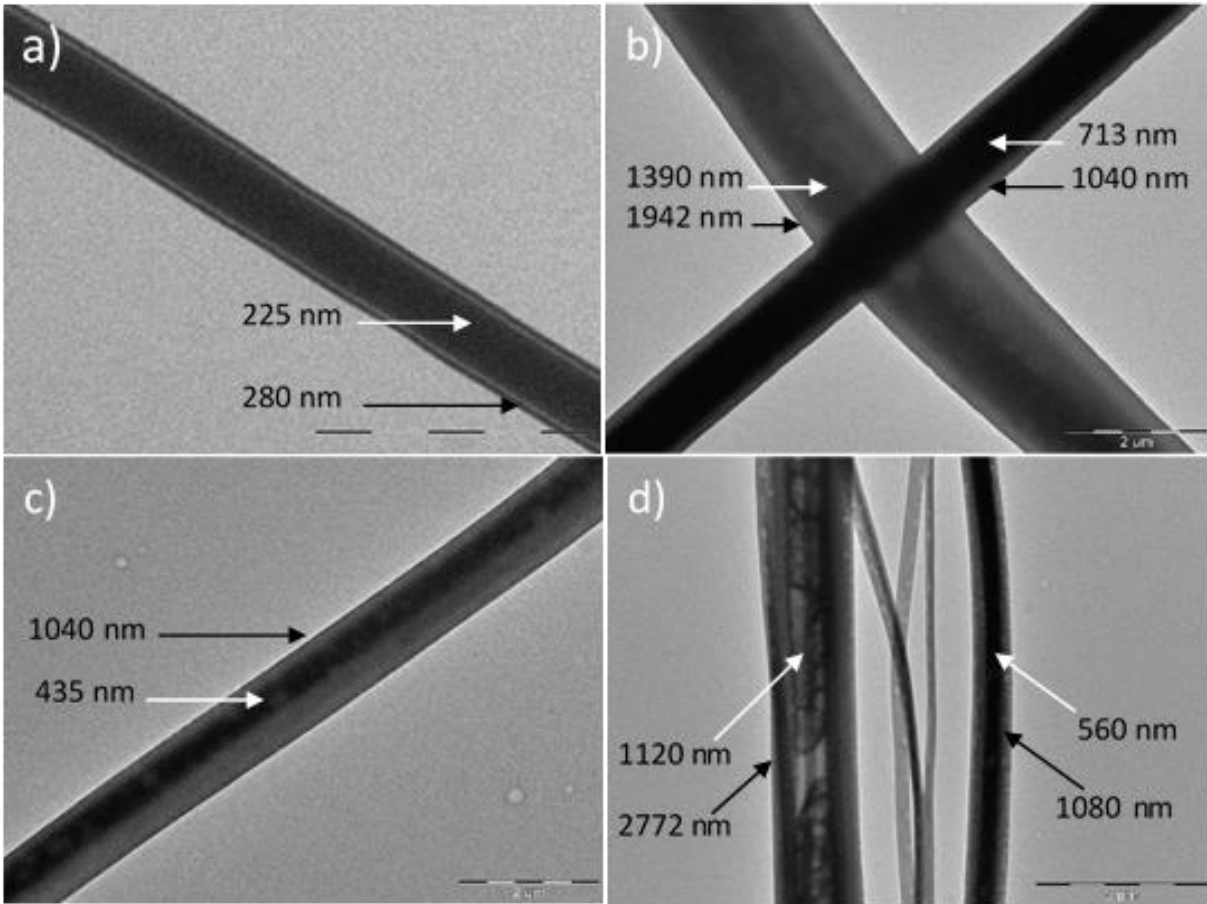


Figure 5.6 TEM images of coaxial nanofibers [P3HT/PS core (white arrow) with BBL shell (black arrow)] created simultaneously within a single run of the electrospinning technique. Scale bars are 1 μm (a), 2 μm (b, c) and 5 μm (d).

With the electrospinning technique, a variety of fiber sizes can be generated within a single production run; however, the diameters of the coaxial nanofiber can be controlled (e.g., concentration of the solutions, molecular weights, pump rate). Figure 5.6 shows electrospun fibers from a single run, with outside diameters ranging from approximately 280 (a) to 2772 (d) nanometers. The variety of sizes is due to weak agglomeration at the syringe tip, which slightly changes the material extrusion into the electric field. A subsequent production run can yield coaxial nanofibers with a similar range of diameters. Future work will aim to fabricate nanofibers of a single, specific diameter.

5.1.5 Future Work

This work focused on the fabrication parameters of the semiconductive polymer-polymer coaxial fibers; in future work, electrical characterizations involving AFM, photoconductivity, and I-V (Figure 5.7) will be performed. MSA will be used to remove the outer BBL layer and expose the P3HT nanofiber core without damaging it. A small amount of acid will be drop casted with microliter pipette onto the ends of nanofibers mounted on a silicon-silicon dioxide wafer. After rinsing the fibers with deionized water, gold electrodes can be added, and electrical characterizations for diode, FET, and sensor capabilities (e.g., organic gases, UV radiation) can be performed. We expect that this coaxial structure will not only support the development of flexible, multifunctional electronic devices, including tunable diodes for UV radiation detectors and rectifiers for integrated intelligent textiles, but will also be able to sense, communicate and generate its own energy, all in a single nanofiber. The ability to use the electrospinning technique to make electroactive coaxial nanofibers from novel organic polymer-based structures will have profound implications for the construction of the mentioned electronic devices.

5.1.6 Conclusions

We have described here for the first time the electrospinning fabrication of pure-polymer, composite coaxial P3HT/PS–BBL fibers to form a p-n junction coaxial structure. The electrically active materials used in this work is the electronic grade, regioregular P3HT and the ladder polymer BBL, with PS providing mechanical support for the thin fiber P3HT core. UV-VIS analysis shows that no chemical or physical changes occurred when the P3HT was blended with the PS. Strategic solvent selection ensures the formation of electrospun fibers that are simultaneously coated with a protective BBL shell. TEM imaging characterizations shows that the formed composite fibers had diameters ranging from approximately 280 to 2772 nm.

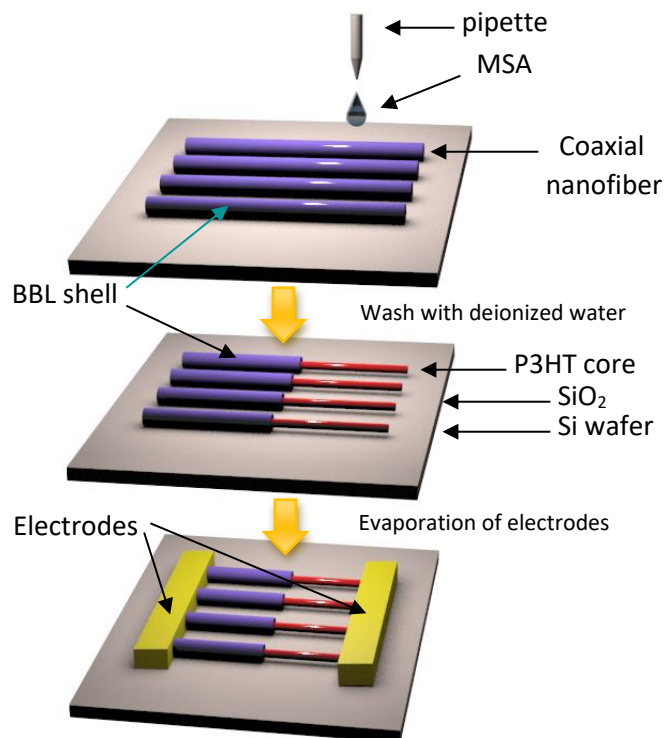


Figure 5.7 Future work, electrical characterizations will be performed by using a small amount of MSA to remove the BBL shell and expose the P3HT core. Electrodes will be evaporated at the shell and the core. The resulting devices are expected to work as diodes, FETs, and sensors, as well as photoactive devices for organic solar-cell meshes.

5.2 References

1. W. Ma, C. Yang, X. Gong, K. Lee, Alan J. Heeger, *Adv. Funct. Mater.* 2005, 15, 1617.
2. a) K. Fukuda, Y. Takeda, M. Mizukami, D. Kumaki, S. Tokito, *Scientific Reports* 2014, 4, 3947; b) A. Luzio, E. V. Canesi, C. Bertarelli, M. Caironi, *Materials*. 2014, 7, 906.
3. a) A. T. Kleinschmidt, S. E. Root, D. J. Lipomi, *J. Mater. Chem.* 2017, 5, 11396; b) H. C. Chang, C. L. Liu, W. C. Chen, *Adv. Funct. Mater.* 2013, 23, 4960.
4. a) M. Irimia-Vladu, *Chem. Soc. Rev.* 2014, 43, 588; b) G. Jin, M.P. Prabhakaran, D. Kai, M. Kotaki, S. Ramakrishna, *Photochem. Photobiol. Sci.* 2013, 12, 124.
5. a) V. Guarino, R. Altobelli, V. Cirillo, A. Cummaro, L. Ambrosio, *Polym. Adv. Technol.* 2015, 26, 1359; b) A. K. Moge, B. S. Gupta, *Polym. Rev.* 2008, 48, 353.

6. a) Q. Li, S. Ding, W. Zhu, L. Feng, H. Dong, W. Hu, *J. Mater. Chem. C* 2016, 4, 9388.
7. a) G. Jin, M.P. Prabhakaran, D. Kai, M. Kotaki, S. Ramakrishna, *Photochem. Photobiol. Sci.* 2013, 12, 124.
8. A. T. Kleinschmidt, S. E. Root, D. J. Lipomi, *J. Mater. Chem. A* 2017, 5, 11396.
9. R. Gonzales, N. J. Pinto, *Synth Met* 2005, 151, 275.
10. J. F. Chang, B. Sun, D. W. Breiby, M. M. Nielsen, T. I. Sölling, M. Giles, I. McCulloch, H. Sirringhaus, *Chem. Mater.* 2004, 16, 4772.
11. a) A. Babel, S. A. Jenekhe, *JACS* 2003, 125, 13656; b) A. L. Briseno, S. C. B. Mansfeld, P. J Shamberger, F. S. Ohuchi, Z. Bao, S. A. Jenekhe, Y. Xia, *Chem. Mater.* 2008, 20, 4712.
12. a) A. Babel, S. A. Jenekhe, *JACS* 2003, 125, 13656; b) W. Serrano, N. J. Pinto, *Ferroelectrics* 2012, 432, 41; c) W. Serrano, A. Meléndez, I. Ramos, N. J. Pinto, *Polym Int* 2016, 65, 503.
13. a) H. S. Yoo, T. G. Kim, T. G. Park, *Adv. Drg. Deliv. Rev.* 2009, 61, 1033.
14. a) M. O. Reese, A. J. Morfa, M. S. White, N. Kopidakis, S. E. Shaheen, G. Rumbles, D. S. Ginley, *Solar Energy Mater & Solar Cells* 2008, 92, 746.
15. a) A. L. Briseno, F. S. Kim, A. Babel, Y. Xia, S. A. Jenekhe, *J. Mater. Chem.* 2011, 21, 16461.
16. a) J. E. Anthony, *Nat. Mater.* 2014, 13, 773.
17. A. L. Briseno, S. C. B. Mansfeld, P. J Shamberger, F. S. Ohuchi, Z. Bao, S. A. Jenekhe, Y. Xia, *Chem. Mater.* 2008, 20, 4712.
18. N. J. Pinto, K. V. Carrasquillo, C. M. Rodd, R. Agarwal, *Appl. Phys. Lett.* 2009, 94, 083504.

19. Q. Gao, H. Meguro, S. Okamoto, M. Kimura, *Langmuir* 2012, 28, 17593.
20. a) A. Babel, S. A. Jenekhe, *JACS* 2003, 125, 13656; b) S. Lee, G. D. Moon, U. Jeong, *J. Mater. Chem.* 2009, 19, 743; c) S. W. Lee, H. J. Lee, J. H. Choi, W. G. Koh, J. M. Myoung, J. H. Hur, J. J. Park, J. H. Cho, U. Jeong, *Nano. Lett.* 2010, 10, 347; d) A. Babel, J. D. Wind, S. A. Jenekhe, *Adv. Funct. Mater.* 2004, 14, 891.
21. a) S. Sundarrajan, R. Murugan, A. S. Nair, S. Ramakrishna, *Mater. Lett.* 2010, 64, 2369; b) S. A. Jenekhe, S. Yi, *Appl. Phys. Lett.* 2000, 77, 2635; c) M. M. Alam, S. A. Jenekhe, *Chem. Mater.* 2004, 16, 4647.
22. a) L. Qiu, X. Wang, W. H. Lee, J. A. Lim, J. S. Kim, D. Kwak, K. Cho, *Chem. Mater.* 2009, 21, 4380; b) J. Hur, S. N. Cha, K. Im, S. W. Lee, U. Jeong, J. Kim, J. J. Park, *10th IEEE Int. Conf. Nanotech.* 2010, Seoul, 533.
23. a) W. Serrano, A. Meléndez, I. Ramos, N. J. Pinto, *Polym.* 2014, 55, 5727
24. a) W. Serrano, A. Meléndez, I. Ramos, N. J. Pinto, *Polym Int* 2016, 65, 503.
25. a) S. A. Jenekhe, L. R. de Paor, X. L. Chen, R. M. Tarkka, *Chem. Mater.* 1996, 8, 2401; b) M. M. Alam, S. A. Jenekhe, *Chem. Mater.* 2004, 16, 4647.
26. a) K. S. Narayan, B. E. Taylor-Hamilton, R. J. Spry, J. B. Ferguson, *J. Appl. Phys.* 1995, 77, 3938.
27. a) A. Sun, K. Park, L. J. Dai, *Phys Chem C* 2009, 113, 7892; b) K. S. Narayan, B. E. Taylor-Hamilton, R. J. Spry, J. B. Ferguson, *J. Appl. Phys.* 1995, 77, 3938.

Chapter 6: Conclusions and Future Work

6.1 Conclusions

A general approach with direct steps and results for the fabrication of electronic devices using semiconducting polymers and the electrospinning technique has been provided. For the first time, we presented the fabrication of P3HT loaded fibers for the adsorption of negatively charged molecules that can act as a core fiber, characterization of BBL for different volatile organic compounds (VOC's) that could be the shell of the core fiber, and finally, a coaxial nanofiber comprising P3HT and BBL. In summary, this work has accomplished the fabrication and characterization of electroactive P3HT fibers, self-assembled fabrication of BBL thin films for VOC's sensing, and coaxial P3HT/BBL nanofibers.

Nanofiber's technology has been shown to be successfully used in electronic devices and wearable technology as presented in Chapter 1. Chapter 2 focuses on the application of electrospinning for sensing applications and introduces the usage of P3HT as a nanofiber enhancer and electronic devices active material. Chapter 3 presents the idealization of a P3HT/BBL coaxial fiber. Chapter 4 discusses the capabilities of fabricating a coaxial nanofiber of P3HT and BBL that could lead to various applications such as diodes, field effect diodes (FED), field effect transistors (FET), sensors, and many other arrangements. Chapter 5 contains further characterizations of P3HT fibers as negatively charged molecule adsorption and BBL behavior under various VOC's for sensing applications. This chapter concludes the study with the fabrication of a P3HT/BBL core-shell structure and its morphological characterization.

6.2 Future Work

6.2.1 Electrical Characterizations of Coaxial Structured All-polymer p-n Junctions

The electrospinning technique, a cost-effective electrostatic procedure to fabricate nanofibers, has been used for the fabrication of an all-polymer p-n junction. The fabrication and production are naturally improved by the orthogonality of the solvents. This promotes the fabrication of coaxial structured nanofibers by the continuous extrusion of the core, which is covered by the shell due to the insolubility of the polymers in the counterpart solvents. Past work has shown the continuous and well-formed interface by TEM; however, internal percolation and interface coupling is not totally understood.

The usage of a TEM coupled with an EDAX system will let us understand the distribution of the polymer in the interface. This will be done by taking advantage of the molecular structure of each polymer. The polymers that are used in the current structure are the regioregular p-type P3HT and the ladder n-type BBL. These polymers are distinguished by Sulfur and Nitrogen respectively, permitting us to characterize and determine the interface validating the usage of EDAX.

6.2.2 Morphological and Electrical Characterizations of P3HT - BBL Junction Devices

For the final coaxial structured devices, SEM will be used to determine the morphological structures of the fibers while the STEM - EDAX will be used to determine the core/shell structure and interface distribution. By using AFM (KPFM) and semiconductor set-ups for electrical characterizations, we will be able to characterize the percolation, diode and FET characteristic curves, and generation/recombination behavior by irradiating white light (Kelvin probe). Also, taking into account the junction structures, photoconductivity characterizations are envisioned. Indeed, this characterization will overcome the actual gap in fiber devices by fabricating, for the

first time, BBL nanofibers [no studies have been performed or reported] and characterizing the polymer-polymer 1D junctions that are a challenging task in this field.

The expectations rely on the fact that the P3HT/BBL fibers, not published before, will open a new window in the understanding of all-polymer coaxial based devices that can perform as diodes, FET, sensors, and solar cells. This is envisioned to be tethered in textiles forming textile-like devices that share the flexible, durable, and general usage of textiles with the electroactive characteristics of electronic materials which again, are able to sense, compute, and possibly convert their own energy (light or piezo-triboelectricity in the case of other polymers), all in a single nanofiber, yarn or non-woven matrix.

Past research has shown these polymers to be excellent candidates for the proposed characterizations with this coaxial structure. For example, P3HT have been studied in their fiber form and characterized as diode with an ideality factor less than 2 with threshold voltages smaller than 2V. As a field effect transistor, mobility in the range of 10^{-5} to $0.1 \text{ cm}^2/\text{Vs}$ have been reported. A specific case for a thin film structure has reported mobility of $7.2 \times 10^{-4} \text{ cm}^2/\text{Vs}$. In the case of BBL, thin film transistor has been reported to have a mobility of $6.2 \times 10^{-4} \text{ cm}^2/\text{Vs}$ and formed an inverter circuitry with the P3HT thin film FET expressed above. After exhaustive characterizations on P3HT and BBL, to date, no previous research has been performed on the BBL nanofibers, P3HT/BBL nanofiber-based structures, on an all-polymer, electroactive, coaxial structure.

For this process, electrical characterizations are required and will be performed between thin-film and fiber structures to compare and prove the advantage of nanofiber structures over the thin-film devices (which includes higher surface area to volume, basic 1D structure and extended degrees of flexibility than a 2D device) and develop a fundamental understanding of the coaxial structure.

For the fabrication of the BBL nanofibers, the next methodology will be used:

- Dissolve BBL in MSA and PS in CHCl_3 .
- Use BBL solution as a core and PS as the sheath (shell).
- Core solution should run at 0.1ml/hr while Sheath should run at 0.3 to 0.5 ml/hr.
- Recollected fibers in Si wafer and Al foil will be immersed in CHCl_3 to remove the shell and comprise the BBL fiber.
- Fibers of BBL will be immersed in Methanol, followed by DI water to remove any trace of MSA.
- Fibers will be dried at 70°C and then annealed at 100°C for 5 to 10 min.
- Electrical characterizations, SEM, AFM, TEM, WAXD will be performed.

6.2.3 Expectations

Crystalline but flexible fibers will be formed down to 100nm. SEM, AFM pictures should show smooth surfaces if the crystallization begins from the surface (from CHCl_3) and then is stretched by the electrostatic force. However, rough surfaces can be also expected after PS removal. TEM and WAXD should show the excellent crystalline structure in the fiber (expected to be orthorhombic). Assuming the fiber formation led to an improved crystalline structure and continuous π - π bonding's, with total acid remotion, and an annealed improved structure, the lowest mobility should be $0.1\text{cm}^2/(\text{Vs})$.

Appendix A: Copyright Permissions

The permission below is for the content used in chapter 1: General Introduction to the Electrospinning Technique and Polymeric Composites.

[Can I use material from my Elsevier journal article within my thesis/dissertation? –](#)

As an Elsevier journal author, you have the right to Include the article in a thesis or dissertation (provided that this is not to be published commercially) whether in full or in part, subject to proper acknowledgment; see [the Copyright page](#) for more information. No written permission from Elsevier is necessary.

This right extends to the posting of your thesis to your university's repository provided that if you include the published journal article, it is embedded in your thesis and not separately downloadable.

3/2/2021

RightsLink Printable License

ELSEVIER LICENSE TERMS AND CONDITIONS

Mar 02, 2021

This Agreement between University of South Florida -- William Serrano ("You") and Elsevier ("Elsevier") consists of your license details and the terms and conditions provided by Elsevier and Copyright Clearance Center.

License Number	5021030967101
License date	Mar 02, 2021
Licensed Content Publisher	Elsevier
Licensed Content Publication	Elsevier Books
Licensed Content Title	Advances in Nanostructured Materials and Nanopatterning Technologies
Licensed Content Author	Sylvia W. Thomas, Ridita Rahman Khan, Kavyashree Puttananjegowda, William Serrano-Garcia
Licensed Content Date	Jan 1, 2020
Licensed Content Pages	29
Start Page	243
End Page	271
Type of Use	reuse in a thesis/dissertation

<https://s100.copyright.com/AppDispatchServlet>

1/8

The permission below is for the content used in chapter 2: Background Research.

3/1/2021

RightsLink Printable License

SPRINGER NATURE LICENSE
TERMS AND CONDITIONS

Mar 01, 2021

This Agreement between University of South Florida -- William Serrano ("You") and Springer Nature ("Springer Nature") consists of your license details and the terms and conditions provided by Springer Nature and Copyright Clearance Center.

License Number	5020441206904
License date	Mar 01, 2021
Licensed Content Publisher	Springer Nature
Licensed Content Publication	Science China Technological Sciences
Licensed Content Title	Nanocomposites for electronic applications that can be embedded for textiles and wearables
Licensed Content Author	William Serrano-Garcia et al
Licensed Content Date	May 7, 2019
Type of Use	Thesis/Dissertation
Requestor type	academic/university or research institute
Format	print and electronic
Portion	full article/chapter
Will you be translating?	no

<https://s100.copyright.com/AppDispatchServlet>

1/6

The permission below is for the content used in section 2.1: Nanocomposites for Electronic Applications That Can Be Embedded for Textiles and Wearables.



Sensor response of electrospun poly(lactic acid)/polyaniline nanofibers to aliphatic alcohol vapors of varying sizes

Conference Proceedings: 2014 IEEE 9th IberoAmerican Congress on Sensors

Author: William Serrano

Publisher: IEEE

Date: Oct. 2014

Copyright © 2014, IEEE

Thesis / Dissertation Reuse

The IEEE does not require individuals working on a thesis to obtain a formal reuse license, however, you may print out this statement to be used as a permission grant:

Requirements to be followed when using any portion (e.g., figure, graph, table, or textual material) of an IEEE copyrighted paper in a thesis:

- 1) In the case of textual material (e.g., using short quotes or referring to the work within these papers) users must give full credit to the original source (author, paper, publication) followed by the IEEE copyright line © 2011 IEEE.
- 2) In the case of illustrations or tabular material, we require that the copyright line © [Year of original publication] IEEE appear prominently with each reprinted figure and/or table.
- 3) If a substantial portion of the original paper is to be used, and if you are not the senior author, also obtain the senior author's approval.

Requirements to be followed when using an entire IEEE copyrighted paper in a thesis:


- 1) The following IEEE copyright/ credit notice should be placed prominently in the references: © [year of original publication] IEEE. Reprinted, with permission, from [author names, paper title, IEEE publication title, and month/year of publication]
- 2) Only the accepted version of an IEEE copyrighted paper can be used when posting the paper or your thesis on-line.
- 3) In placing the thesis on the author's university website, please display the following message in a prominent place on the website: In reference to IEEE copyrighted material which is used with permission in this thesis, the IEEE does not endorse any of [university/educational entity's name goes here]'s products or services. Internal or personal use of this material is permitted. If interested in reprinting/republishing IEEE copyrighted material for advertising or promotional purposes or for creating new collective works for resale or redistribution, please go to http://www.ieee.org/publications_standards/publications/rights/rights_link.html to learn how to obtain a License from RightsLink.

If applicable, University Microfilms and/or ProQuest Library, or the Archives of Canada may supply single copies of the dissertation.

BACK

CLOSE WINDOW

The permission below is for the content used in section 2.2: Electrospinning for Sensing Devices.



Taylor & Francis
Taylor & Francis Group

Ferroelectrics

Electrospun Fibers of Poly(Vinylidene Fluoride-Trifluoroethylene)/Poly(3-Hexylthiophene) Blends from Tetrahydrofuran

Author: William Serrano, , Nicholas J. Pinto

Publication: Ferroelectrics

Publisher: Taylor & Francis

Date: Jan 1, 2012

Rights managed by Taylor & Francis

Thesis/Dissertation Reuse Request

Taylor & Francis is pleased to offer reuses of its content for a thesis or dissertation free of charge contingent on resubmission of permission request if work is published.

BACK

CLOSE

The permission below is for the content used in section 2.3: Applications of Poly(3-Hexylthiophene) (P3HT).

3/2/2021

RightsLink Printable License

JOHN WILEY AND SONS LICENSE
TERMS AND CONDITIONS

Mar 02, 2021

This Agreement between University of South Florida -- William Serrano ("You") and John Wiley and Sons ("John Wiley and Sons") consists of your license details and the terms and conditions provided by John Wiley and Sons and Copyright Clearance Center.

License Number	5020911045729
License date	Mar 02, 2021
Licensed Content Publisher	John Wiley and Sons
Licensed Content Publication	Polymer International
Licensed Content Title	Poly(lactic acid)/poly(3-hexylthiophene) composite nanofiber fabrication for electronic applications
Licensed Content Author	William Serrano, Anamaris Meléndez, Idalia Ramos, et al
Licensed Content Date	Feb 24, 2016
Licensed Content Volume	65
Licensed Content Issue	5
Licensed Content Pages	5

<https://s100.copyright.com/AppDispatchServlet>

1/8

About the Author

William Serrano Garcia earned his B.Sc. in Physics Applied to Electronics from the University of Puerto Rico at Humacao (UPRH), Puerto Rico, in 2015. As a participant in the NSF Partnerships for Research and Education in Materials Research (PREM) program, he coauthored eight journal and conference papers focusing on the fabrication and characterization of organic polymers and nanofiber electronics.

After enrolling at the University of South Florida (USF), the author completed his Master's in Electrical Engineering (M.S.E.E.) as a member of the Advanced Materials for Bio & Integration Research Laboratory (AMBIR). He is a member of the National Academy of Inventors and holds a patent for the fabrication of electroactive coaxial structures and has coauthored seven journal papers and book chapters studying conducting and semiconducting polymers for nanoscale fiber-based electronic devices.

During his graduate years, the author initiated global collaborations as an NSF East Asia Pacific Summer Institute (EAPSI) fellow and U.S. Fulbright U.S. Student Program grant recipient to advance knowledge gaps in fiber technologies. His current research is focused on the development of new structures for organic electronic devices, nanofibers and their applications in energy, personal protection equipment (PPE), communications, sensors, and actuators.